Compensation of Nonlinearities in Transducers

Martin Rune Andersen

Kgs. Lyngby 2005
IMM-THESIS-2005-35

Technical University of Denmark
Informatics and Mathematical Modelling
Building 321, DK-2800 Lyngby, Denmark
Phone +45 45253351, Fax +45 45882673
reception@imm.dtu.dk
www.imm.dtu.dk

IMM-THESIS: ISSN 1601-233X

Abstract

This thesis is concerned with the topic of compensation algorithms for the nonlinearities in transducers for use in hifi-loudspeaker. The thesis contains a examination of the general ideal loudspeaker model. Furthermore, nonlinearities that influences the performance of the loudspeaker are described, and measurement are done on what they does to the loudspeaker.

The loudspeaker model is from here transformed into the digital domain, in preparation for constructing a control system later. In order to make this model complete, appropriate functions are fitted to the nonlinearities and added to the model.

Furthermore, a text based toolbox for Matlab is made for simulations and evaluations of different properties in both the loudspeaker and in the upcoming compensation algorithm.

Finally, two interesting feedforward controller systems are presented. The first is the "state space" compensator and the second is the "Mirror filter" derived by Wolfgang Klippel. Later research has shown that they are of same controller type.

Resumé

Denne rapport omhandler emnet kompenserings algoritmer for ikke-lineariteter i transducere til brug i hi-fi højttalere. Rapporten indeholder en gennemgang af den generelle ideelle højttaler model. Yderligere er ikke-lineariteterne der forringer ydelsen af højttaleren beskrevet og målinger, omkring hvad det gør ved denne, er foretaget.

Herfra overføres højttaler modellen til det digitale domæne med henblik på senere at konstruere et regulering system til denne. Og for at gøre modellen komplet i forhold til højttaleren, tilpasses en passende funktion til ikke-lineariteterne så disse kan inkluderes.

Desuden præsenteres en Matlab toolbox til hjælp med at simulere og evaluere de forskellige egenskaber i både højttalere og også i de senere kompenseringsalgoritmer.

Til sidst gennemgås to interessante prekompensering algoritmer. Den ene er "state-space" kompensatoren og den anden er Wolfgang Klippels "Mirror filter". Ved senere tids forskning har det dog vist sig, at disse to er af samme type reguleringssystem.

Preface

This thesis was written to fulfil the requirements to obtain a master of science degree in engineering from the Technical University of Denmark.
It was carried out in corporation with Oticon A/S, at IMM-DTU and Oersted-DTU. Furthermore, i would like to thank Bang & Olufsen ICEpower A/S for supplying me with articles from audio engineer society (AES), and giving me the opportunity for a one day trip to Bang & Olufsen in Struer.

I would like to thank my supervisors Ole Winther, Jan Larsen, Finn Agerkvist and Steen M. Munk for giving my constructive feedback, which helped me in writing my thesis.
I would like thank my girlfriend Jeanette for her support during my project and for her house keeping in the end of my project while I was stocked with my project at DTU (I hope she will continue with that :)).
I would like to thank Fares El Azm and Crilles Bak Rasmussen for relevant technical discussions and for proofreading my thesis. Finally, I would like to thank some of my friends, Martin, Denis, Maya, Robert, Fares and Daniel, for a good atmosphere while writing our thesis.

Martin Rune Andersen, 25th May 2005, Lyngby

Contents

1 Introduction **1**
1.1 History . . . 1
1.2 Purpose of the thesis . . . 2
1.3 Organization of the thesis . . . 2

2 Linear transducer model **5**
2.1 Transducer construction . . . 5
2.2 Electrical circuit . . . 7
2.3 Mechanical circuit . . . 7
2.4 Electro-mechanical transduction . . . 8
2.5 Acoustical circuit . . . 9
2.5.1 Closed box . . . 9
2.5.2 Vented box . . . 11
2.5.3 Acoustic response . . . 12
2.5.4 Linear frequency responds . . . 13
2.6 Extensions to the linear model . . . 15
2.6.1 Temperature model . . . 15
2.6.2 Eddy currents . . . 18
2.6.3 Frequency modulation (Doppler effect) . . . 18
2.7 Speaker construction . . . 19
2.7.1 Loudspeaker alignment . . . 20
2.7.2 Box construction and measurements . . . 22

3 Nonlinearities in the transducer model **27**
3.1 Parametric non-uniformity . . . 27
3.1.1 Electro-mechanical part . . . 27
3.1.2 Mechanical part . . . 29
3.1.3 Others . . . 31
3.1.4 Analysis of importance of the nonlinearities . . . 33
3.2 Evaluation of nonlinear loudspeakers . . . 34
3.2.1 Variation in filter characteristic . . . 34
3.2.2 DC offset . . . 34
3.2.3 Total harmonic distortion and Intermodulation distortion . . . 34
3.2.4 Summary . . . 36

4 Modeling of nonlinearities **39**
4.1 Least Squares . . . 39
4.2 Polynomial fit . . . 40
4.3 Exponential fit . . . 42
4.4 Alternative functions . . . 43

4.5 Fitting models with soft clipping . . . 47
4.6 Summary . . . 47

5 Discrete nonlinear simulation **49**
5.1 Discrete representation of differential equations . . . 49
5.1.1 Discrete difference . . . 52
5.2 Digital filter description of transducer . . . 53
5.3 State space model of transducer . . . 55
5.3.1 Closed box . . . 55
5.3.2 Vented box . . . 55
5.4 Matlab simulation toolbox . . . 56
5.4.1 Layer 1: Settings . . . 56
5.4.2 Layer 2: Signal generation . . . 56
5.4.3 Layer 3: Simulation . . . 58
5.4.4 Layer 4: Signal processing . . . 58
5.4.5 Layer 5: plotting . . . 58
5.5 THD and IMD evaluation of nonlinear plant model . . . 58

6 Controllers **61**
6.1 Controller theory . . . 61
6.1.1 Plant measurement . . . 63
6.2 State-space compensator . . . 65
6.2.1 Inverse dynamics . . . 65
6.2.2 State observer . . . 67
6.2.3 Pre-estimation of states assuming ideal alignment . . . 67
6.2.4 Simulation . . . 69
6.3 Mirror filter . . . 70
6.3.1 Algorithm . . . 70
6.3.2 Simulation . . . 71

7 Future work **73**

8 Conclusion **75**

Bibliography **79**

A Data coefficients **81**
A.1 Digital filters . . . 81
A.1.1 Closed box . . . 81
A.1.2 Vented box . . . 81
A.2 Bessel and Struve functions . . . 82

B Parameters of the test loudspeaker **83**
B.1 Linear parameters . . . 83
B.2 Nonlinear coefficients . . . 84
B.2.1 Polynomial fit . . . 84
B.2.2 Exponential fit . . . 84
B.2.3 Sigmoid fit . . . 85

List of Figures

1.1 Commercial surround systems with wireless speakers (a) Sony HT SL900, (b) Pioneer DCS 515 . . . 2

2.1 Typical transducer construction . . . 6
2.2 (a) Overhung voice-coil, (b) Underhung voice-coil . . . 6
2.3 Schematic of electric circuit of an transducer . . . 7
2.4 SDOF mechanical diagram for the transducer . . . 8
2.5 Speaker mounted in a closed-box enclosure (cavity) . . . 10
2.6 Speaker mounted in a vented-box enclosure . . . 11
2.7 Acoustic radiation impedance and approximations to it . . . 13
2.8 SPL at 1m for a closed box loudspeaker . . . 14
2.9 Displacement for a closed box loudspeaker, 0dB = 1mm . . . 15
2.10 SPL at 1m for a vented box loudspeaker . . . 16
2.11 Displacement for a vented box loudspeaker, 0dB = 1mm . . . 16
2.12 Linear thermal model . . . 17
2.13 Circuit of electrical part with eddy current loss . . . 18
2.14 measured impedance and fitted impedance, (a) s1, (b) s2 . . . 20
2.15 Drawings of the loudspeaker box . . . 23
2.16 Measurements of box alignment, (a) corrected sound pressure insight of box, (b) electrical impedance . . . 25

3.1 Nonlinear force factor $B(x_D)l$, and mirrored to get a better asymmetry view . . . 28
3.2 Nonlinear inductance $L_E(x_D)$ of the voice-coil . . . 28
3.3 Nonlinear compliance $C_D(x_D)$, and mirrored to get a better asymmetry view . . . 29
3.4 Cross section of typical single roll suspension . . . 30
3.5 Deviation of the sound pressure compared to the inverted impedance . . . 31
3.6 (a) Resonance frequency f_s and (b) quality factor Q_{TS}, at different displacements . . . 34
3.7 Normalized SPL at low frequencies, measured inside box . . . 35
3.8 DC in diaphragm displacement at different driving levels . . . 35
3.9 (a) Total harmonic distortion (b) Intermodulation distortion . . . 36
3.10 Simulated total harmonic distortion, only Bl nonlinearity . . . 37
3.11 Simulated total harmonic distortion, only C_D nonlinearity . . . 37
3.12 Simulated total harmonic distortion, only L_E nonlinearity . . . 37
3.13 Simulated intermodulation distortion, only Bl nonlinearity . . . 38
3.14 Simulated intermodulation distortion, only C_D nonlinearity . . . 38
3.15 Simulated intermodulation distortion, only L_E nonlinearity . . . 38

4.1 Fit on data . . . 41
4.2 Polynomial fit on force factor data data . . . 41
4.3 Polynomial fit on force factor data data . . . 42
4.4 Polynomial fit on force factor data data . . . 43

4.5 Sum of squares error . . . 44
4.6 Bad fits, (a) $\sigma_l = 1$, (b) $\sigma_l = 4.5$ . . . 44
4.7 $\sigma = 2.81$, range of centers $\{-7\text{mm}; 7\text{mm}\}$, no offset . . . 45
4.8 $\sigma = 2.55$, range of centers $\{-7\text{mm}; 7\text{mm}\}$, no offset . . . 45
4.9 $\sigma = 3$, range of centers $\{-6\text{mm}; 6\text{mm}\}$, offset equal to $Bl(0)$ . . . 45
4.10 Fit on inductance data with sigmoid function, (a) iterations in fit, (b) final result . . . 47
4.11 Polynomial fit on compliance data, where only offset is changed . . . 48

5.1 Transfer function of discrete derivatives, $f_s = 48\text{kHz}$, (a) magnitude, (b) phase . . . 51
5.2 Block diagram of loudspeaker compensation toolbox in Matlab . . . 57
5.3 THD simulation plotted along with belonging measurements . . . 59
5.4 IMD simulation plotted along with belonging measurements . . . 60

6.1 Three types of controller systems, (a) feed-forward, (b) feedback, (c) adaptive feed-forward 62
6.2 State-space compensator . . . 65
6.3 State-space compensator with state observer . . . 68
6.4 State-space compensator with pre-simulated states . . . 68
6.5 THD and IMD simulations at different driving levels, (a) THD, (b) IMD . . . 69
6.6 THD and IMD simulations at different driving levels, (a) THD, (b) IMD . . . 71

List of Tables

2.1 Linear parameters for the drivers used in the test loudspeaker 21
2.2 Calculated box parameters in alignment 22
2.3 Measured box parameters in alignment 24

Abbreviation

B&K	Brüel & Kjear
DST	Danish Sound Technology
EMF	Elector magnetic force
IMD	InterModulation distortion
PA	Public address
SDOF	Single-degree of freedom
THD	Total Harmonic Distortion

Notation

a_D	Acceleration of diaphragm [m/s^2]
B	Magnetic flux density [T]
c	Speed of sound [343 m/s]
C_D	Mechanical compliance of diaphragm suspension [m/N]
C_t	Mechanical compliance of diaphragm suspension and mechanical equivalent of acoustic compliance [m/N]
C_{tb}	Thermal capacity of box
C_{tm}	Thermal capacity of magnet
C_{tv}	Thermal capacity of voice-coil
f	Frequency [1/s]
f_B	Helmholtz resonance frequency [1/s]
F_D	Force on voice-coil [N]
F_MD	Force produced from the mass of diaphragm when moving [N]
F_RD	Force produced from the resistance of diaphragm when moving [N]
F_CD	Force produced from the compliance of diaphragm when moving [N]
i_c	Current flow in voice-coil [A]
l	Effective length of voice-coil wire in the magnetic field [m]
K_D	Mechanical stiffness of diaphragm suspension [N/m]
L_2	Para-inductance of voice-coil [H]
L_E	Inductance of voice-coil [H]
L_P	Length of vent [m]
$L_{P,eff}$	Effective length of vent [m]
M_{A1}	Acoustical mass in front of the diaphragm
M_{AB}	Acoustical mass behind of the diaphragm
M_D	Mass of diaphragm and coil assembly [kg]
M_t	Mass of diaphragm and coil assembly and mechanical equivalent of acoustic mass [kg]
P_t	Input power in thermal model [W]
Q_0	Total quality factor of driver in vented box
Q_{TC}	Total quality factor of driver in closed box
Q_{TS}	Total quality factor of driver in free air
Q_L	Quality factor of loss
Q_E	Electrical quality factor of driver in free air
Q_M	Mechanical quality factor of driver in free air
p_D	Pressure difference between front and back of diaphragm [Pa]
p_c	Pressure inside box [Pa]
R_2	Electrical resistance due to eddy current losses
R_E	Resistance in coil wire [Ω]
R_D	Mechanical resistance of diaphragm suspension [N·s/m]
R_t	Mechanical resistance of diaphragm and coil assembly and mechanical equivalent of acoustic resistance [N·s/m]

R_{tb}	Thermal resistance of box
R_{tm}	Thermal resistance of magnet
R_{tv}	Thermal resistance of voice-coil
s	Laplace frequency, notation for $-j\omega$ in phasor equations [s^{-1}]
S_B	Inside cross area of front plate [m^2]
S_D	Cross area of diaphragm [m^2]
S_P	Cross area of vent [m^2]
T_a	Ambient temperature [°C]
T_b	Box temperature [°C]
T_m	Temperature of magnet [°C]
T_v	Temperature of voice-coil [°C]
u	Voltage applied on the terminals [V]
u_D	Mechanical velocity of the diaphragm [m/s]
U_B	Volume velocity emitted into the box
U_D	Volume velocity emitted by the diaphragm
U_L	Volume velocity emitted by air leaks
U_0	Total volume velocity emitted by loudspeaker
U_P	Volume velocity emitted by vent
v	Voltage applied to the compensation system [V]
v_c	Voltage drop across the terminals of the voice-coil [V]
V_c	Volume of box [l]
V_{AB}	Effective volume of box [l]
w	Voltage applied to the linear dynamics [V]
x_D	Diaphragm displacement [m]
Z_{rad_b}	Acoustic radiation impedance in back of the diaphragm
Z_{rad_F}	Acoustic radiation impedance in front of the diaphragm
Z_{rad}	Acoustic radiation impedance
Z_E	Impedance of voice-coil [Ω]
Z_{EB}	Impedance of blocked voice-coil (no diaphragm movements) [Ω]
Z_M	Mechanical impedance [Ω]
Z_{rm}	Mechanical equivalent of acoustical impedance
ΔT_c	Increase of cabinet temperature [°C]
ΔT_m	Increase of magnet temperature [°C]
ΔT_{mss}	Steady-state magnet temperature [°C]
ΔT_v	Increase of voice-coil temperature [°C]
ΔT_{vss}	Steady-state voice-coil temperature [°C]
ρ_0	Density of air 1.18 at 20°C
ρ	Effective density
λ	Wavelength of sound c/f
ω	Angular frequency $2\pi f$ [rad/s]
ω_s	Undamped natural frequency driver in free air [s^{-1}]
ω_s	Natural frequency driver in closed box [s^{-1}]
ξ	Damping ratio of the mechanical system without acoustical loading

Chapter 1

Introduction

There exists clear division between people who are willing to pay a lot for hifi-systems and people who are not.
The group which are willing to pay more do not compromise the performance in terms of the price, and tend to spend a fortune on components which only slightly increase the performance. On the other hand the second group consider the price more important than the performance.
The intension for doing this project was to challenge both of the two worlds by looking at the perspective from a different point of view. This would be done by taking a cheap hifi-system, and then digitally compensating for the distortion, only modestly increasing the price to the extent that the last of the two groups would accept the increase in the price.
During thesis a symposium, that took place the December 2. at IMM-DTU in corporation with Oersted-DTU, was arranged, where two experts within transducer linearization, Dr. Wolfgang Klippel and PhD. Andrew Bright from Nokia, were invited. The symposium ended up in a panel discussion, where also some among the industry joined. The topic was "how far are we from commercial products?". The overall conclusion of the discussion was that in order to see commercial success, the implementation must be done in a application where a DSP-processor already is available. Furthermore, the compensation algorithm must be less complex than the rest of the DSP code.
In figure 1.1 two products, from respectively Sony and Pioneer, that are on the market are shown. The interesting with these systems are that they include wireless speakers, which then leads to active speakers with digital inputs. So the speaker in these systems already contain some kind of digital processing. Furthermore, the amplifier in the Sony system is their digital one with S-master technology, which makes the electronics in the Sony speaker completely digital.

Of other applications of interest to this thesis are mobile units in general, as mobile phones, hand held computers and hearing aids.

1.1 History

The moving-coil transducer for audio reproduction was first described in 1874 by Ernst Werner Siemens. But not until 1925 the transducer appeared as a loudspeaker as we know it today, developed by Chester W. Rice and Edward W. Kellogg.
From the beginning research, on compensating the nonlinearities in a transducer, has been done, but not until the last decade useable proposals have been made and furthermore, not until the last few years has the proposals been realizable.

(a) (b)

Figure 1.1: Commercial surround systems with wireless speakers (a) Sony HT SL900, (b) Pioneer DCS 515

1.2 Purpose of the thesis

The purpose of this thesis is to look into the theory of loudspeaker compensation and how to apply it on existing loudspeakers, thus optimization of the loudspeaker design is not considered in here. As many attempts have been done in the past, these must be studied and a short overview will be given.
The following short list describes the topics that need to be investigated:

- Transducers theory, how they are used in a loudspeaker and how they are modeled.
- Nonlinearities that must be added to the model, in order to describe it at large signals
- Attempts in the past to make control systems
- How to use loudspeaker compensation in applications

Furthermore, one or two algorithms must be investigated even further and be implemented in Matlab with real transducer data. Of this reason a simple test loudspeaker must be constructed to achieve these data.

1.3 Organization of the thesis

Chapter 1. Introduction

Chapter 2. Linear transducer model: Classical linear models of the loudspeaker are reviewed. Furthermore, a test loudspeaker is constructed, where its parameters are used in later simulations.

Chapter 3. Nonlinearities in the transducer model: Nonlinearities in the transducer model are discussed, and it is finally decided which ones of biggest importance. Furthermore, distortion in the test loudspeaker is measured.

Chapter 4. Modeling of nonlinearities: This chapter focusses on fitting models to the nonlinearities. Different functions are applied and their advantages and disadvantages are discussed. Finally an idea for adding soft clipping to the transducer is presented.

Chapter 5. Discrete nonlinear simulation: In this chapter the transducer model is transformed into discrete time difference equations. From these general digital filters are derived, both linear and nonlinear filters. Finally a Matlab toolbox for simulating loudspeakers and compensation systems, is presented.

Chapter 6. Control: Some general control theory are reviewed. Later two feedforward compensator algorithms are presented and they are evaluated on the discrete nonlinear model.

Chapter 7. Future work: Based on the work done in this thesis, a schedule for how to carry on, is given.

Chapter 8. Conclusions: Conclusions are drawn on active control of loudspeakers using feedforward processing.

Appendix A. Data coefficients: Filter coefficients and other data are given in here.

Appendix B. Parameters of the test loudspeaker: Parameters for the drivers used in the loudspeaker and the loudspeaker coefficient, are given.

Chapter 2

Linear transducer model

In the this chapter the basic linear transducer model is described. The model, which can be written as basic filters, was completed by Thiele [Thiele, 1961] and in a series of papers by Small [Small, 1971], [Small, 1972], [Small, 1973a], [Small, 1973b], [Small, 1973c], [Small, 1973d] and [Small, 1973e]. Though Thiele and Small's papers gives a full description of the model, [Leach, 1999] and [Bright, 2002] have been a great inspiration for the study of the linear transducer model.

At the end of this chapter, a vented-box loudspeaker is constructed. The parameters of the transducer used in this, is used in Matlab simulations throughout this thesis and the loudspeaker is used for testing the derived control systems.

2.1 Transducer construction

A typical construction of a moving-coil transducer is seen at figure 2.1. The transducer consists of three circuits:

- The electrical circuit, which is a voice-coil and the resistance in the coil wire.
- The mechanical circuit, which is a single-degree-of-freedom (SDOF) mechanical oscillator.
- The acoustical circuit, which is the air loading both in front and in back of the diaphragm.

The sound is radiated by the diaphragm, which is the moving surface. The diaphragm is moved by the voice-coil, which is a part of the electromagnetic network. The other part of the electromagnetic network is the magnet and its circuit (pole pieces). If current is applied to the voice-coil in the magnetic field, a force will move the voice-coil. If the current is reversed, the force is reversed too. The force on the diaphragm is linearly related to the current in the voice-coil if the number of turns of wire in the magnetic field does not change when the diaphragm moves. In figure 2.2, two methods of how this is achieved, is seen. If the coil is overhung as in figure 2.2a, then as the coil moves in one direction, some turns leave the gap while others enter it in the other end and the total number of turns of wire is kept constant. In 2.2b the underhung method is seen, when the coil moves no turns of wire leave the gap and non enter, thus keeping the number of turns constant.
If the transducer is pushed too far, the coil moves out of the gap decreasing the number of turns of wire, and it becomes nonlinear.
An air vent is often used to prevent the air in the small cavity behind the dust cap from being nonlinear and furthermore it increases the air convection which gives a much better cooling of the coil, see [Klippel, 2003]. The diaphragm is kept in place by the spider and the outer suspension. As here, two suspensions is often used, but in micro-transducers only the outer suspension is used.

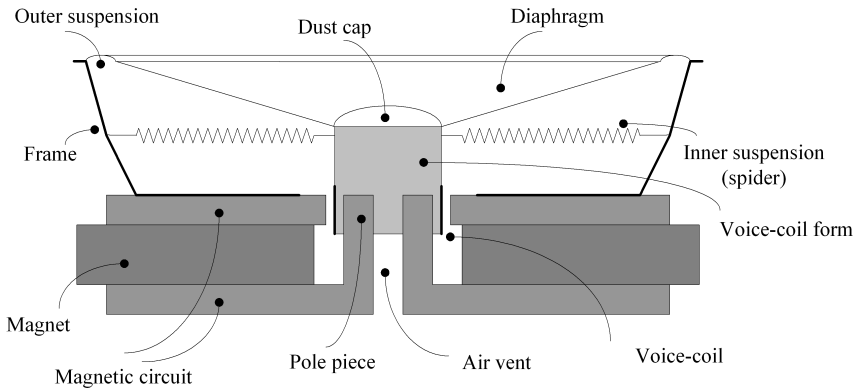

Figure 2.1: Typical transducer construction

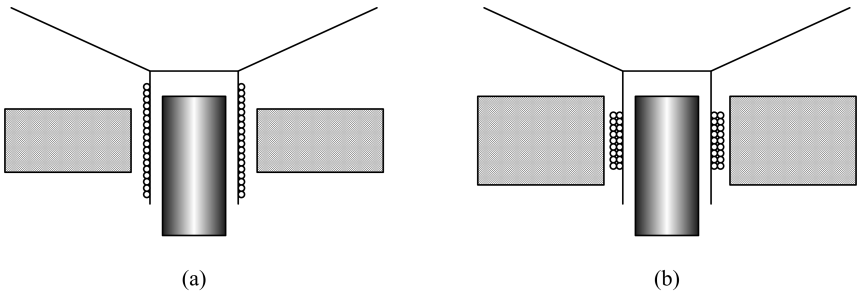

Figure 2.2: (a) Overhung voice-coil, (b) Underhung voice-coil

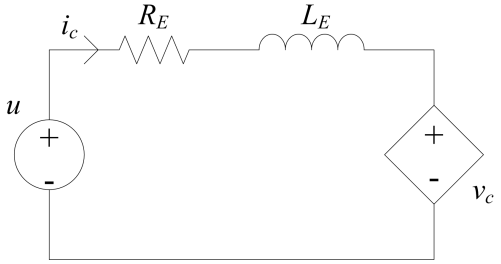

Figure 2.3: Schematic of electric circuit of an transducer

2.2 Electrical circuit

The electrical circuit consists of the voice-coil, a electrical resistance in the wire and voltage applied on the coil when moving in a magnet field. The schematic of the electrical circuit is seen in figure 2.3. u is the input voltage and v_c is the voltage on the voice-coil when moving in a magnet field, also called the back electro magnetic force (back EMF). The value of the voltage is proportional to the velocity of the voice-coil and thus becomes as a controlled voltage source in the electrical circuit. R_E is the resistance in the coil wire, L_E is the inductance and i_c is the current in the voice-coil. From this the voltage equation can be written as:

$$u(t) = R_E i_c(t) + L_E \frac{di_c(t)}{dt} + v_c(t) \tag{2.1}$$

All parameters in the equation are constant and it is therefore solved easily with the Laplace transform, and thus the voltage equation can be written as:

$$u(s) = R_E i_c(s) + L_E s i_c + v_c(s) \tag{2.2}$$

where s is the 'Laplace variable' equal to $-j\omega$, $\omega = 2\pi f$ and f is the frequency hertz. And finally, grouping R_E and L_E to a electrical impedance Z_{EB}, which is the blocked electrical impedance as the electrical impedance, caused by the movements of the diaphragm (see section 2.4), is left out:

$$u(s) = Z_{EB}(s) i_c + v_c(s) \tag{2.3}$$

2.3 Mechanical circuit

The mechanical SDOF network is the diaphragm with coil assembly and the two suspensions. A diagram of this is seen in figure 2.4. M_D is the mass of the diaphragm and coil assembly, R_D is the loss in the diaphragm suspension, C_D is the compliance of the suspension and $K_D = 1/C_D$ is the stiffness of the suspension. Z_{rm} is the mechanical-equivalent of the acoustical radiation impedance and is dealt with in the next section. Each of these three components produce a force when the diaphragm is moving:

$$F_{MD}(t) = M_D \frac{d^2 x_D(t)}{dt^2} \qquad F_{RD}(t) = R_D \frac{dx_D(t)}{dt} \qquad F_{CD}(t) = \frac{1}{C_D} x_D(t) \tag{2.4}$$

The first of the equations is Newton's second law, where the second order derivative of the diaphragms displacement is the acceleration. The second equation is the force occurring when a object is moving with a certain speed and a resistance is applied on it; where the first order derivative of the diaphragms displacement is the velocity of it. The force has the opposite direction as the velocity, stopping the diaphragm. The last equation is the spring equation. In this, the direction of the force is always towards the rest position of the diaphragm.

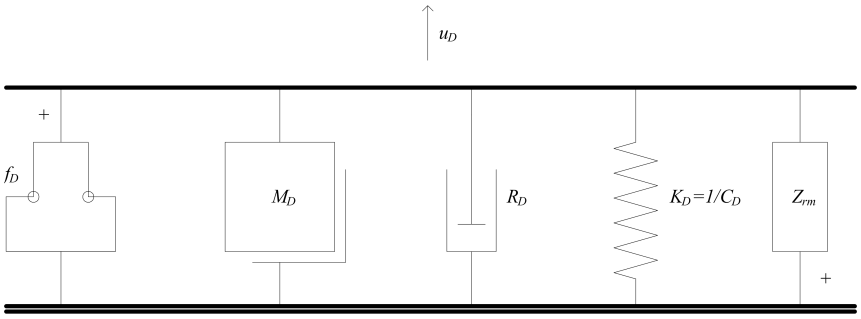

Figure 2.4: SDOF mechanical diagram for the transducer

Hereof the system can be described by the second-order inhomogeneous differential equation:

$$F_D(t) = M_D\ddot{x}_D(t) + R_D\dot{x}_D(t) + \frac{1}{C_D}x_D(t) + Z_{rm}x_D(t) \tag{2.5}$$

where $F_D(t)$ is the force applied on the diaphragm and coil assembly when current flows in the coil. Taking the Laplace transformation of it gives:

$$F_D(s) = (M_D s^2 + R_D s + \frac{1}{C_D} + Z_{rm})x_D(s) \tag{2.6}$$

If the acoustical loading is left out, the mechanical impedance can be found:

$$Z_{M0}(s) = \left.\frac{F_D(s)}{u_D(s)}\right|_{\substack{i_c(s)=0 \\ p_D(s)=0}} = M_D s + R_D + \frac{1}{C_D s} \tag{2.7}$$

where $u_D(s) = \dot{x}_D(s)$. Here the voice-coil is open circuited and there is no acoustical loading (pressure difference from front to back of the diaphragm, p_D, is zero).

With the electrical and mechanical circuit, the resonance frequency and total quality factor for the driver in free air, is given by:

$$\omega_s = 2\pi f_s = \frac{1}{\sqrt{M_t C_D}} \tag{2.8}$$

$$Q_{TS} = \frac{1}{Bl^2/R_E + R_D}\sqrt{\frac{M_t}{C_D}} \tag{2.9}$$

M_t is the mass of the diaphragm and mechanical equivalent of the acoustical loading given in section 2.5.1. The combination of the electrical and mechanical circuit is described in the following section.

2.4 Electro-mechanical transduction

The classical electrodynamic interaction of the line currents and static magnetic field causes a force applied on the voice-coil. It is given by the effective length of the voice-coil wire in the magnetic field times the magnetic force factor times the current in the electrical circuit:

$$F_D(t) = Bli_c(t) \tag{2.10}$$

This is also called the electro magnetic force (EMF). The two first products on the right hand side (RHS) is referred to as the $B \cdot l$ product.

The back EMF as given in the last term on the RHS in 2.1 applies a voltage on the voice-coil:

$$v_c(t) = Blu_D(t) \tag{2.11}$$

This shows that the speaker is a regressive network.

2.5 Acoustical circuit

The acoustical circuit is the load on the loudspeaker, both in back of the diaphragm Z_{rad_b} and in front of it Z_{rad_f}. The load in front is the room and the load in back of the diaphragm is a fixed box. The most commonly used types of rear loads is:

- Closed box.
- Vented box.
- Transmission line speaker.
- Dipole speaker.
- Infinite baffle.
- Horn loaded speaker.

The two first are the most commonly used constructions for amateur hifi and surround systems. The remaining are more seldom and are often used by enthusiastic persons or, for public address (PA) equipment. As this thesis aims at the cheap part of the amateur market, the first two are the ones dealt with in this thesis.

The closed box loudspeaker has a certain volume and separates the front from the back of the diaphragm. This is the most simple type of loudspeaker existing.
The vented box loudspeaker is a closed box loudspeaker with a vent and which forms a resonating circuit. The advantage of vented box loudspeakers is, if properly designed, the lower cut off frequency would be lower than with a properly designed closed box. The volume of the vented box would be bigger than it would for the closed box, though the efficiency is the same.

2.5.1 Closed box

Figure 2.5 is a closed box speaker system. The box has the volume V_C and the internal pressure $p_C(t)$. If the wavelength is about five times greater than any of the box dimensions, $\lambda >\sim 5 \cdot (h, w, d)$, the pressure is assumed to be constant throughout the cavity; the wavelength is found by $\lambda = c/f$, where c is the velocity of sound and f is the frequency. S_D is the cross area of the diaphragm.
The pressure difference between the front and the back of the diaphragm is given by:

$$p_D(t) = U_D(t)\left(M_{AB}s + R_{AB} + \frac{1}{C_{AB}s}\right) + U_D(t)(M_{A1}s) \tag{2.12}$$

where $U_D = S_D u_D$ is the volume velocity radiated by the diaphragm, M_{AB} is the mass behind the diaphragm, M_{A1} is the mass seen in front of the it, R_{AB} is the resistance in the box and C_{AB} is the compliance of the box. The acoustical radiation impedance for both the front and the back is written as:

$$Z_{rad_b} = M_{AB}s + R_{AB} + \frac{1}{C_{AB}s} \qquad Z_{rad_f} = M_{A1} \tag{2.13}$$

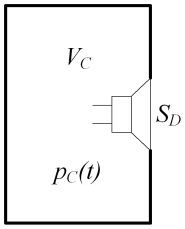

Figure 2.5: Speaker mounted in a closed-box enclosure (cavity)

Only the mass and compliance in Z_{rad_b} can be calculated, the resistance must be measured as it depends on how much filling there is put into the box. The mass and compliance is calculated as:

$$M_{AB} = \frac{B\rho}{\pi a} \text{ [kg/m}^4\text{]} \qquad C_{AB} = \frac{V_{AB}}{\rho_0 c^2} \text{ [m}^5\text{/N]} \tag{2.14}$$

where V_{AB} is effective acoustic volume, ρ_0 is the density of air, ρ is effective density of the combined air and fiber filling in the box, B is the mass loading factor and a is the radius of the diaphragm. The effective volume (volume seen by the loudspeaker) is increased when filled with uncompressed fiber material. This is due to the fact that the filling fibers do not necessarily move with the same velocity as the air particles and furthermore, the specific heat is different for the two. Sometimes it is assumed that the increase of volume, when a closed box is used, is about 25%. With a vented box system the increase is less because normally only the inside walls are covered with filling.
The mass loading factor given in [Leach, 1999] is defined by the dimension of the box:

$$B = \frac{d\sqrt{\pi}}{3} \cdot \frac{S_D^{3/2}}{S_B^2} + \frac{8}{3\pi}\left[1 - \frac{S_D}{S_B}\right] \tag{2.15}$$

where d is the depth of the box and S_B is the inside area of the wall in which the loudspeaker is mounted. As mentioned the resistance R_{AB} can not be calculated, thus it needs to be measured. The measurement is not done in this thesis

The acoustical loading in front of the diaphragm is, despite the simple mass model M_{A1}, very complex. The impedance can be well approximated with a mass, but the mass depends on the dimensions of the box or baffle it is mounted in. If the wavelength of sound is short (high frequencies) compared to the dimensions of the baffle, then the mass is equal to the one when mounted in a infinite baffle. But at very low frequencies where the wavelength is very long compared to the dimensions of the baffle, then the mass of a point source might be used; the mass when mounted in a infinite baffle is two times bigger than the mass seen by a point source. For both these cases, it is assumed that the sound is radiated as simple spherical waves; for the infinite baffle in 2π space and for the point source in 4π space.
In [Leach, 1999][1] a third option is given, which is an alternative between the two. Here the driver is mounted in the end of a long tube where the sound waves diffracts into the space behind the box, and now simple spherical waves cannot be assumed. This model is considered to be the most optimal if the speaker is placed away from the wall, else the infinite baffle will suite best as the wall can be considered as a extension to the front of the speaker.
At high frequencies the infinite baffle would always be the optimal choice, but since the displacement behaves as a low-pass filter, as shown later, the greatest displacements are exhibited at low frequencies, thus the model that describes the low frequencies best must be chosen. Therefore the last described model is used in this thesis and it is given by:

$$M_{A1} = \frac{0.6133\rho_0}{\pi a} \text{ [kg/m}^4\text{]} \tag{2.16}$$

[1] Page 67

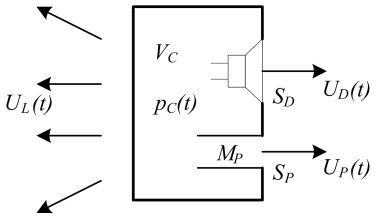

Figure 2.6: Speaker mounted in a vented-box enclosure

The acoustical impedance is easily converted to a mechanical equivalent where it is added to the mechanical impedance:

$$Z_M = Z_{M0} + S_D^2(Z_{rad_r} + Z_{rad_f}) \tag{2.17}$$

Now the three parameters in (2.5) are written as, M_t which is the total mass of the diaphragm with assembly and air load, R_t which is the total resistance and C_t which is the total compliance of the suspension and air in box.

2.5.2 Vented box

The vented box loudspeaker is seen in figure 2.6. Here M_{AP} is the mass of the air in the vent and S_P is the cross-section of it.
Before the vented box circuit is written, the acoustic mass seen by the diaphragm must be converted to a mechanical equivalent and added to the mechanical mass. Both the acoustical masses M_{AB} and M_{A1} are defined for the vented box loudspeaker the same way as for the closed box and can be added to the mechanical impedance in (2.7):

$$Z_{M1} = Z_{M0} + S_D^2(M_{AB} + M_{A1})s \tag{2.18}$$

The compliance and resistance, can not directly be converted into a mechanical equivalent as for the closed box system and thus a new acoustical impedance for the back of the diaphragm must be derived.
The total volume velocity emitted by the speaker U_0 is:

$$U_0(t) = U_D(t) + U_P(t) + U_L(t) = -U_B(t) \tag{2.19}$$

where U_D, U_P and U_L is the contribution from the diaphragm, port (vent) and losses, and U_B is the volume velocity emitted into the box. The losses are due to the fact that the box is not ideal and some of the sound energy travels through the walls and air leaks. This is also the case for the closed box speaker, but in contrast to here, the effect with respect to the displacement is very small. The losses affects the displacement around the Helmholtz resonance.
Inserting the formulas in Laplace time for each volume velocity into (2.19) gives:

$$U_0(s) = S_D u_D(s) + \frac{p_c(s)}{M_{AP}s} + \frac{p_c(s)}{R_{AL}} = -p_c(s)C_{AB}s \tag{2.20}$$

By calculating the Laplace transform to this and rewriting it, the impedance $Z_{rad_{VB}}$ can be written:

$$Z_{rad_{VB}}(s) = -\frac{p_c(s)}{S_D u_D(s)} = -\frac{p_c(s)}{U_D(s)} = \frac{M_{AP}R_{AL}s}{M_{AP}C_{AB}R_{AL}s^2 + M_{AP}s + R_{AL}} \tag{2.21}$$

The mass M_{AP} and the compliance C_{AB} forms a resonating circuit, with the resonance frequency, called the Helmholtz frequency, given by:

$$\omega_B = 2\pi f_B = \frac{1}{\sqrt{M_{AP}C_{AB}}} \tag{2.22}$$

Here the diaphragm is short circuited and does not move (the loss causes it to move little), instead the vent and box resonate resulting a sound pressure. Furthermore, the quality factor Q_L can be written as:

$$Q_L = R_{AL}\sqrt{\frac{C_{AB}}{M_{AP}}} \tag{2.23}$$

The loss resistor R_{AL} can not be calculated and can be very hard to measure. In [Leach, 1999] a thumb of rule is given. If the volume of the box is around 55l to 85l, then $Q_L = 7$ is a good guess. If the volume is bigger then Q_L must be less and vice versa.
The compliance is the same as for the closed box given in (2.14). The mass of the air in the vent is given by:

$$M_{AP} = \frac{\rho_0}{S_P} L_{P,eff} \tag{2.24}$$

where $L_{P,eff}$ is the effective length of the vent. The radiation impedance of a flanged tube with a radius a_p is:

$$Z_{a,r} = \frac{\rho_0 c}{S_p}\left(1 - \frac{\mathrm{J}_1(2\omega a_p/c)}{\omega a_p/c} + j\frac{\mathrm{H}_1(2\omega a_p/c)}{\omega a_p/c}\right) \tag{2.25}$$

where J_1 is the Bessel function and H_1 is the Struve function, both of first order; Their definition is given in appendix A.2. A good approximation is found for frequencies below $\omega a_p/c < 0.5$:

$$Z_{a,r} \approx \frac{\rho_0 c}{S_p}\left(\frac{1}{2}(\omega a_p/c)^2 + j\frac{8}{3\pi}\omega a_p/c\right) \tag{2.26}$$

The radiation impedance of an unflanged tube can be approximated as:

$$Z_{a,r} \approx \frac{\rho_0 c}{S_p}\left(\frac{1}{4}(\omega a_p/c)^2 + \mathrm{j}0.61 \cdot \omega a_p/c\right) \tag{2.27}$$

The last term in the brackets in both cases is the impedance of a acoustic mass corresponding to an extension in the length of the tube equal to $8a_p/3\pi$ and $0.61a_p$. The typical use of a vent mounted in a box, one end is flanged and one is unflanged, gives the effective length of it:

$$L_{P,eff} = L_{P,phy} + \Delta L_P = L_{P,phy} + \left(\frac{8}{3\pi} + 0.61\right) a_p \tag{2.28}$$

The magnitude and phase response for the true, the approximated and an acoustic mass respectively, is shown in figure 2.7. As will be shown in section 2.5.4, the vent only contributes to the sound pressure below about 200 Hz. Therefore the radiation impedance used throughout this thesis is the simple impedance of a acoustic mass.

Now the acoustic impedance for the vented box can be added to (2.18):

$$Z_M = Z_{M1} + S_D^2 Z_{rad_{VB}}(s) \tag{2.29}$$

Finally the transfer function for the volume velocity emitted from the vent can be written by combining (2.19) and (2.20):

$$\frac{U_P(s)}{U_D(s)} = \frac{1}{C_{AB}M_{AP}s^2 + \frac{M_{AP}}{R_{AL}} + 1} \tag{2.30}$$

2.5.3 Acoustic response

The on-axis sound pressure radiated by a circular piston (diaphragm) can be written as a point monopole source in free space if the shortest wavelength of sound considered is longer than any dimension of the loudspeaker:

$$p_r(s) = \rho_0 s U_D(s)\frac{e^{-jkr}}{4\pi r} \tag{2.31}$$

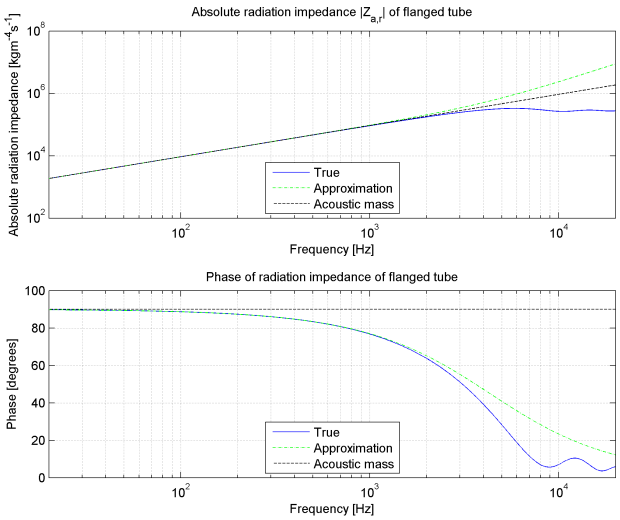

Figure 2.7: Acoustic radiation impedance and approximations to it

where $U_D = S_D u_D$ is the volume velocity, $k = \omega/c$ is the wave number and r is the distance from the diaphragm to the observation point. The complex exponential represents the phase delay caused by the propagation time delay from the diaphragm to the observation point. If the diaphragm is assumed to be mounted in a baffle (the longest wavelength of sound considered is shorter than any dimension of the loudspeaker), the term $4\pi r$ will be replaced by $2\pi r$.
The observation point is from now on considered to be 1m from the diaphragm, and then the pressure can be written as:

$$p_{1\mathrm{m}}(s) = \frac{\rho_0}{4\pi} s U_D(s) \tag{2.32}$$

For the vented box system the sum of the volume velocities from the diaphragm and vent must be used:

$$p_{1\mathrm{m}}(s) = \frac{\rho_0}{4\pi} s(U_D(s) + U_P(s)) \tag{2.33}$$

2.5.4 Linear frequency responds

If the voltage equation (2.2) and the force equation (2.6) is combined and the electrical impedance Z_{EB} and mechanical impedance Z_M are used, then the transfer function for the velocity with the voltage u can be derived:

$$\frac{u_D(s)}{u(s)} = \frac{Bl}{Z_E(s)Z_M(s) + Bl^2} \tag{2.34}$$

And given that $U_D = S_D u_D$ the pressure transfer function is nearly derived.

Closed box response

In the actual pressure response derived here, the electrical inductance is left out and given in a simple first order low-pass filter. This is often done, as it is the low frequencies there is of interest and the inductance only has a effect at high frequencies. With this R_E replaces Z_E in (2.34) and inserting it in (2.32) and rearranging it gives the pressure transfer function:

$$p_{1\mathrm{m}}(s) = \frac{\rho_0}{4\pi} \frac{Bl S_D u(s)}{R_E M_t} \frac{(s/\omega_C)^2}{(s/\omega_C)^2 + (1/Q_{TC})(s/\omega_C) + 1} \tag{2.35}$$

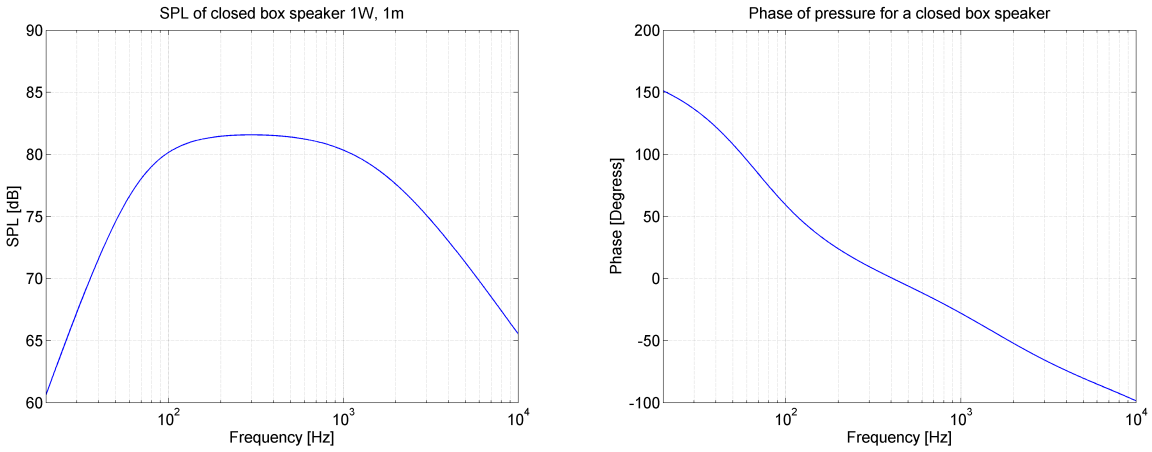

(a) (b)

Figure 2.8: SPL at 1m for a closed box loudspeaker

where ω_C is the closed box system resonance frequency and Q_{TS} is its quality factor, given by:

$$\omega_C = \frac{1}{\sqrt{M_t C_t}} \tag{2.36}$$

$$Q_{TC} = \frac{1}{R_t + Bl^2/R_E}\sqrt{\frac{M_t}{C_t}} \tag{2.37}$$

The low-pass properties of the driver due to the inductance, can be written as a simple first order low-pass filter:

$$T_{u1}(s) = \frac{1}{1 + s/\omega_{u1}} \tag{2.38}$$

where ω_{u1} is given by:

$$\omega_{u1} = \frac{R_E M_t}{L_E M_D} \tag{2.39}$$

The sound pressure level and its phase is calculate and plotted in figure 2.8. The parameters for the loudspeaker constructed in section 2.7 has been used; the vent is blocked so the loudspeaker is assumed to be a closed box. As seen, the low frequency slope is 40dB/dec and the high frequency slope is 20dB/dec. The upper cutoff frequency f_{u1} is at 1781Hz, which is much lower than shown in the datasheet. Actually it is because the model does not fit well at high frequencies due to eddy currents, see section 2.6.2 and diaphragm break up see section 3.1.2. In figure 2.9 the displacement response and its phase are plotted. It can be seen that the displacement is a second order low-pass filter.

Vented box response

Again the electrical inductance is excluded and the pressure transfer function of a vented-box loudspeaker is given by:

$$p_{1\mathrm{m}}(s) = \frac{\rho_0}{4\pi}\frac{BlS_D u(s)}{R_E M_t} G_V(s) \tag{2.40}$$

Where $G_V(s)$ is the unity gain pressure transfer function and given by:

$$G_V(s) = \frac{(s/\omega_0)^4}{(s/\omega_0)^4 + a_3(s/\omega_0)^3 + a_2(s/\omega_0)^2 + a_1(s/\omega_0)^1 + 1} \tag{2.41}$$

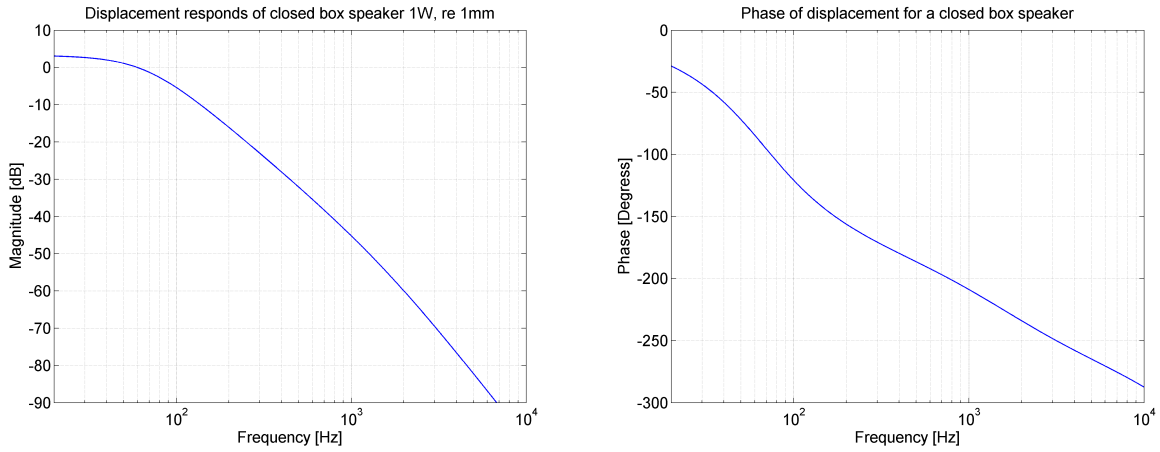

(a) (b)

Figure 2.9: Displacement for a closed box loudspeaker, 0dB = 1mm

The coefficients are written as:

$$a_1 = \frac{1}{Q_L\sqrt{h}} + \frac{\sqrt{h}}{Q_{TS}} \qquad a_2 = \frac{\alpha+1}{h} + h + \frac{1}{Q_L Q_{TS}} \qquad a_3 = \frac{1}{Q_{TS}\sqrt{h}} + \frac{\sqrt{h}}{Q_L} \tag{2.42}$$

where Q_{TS} is the quality factor of the driver in free air, see (2.9) and α and h is given by:

$$\alpha = \frac{V_{AS}}{V_{AB}} \qquad h = \frac{f_B}{f_s} \tag{2.43}$$

In figure 2.10 the sound pressure levels and phases for the diaphragm, vent and their summation, is shown for a vented box system. As seen, at the Helmholtz resonance frequency, the diaphragm hardly moves and the sound pressure is radiated from the vent. Subtracting the vent response from the diaphragm response, gives the total pressure response. As they are in phase below the helmholtz frequency and in inverse phase at and above it, and as the vent is subtracted from the diaphragm, they are in phase at f_B and above, but out of phase below. The displacement function and its phase is seen in figure 2.11. As seen, the displacement is again a low-pass filter, but at f_B it moves only a bit.

2.6 Extensions to the linear model

2.6.1 Temperature model

The variation of the temperature is relatively slow compared with the lowest frequency component used in loudspeakers, thus the electro-mechanical model is considered as a linear but time-variant system; see [Klippel, 2003].
The temperature of the voice-coil is important because firstly, high temperatures might damage the loudspeaker and secondly, changes in the temperature changes the electrical resistance:

$$R_E(T_a + \Delta T_v) = R_E(T_a)(1 + \delta \Delta T_v) \tag{2.44}$$

where T_a is the ambient temperature and ΔT_v is the temperature difference between the ambient and the voice-coil. δ is the conductivity where $\delta = 0.0393K^{-1}$ for copper and $\delta = 0.0377K^{-1}$ for aluminium. The

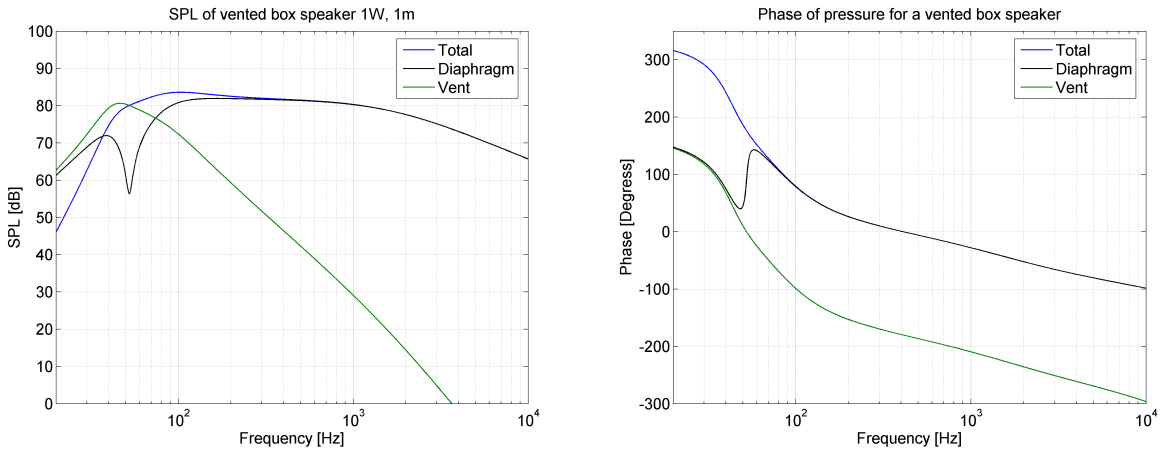

(a) (b)

Figure 2.10: SPL at 1m for a vented box loudspeaker

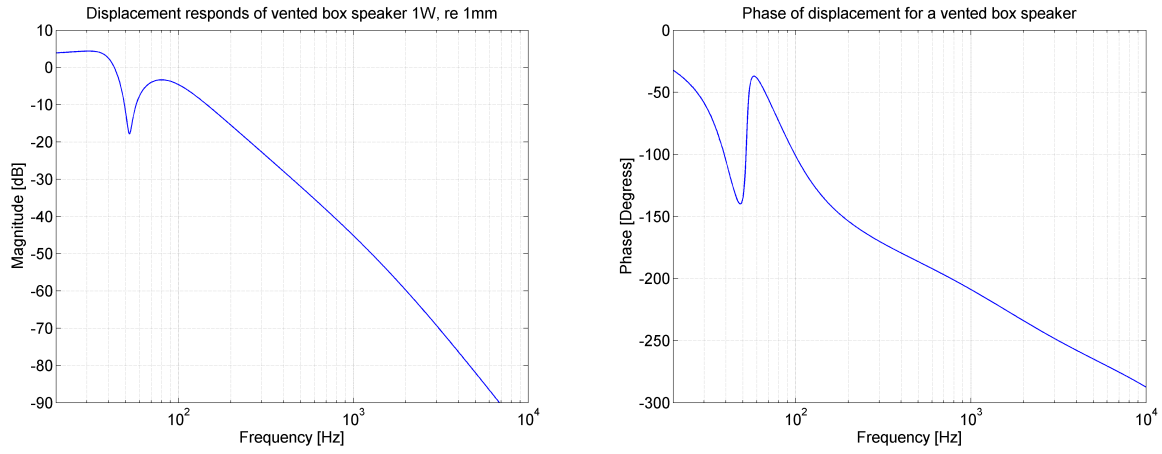

(a) (b)

Figure 2.11: Displacement for a vented box loudspeaker, 0dB = 1mm

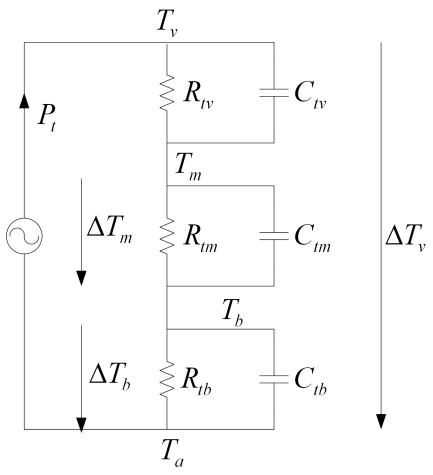

Figure 2.12: Linear thermal model

increased temperature causes power compression and lower efficiency/sensitivity, see **??** and **??**.

So far two models have been presented, the integrator based model by [Henricksen, 1987] and a model by Bang & Olufsen A/S [Chapman, 1998]. The former is the most common used in papers for documentation, but has not been implemented in any products on the market. The latter is the only one that is implemented in a loudspeaker [Chapman, 2000]; the loudspeaker is the Bang & Olufsen Beolab 5. Despite that it does not compensate for the nonlinearities given in chapter 3, it compensates for the temperature changes and is actually the only loudspeaker on the market yet that compensates for unwanted properties of the speaker.

Integrator based model

A thermal model of the loudspeaker is seen in figure 2.12. The thermal model describes the relationship between the input power P_t dissipated into heat and voice-coil temperature T_v and is modeled with a third-order integrator. The first integrator represents the heating of the coil by using the thermal resistance R_{tv} and thermal capacity C_{tv}. The second integrator models the heating of the magnet using R_{tm} and C_{tm} as thermal resistance and capacity and the third models the cabinet heating using R_{tc} and C_{tc}. ΔT_v represent the increase of the voice-coil temperature $\Delta T_v = T_v - T_a$, ΔT_m is the increase of the magnet temperature and ΔT_c is the increase of the cabinet temperature. Often the third integrator is left out besides when using a small sealed enclosure, as suggested by [Behler and Bernhard, 1998].

The input power is given by:

$$P_t = \frac{u^2}{Z_{min}(T_v)} \tag{2.45}$$

where $Z_{min}(T_v)$ is the minimum impedance that is the DC resistance including additional resistance that will generate heat, which is due to eddy currents in the magnet structure; [Button, 1992].

When applying a stimulus with constant power to the loudspeaker the thermal system will go into a thermal equilibrium, given by:

$$\Delta T_{vss} = (R_{tv} + R_{tm})P_t = R_t P_t \tag{2.46}$$

for the voice-coil where ΔT_{vss} is the steady-state temperature. The steady-state magnet temperature is:

$$\Delta T_{mss} = R_{tm} P_t \tag{2.47}$$

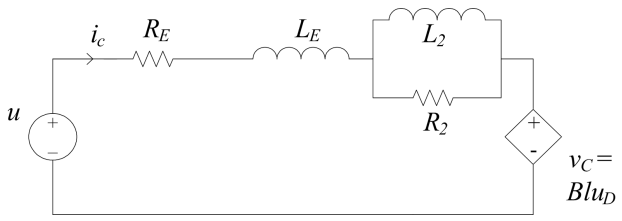

Figure 2.13: Circuit of electrical part with eddy current loss

When switching on the input power, at time $t = t_{s\_on}$, the observed variation of the temperature of the magnet varies exponentially with:

$$\Delta T_m(t) = \Delta T_{mss}(1 - e^{-(t-t_{S\_on})/\tau_m}) \tag{2.48}$$

towards the steady-state temperature ΔT_{mss}. The time constant of the magnet structure is:

$$\tau_m = R_{tm}C_{tm} \tag{2.49}$$

After switching off the input power, at time $t = t_{s\_off}$, the temperature difference between the voice-coil and magnet/frame is:

$$\Delta T_v(t) - \Delta T_m(t) = (\Delta T_{vss} - \Delta T_{mss})e^{-(t-t_{S\_off})/\tau_m} \tag{2.50}$$

with the time constant:

$$\tau_v = R_{tv}C_{tv} \tag{2.51}$$

2.6.2 Eddy currents

Eddy currents in the iron pole structure causes the electrical impedance to behave differently from the normal series network of a resistance and a inductance. The effect was first described in [Thiele, 1961].

The effect is often modeled with a lossy inductor in the model, that is the inductor having a resistor in parallel [Leach, 1999]. This model can be used to fit the impedance as well as necessary over an adequate frequency range.
An extended version is often used, where a resistor R_2 in parallel with an inductor L_2 is put in series in the electrical network, as seen at figure 2.13, [Klippel, 2003]. See appendix B for these values of the test loudspeaker.
A third model is given in [Vanderkooy, 1989]. In here the inductance is said to be varying over frequency with:

$$\mathrm{Im}\{Z_E\} \propto \sqrt{f} \tag{2.52}$$

Vanderkooy shows that this model is better than the first one.

Notice, the eddy currents causes ω_{u1} in (2.39) to change, increasing the upper cutoff frequency.

2.6.3 Frequency modulation (Doppler effect)

Doppler distortion is caused by the moving diaphragm. Short-wavelength components (high frequencies) are affected by resulting frequency modulation (doppler effect) of long-wavelength components, [Moir, 1974] and [Beers and Belar, 1981].

Using the assumption of linear plane wave propagating, an equation is found for the square root of the ratio of the generated side band power to the total power, also known as distortion factor:

$$DF = \sqrt{1 - \left[J_0\left(2\pi\frac{\hat{x}_1}{\hat{\lambda}_2}\right)\right]^2} = \frac{1}{\sqrt{2}}\left(2\pi\frac{\hat{x}_1}{\hat{\lambda}_2}\right) \tag{2.53}$$

where J_0 is the Bessel function of the first kind, $\hat{x}_1$ is the amplitude of the low frequency cone excursion and λ_2 is the wavelength of the modulated frequency.
In [Klippel, 1992a] an algorithm for compensating the doppler distortion can be found.

2.7 Speaker construction

In the progress of this project a test loudspeaker has been developed. The linear and nonlinear (described in chapter 3) parameters of the loudspeaker are used in computer simulations to approach the real world. And at last the control systems are applied on the loudspeaker to support the computer simulations.
The test loudspeaker is a small 2-way vented-box speaker with the following drivers[2]:

- Vifa TC14WG49-08 bass/mid-tone
- Peerless 53 NDT '811435' tweeter

The linear parameter for the drivers, measured with the Klippel analyzer system, are found in appendix [**?**]. Despite that only the bass/mid-tone speaker is going to linearized, a tweeter is included in the design for music playing; music without the high tones and only bass and mid, can be very tiring to listen too.

The tweeter is one of the cheapest from DST (41.90 Dkr + VAT, price at 10.000 pcs.) and therefore it suits well in the concept of a low price loudspeakers with electronic compensation, though it is not compensated here.
As well as the tweeter, also the bass/mid driver is a low cost one from DST (93.99 Dkr + VAT, price at 10.000 pcs.). Actually two bass/middle-tone loudspeakers have been bought; just in case if one is broken. Cheaper drivers can be found made by other manufactures, but the supply of more precise information about the drivers than available at their homepage, and the possibility for personal correspondence, would be lost.

In this section the design of the test loudspeaker is presented. It is designed from the approach recommended in [Leach, 1999], which uses the Thiele-Small parameters:

- f_s, Resonance frequency
- R_E, DC resistance
- Q_{MS}, Mechanical quality factor
- Q_{ES}, Electrical quality factor
- Q_{TS}, Total quality factor
- V_{AS}, Volume equivalent

The Thiele-Small parameters are measured for both of bass/mid drivers, but only the parameters from one of them is used to design the speaker. Two methods have been used for measuring the Thiele-Small parameters:

[2] See www.d-s-t.com

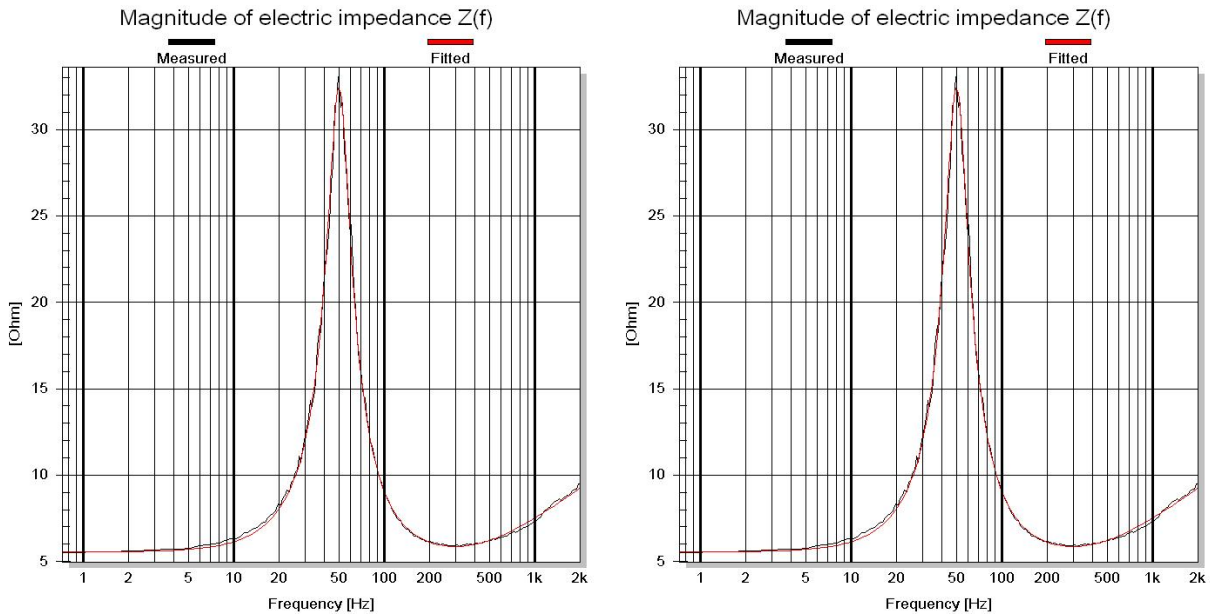

(a) (b)

Figure 2.14: measured impedance and fitted impedance, (a) s1, (b) s2

- Approach given in [Leach, 1999], where the impedance is measured, and the parameters are found by analyzing the result and fitting of the impedance transfer function to it.
- Automatic measurements with "Klippel Analyzer System". The driver is connected to a system that measures and calculates the parameters automatically.

In order to evaluate the two results, the measured impedance were compared to the impedance calculated from the results. It was found that the result measured with the "Klippel Analyzer System" were best. The calculated and measured impedance for both drivers are seen at figure 2.14 and the belonging parameters are given in table 2.1.

At low frequencies the voice-coil inductance L_E is assumed to be short circuit and then the voice-coil impedance, as given in [Leach, 1999], can be written as:

$$Z_{VC}(j2\pi f) = R_E + R_{ES}\frac{j(1/Q_{MS})(f/f_s)}{1-(f/f_s)^2 + j(1/Q_{MS})(f/f_s)} \tag{2.54}$$

where $R_{ES} = R_E Q_{MS}/Q_{ES}$. From the function it can be predicted that $|Z_{VC}(0)| = R_E$, $|Z_{VC}(j2\pi f_s)| = R_E + R_{ES}$ and $|Z_{VC}(j2\pi f)| = R_E$ for $f \gg f_s$.
This equation excludes the voice-coil inductance L_E as it is assumed to be short circuited at low frequencies, where the Thiele-Small parameters are found. If this is the case the impedance function is flat at higher frequencies, and not increasing as in figure 2.14, where the inductance is included. The figure is automatically plotted by the Analyzer System software.

2.7.1 Loudspeaker alignment

The vented-box loudspeaker is designed by specifying an alignment. By defining a specific alignment, the form of the pressure response can be specified. The alignment is adapted by changing the volume of the

	SI	s1	s2	tweeter
R_E	Ω	5.54	5.57	3.57
f_s	Hz	50.1	45.8	1348
Q_{MS}	N/A	2.77	2.49	2.94
Q_{ES}	N/A	0.57	0.50	3.95
Q_{TS}	N/A	0.47	0.41	1.68
V_{AS}	l	10.6	12.99	-

Table 2.1: Linear parameters for the drivers used in the test loudspeaker

box and the dimension of the vent; length and cross area. Specifying the alignment is done in reference to the magnitude-squared function defined by $|G_V(j\omega)|^2$. From (2.41) the magnitude-squared function can be found:

$$|G_V(j2\pi f)|^2 = \frac{(f/f_0)^8}{(f/f_0)^8 + A_3(f/f_0)^6 + A_2(f/f_0)^4 + A_1(f/f_0)^2 + 1} \tag{2.55}$$

where the A coefficients are given by:

$$A_3 = a_3^2 - 2a_2 \qquad A_2 = 2 + a_2^2 - 2a_1a_3 \qquad A_1 = a_1^2 - 2a_2 \tag{2.56}$$

and where a_1, a_2 and a_3 are given in 2.42. One of the three alignments that are commonly used, depending on Q_{TS} [Leach, 1999]:

- Butterworth B4 alignment ($Q_{TS} = 0.4$)
- Quasi-Butterworth QB3 alignment ($Q_{TS} < 0.4$)
- Chebyshev C4 alignment ($Q_{TS} > 0.4$)

As both drivers has a Q_{TS} above 0.4, the Chebyshev alignment is used. In this section the procedure for calculating the C4 alignment, derived in [Leach, 1999], is given and used.

But before starting to derive the alignment, some predefined values are set:

- The volume of the box must be 9l. This volume is chosen because a small speaker is wanted and given the measured values this seems reasonable.
- The vent chosen has a diameter equal to 4.3cm.
- Q_l can not be calculated, but it is needed in order to make the alignment. In [Leach, 1999] a rule of thumb is given. If the volume is between 55l and 85l a good choice would be $Q_l = 7$, if the volume is smaller it must be high and vice versa. Because the volume of this speaker is 9l, $Q_l = 15$.

The C4 alignment has a magnitude-squared function given by:

$$|G_V(j2\pi f)|^2 = \frac{1 + \epsilon^2}{1 + \epsilon^2 C_4^2(f_n/f)} \tag{2.57}$$

where ϵ is a parameter that specifies the amount of ripple and $C4$ is the fourth order Chebyshev polynomial given by:

$$C_4(f_n/f) = 8(f_n/f)^4 - 8(f_n/f)^2 + 1 \tag{2.58}$$

where f_n is a normalization frequency the is related to the lower -3dB cutoff frequency f_l by:

$$f_n = \frac{f_l}{\sqrt{2}} \left[1 + \sqrt{1 + 4\sqrt{2 + 1/\epsilon^2}}\right]^{1/2} \tag{2.59}$$

	SI	Vented-box
V_{AB}	l	9
S_P	cm^2	58.1
L_P	cm	16.7
f_B	Hz	49.25
f_l	Hz	48.4
Q_l	N/A	15
ϵ_{dB}	dB	$0.000009 \approx 0$
k	N/A	0.9477

Table 2.2: Calculated box parameters in alignment

The amount of ripple peak to peak in [dB] can be specified with ϵ_{dB} and ϵ can be calculated:

$$\epsilon = \sqrt{10^{\epsilon_{dB}/10} - 1} \tag{2.60}$$

The a coefficients can be calculated by:

$$a_1 = \frac{k\sqrt{4+2\sqrt{2}}}{D^{1/4}} \qquad a_2 = \frac{1+k^2\left(1+\sqrt{2}\right)}{D^{1/2}} \qquad a_3 = \frac{a_1}{D^{1/2}}\left(1 - \frac{1-k^2}{2\sqrt{2}}\right) \tag{2.61}$$

where k and D are given by:

$$k = \tanh\left[\frac{1}{4}\sinh^{-1}\frac{1}{\epsilon}\right] \qquad D = \frac{k^4+6k^2+1}{8} \tag{2.62}$$

If $k = 1$ then the alignment is equal to the Butterworth alignment and if $k < 1$ it is a chebyshev. Then the following equation is solved for the positive real roots:

$$d^4 - A_3d^3 - A_2d^2 - A_1d - 1 = 0 \tag{2.63}$$

And again for the next equation, it is solved for the positive real roots:

$$r^4 - (a_3Q_L)r^3 - (a_1Q_L)r - 1 = 0 \tag{2.64}$$

And with the solutions for d and r, the Helmholtz resonance frequency f_B and the lower -3dB cutoff frequency can be calculated:

$$f_B = r^2 f_s \qquad f_l = r\sqrt{d} f_s \tag{2.65}$$

In table 2.2 the resulting parameters for the C4 alignment is seen. With the predefined values a theoretically alignment with no ripple is achieved. Given the value of k, it can be concluded that the alignment is close to be a B4 alignment.
At last, the length of the vent can be found by:

$$L_P = \left(\frac{c}{2\pi f_B}\right)^2 \frac{S_P}{V_{AB}} - 1.463\sqrt{\frac{S_P}{\pi}} \tag{2.66}$$

Where the last term is the end correction given in (2.28). The result is found in table 2.2.

2.7.2 Box construction and measurements

In figure 2.15 three drawings of the box, with inside dimensions, are seen, from the front, the side and the top where a cross section half way down is shown. As seen, the two sides, the back and front plate is angled so they are not in parallel with each other. This minimizes the possibility for standing waves

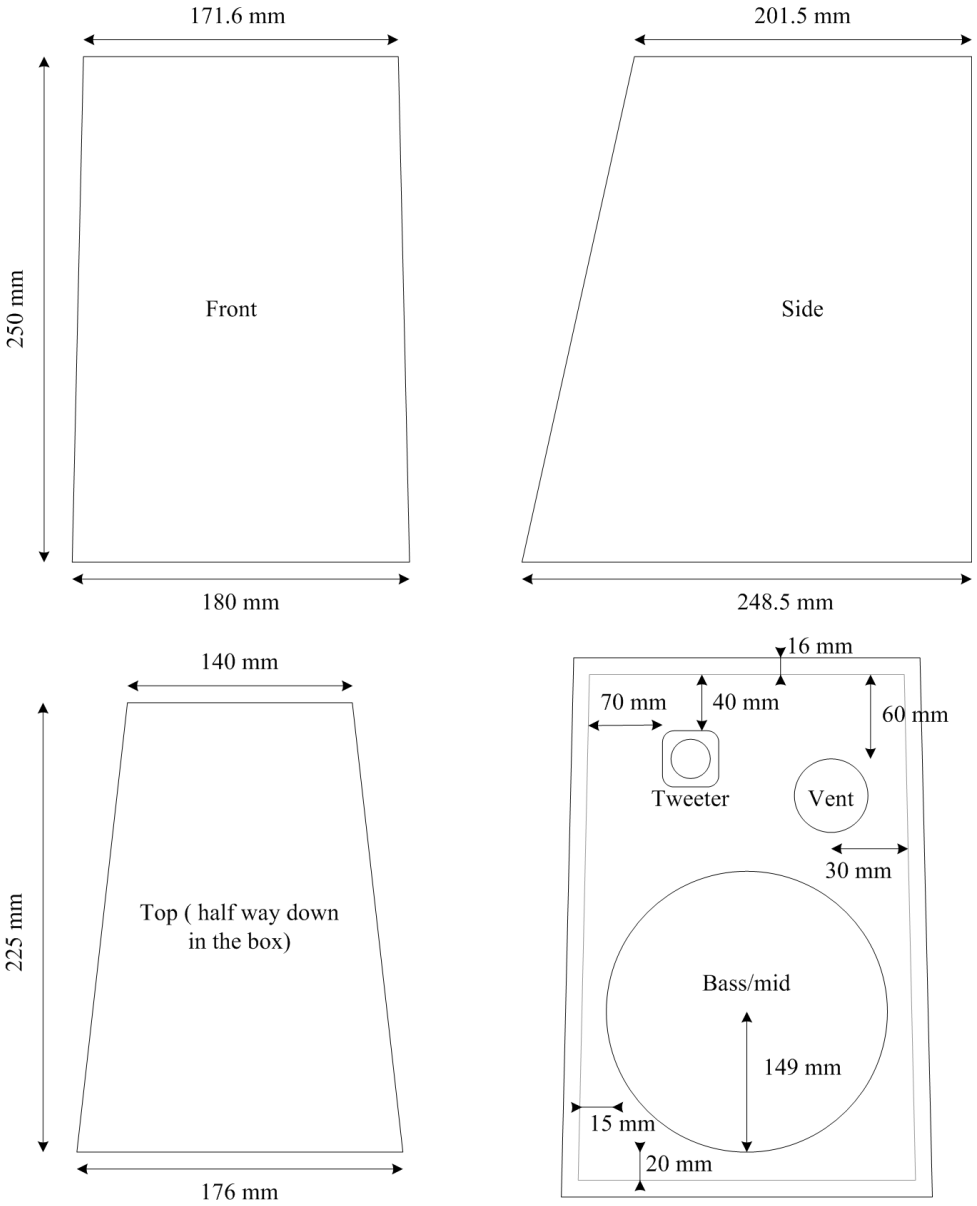

Figure 2.15: Drawings of the loudspeaker box

	SI	Vented-box
V_c	l	9
S_P	cm^2	58.1
L_P	cm	17
f_B	Hz	51
f_l	Hz	60

Table 2.3: Measured box parameters in alignment

inside the box. Standing waves occurs where $i \cdot \lambda$, where i is an integer, is equal to the distance between the two surfaces. They have a resonating effect that results in a deflection at the frequency. Only the top and bottom plate are in parallel.
To suppress standing waves even further, all inside walls, except the front, are lightly covered with fiber fill. The center of the box is not filled, as the air must able to travel between the bass/mid and the vent without resistance.

In order for the air to travel freely from inside of the box into the vent and back, good space from the back plate to the vent opening must be encountered. With the depth of the box in figure 2.15 and the calculated vent length, this is achieved.

The fourth and last drawing in figure 2.15 displays the positions of the bass/mid, vent and tweeter on the front plate. The outer black rectangle is the outside of the box, and the inner grey is the inside. The vent and the bass/mid are placed closely together. This is due to the fact that when measuring with a microphone, in front of the speaker, the radiated sound must sum up in the frequency range measured, and they only do if they are in phase. From that it can be concluded that the distance between the center of the bass/mid and the center of the vent, must be less than the length of half of the shortest wavelength measured.
All sides are made of 16mm MDF.

As a volume velocity is emitted from each of the bass/mid, vent and leaks in the box (2.19), the summed sound pressure can be difficult to measure outside of the box; they must all be measure individually and then added together. If the sound pressure instead is measured inside the box, only one measurement must be done as they are summed at low frequencies when the shortest wavelength of the sound is long compared to the inside dimensions (2.19). When measuring inside a box, the resulting pressure is somewhat different as if measure outside of the box. That is due to the fact that the impedance, for the sound radiated from the front of the diaphragm, is a mass sM_{A1} and the impedance for the sound radiated in back of the diaphragm is a compliance $1/sC_{AB}$. This affects the pressure response and in order to get the correct response, the measured response must be differentiated two times, or equivalent, multiplying the response with f^2.
In figure 2.16 a measurement of the sound pressure inside the box, after it is corrected, is seen. In table 2.3 the measured box parameters are seen.

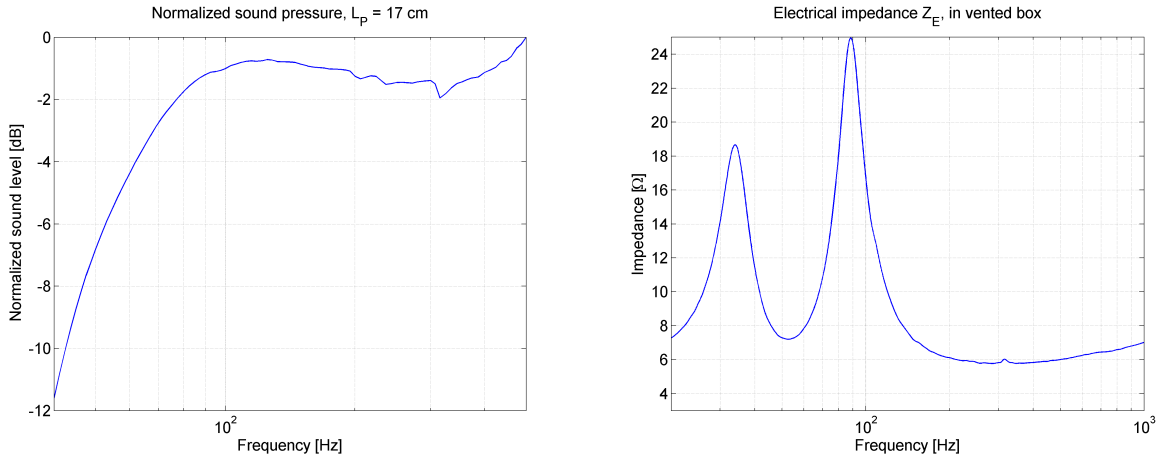

(a) (b)

Figure 2.16: Measurements of box alignment, (a) corrected sound pressure insight of box, (b) electrical impedance

Chapter 3

Nonlinearities in the transducer model

In chapter 2 the ideal transducer model was described. This model is only approximately true when small input signals are applied to the transducer, at larger signals it becomes nonlinear with respect to the displacement, thus the nonlinearities must be added to the model.
In this chapter nonlinear parameters are included in the ideal model, thus the model also is assumed to be true when larger signals are applied. Figures of the nonlinearities are measurements of the 's1' driver used for the test loudspeaker, see section 2.7.
First each nonlinearity is described and later the importance of each of them are discussed and compared, and which nonlinearities that will be dealt with throughout this thesis is chosen.
Finally, the resulting distortion is explained. Note that investigation in improvements of transducer designs is found in [Klippel, 2000].

3.1 Parametric non-uniformity

3.1.1 Electro-mechanical part

Magnetic force factor Bl

3.1.1 In section 2.2 and 2.4 the force factor Bl in the loudspeaker magnet system was described by a constant; uniform in relation to the diaphragm displacement x_D. This is in fact only true at very small displacements. A measurement of the Bl product, for the test loudspeaker driver 's1', is seen in figure 3.1. The force factor is highest around the rest position $x_D = 0$ and decreases towards higher displacements. Furthermore, the measurement shows a small asymmetry. From this the effective transduction coefficient $B(x_D)l$ is calculated as:

$$B(x_D)l = \int_{h/2}^{h/2} B(\xi - x_D)d\xi \tag{3.1}$$

The effective length of the voice-coil l is constant and h is the height of it. The resulting nonlinear behavior is caused by the fact that when the diaphragm moves out of or into the speaker box, it moves away from the magnetic field.

Inductance

The inductance varies with the coil position. This is due to the fact that, as the coil moves away from the magnetic system, less ferromagnetic material is 'seen' by the magnetic field generated by the coil, causing

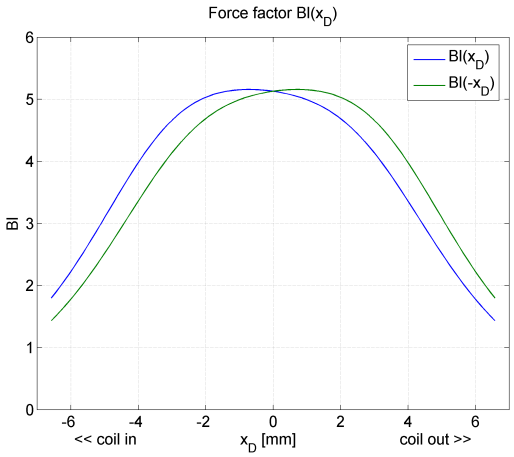

Figure 3.1: Nonlinear force factor $B(x_D)l$, and mirrored to get a better asymmetry view

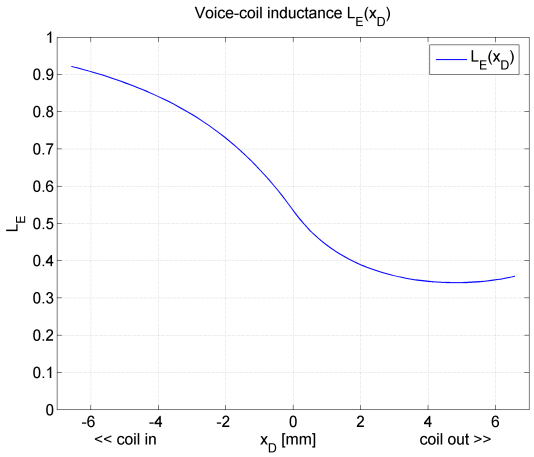

Figure 3.2: Nonlinear inductance $L_E(x_D)$ of the voice-coil

a lower electrical inductance. In figure 3.2 the voice-coil inductance with respect to the displacement is seen. As it is seen, the curve is strongly asymmetric around the rest position for this specific transducer; it is not always like this, for other loudspeakers it can have a shape like the one in figure 3.1 and 3.3, see [Klippel, 2000].

Magnetic attraction force

The magnetic attraction force is a 'solenoid' effect and was described first by [Cunningham, 1949]. It is a result of the classical electrodynamic effect of the attractive force existing in a current-carrying wire, on any ferromagnetic material in its vicinity. The coil will exhibit this force in the magnet and magnet circuit. The force is related to the spatial derivative of the internal inductance of the coil and thus is dependent on the non-uniformity in the electrical inductance:

$$F_{ma} = \frac{1}{2} i_c^2(t) \frac{dL_E\left(x_D(t)\right)}{dx_D(t)} \tag{3.2}$$

The magnetic attraction force problem is biggest in transducers with largely overhung voice-coils, thus the effect is reduced if the ferromagnetic material in the magnet system is near or at magnetic saturation.

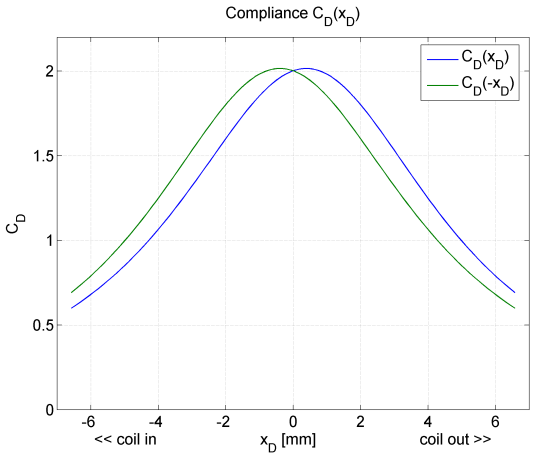

Figure 3.3: Nonlinear compliance $C_D(x_D)$, and mirrored to get a better asymmetry view

The forcing term F_{ma} must be subtracted from the left-hand-side of (2.5).

Klippel states in [Klippel, 1998][1] that in most cases, the magnetic attraction force only has a minor influence.

3.1.2 Mechanical part

Suspension stiffness/compliance

Again, the stiffness or compliance of the suspension is not constant as described in section 2.3. Three types of nonuniformity are causing distortion, which are:

- Suspension exhibits as a smooth memory-less function of displacement.
- Suspension exhibits as a hysteretic function.
- Suspension exhibits as a discontinuous function.
- Suspension changes under high playing levels.

The gradual (smooth) variation in the suspension is also known in mechanics as a hardening spring. For a typical transducer the compliance will decrease at higher displacements, as seen at figure 3.3. The decreasing compliance causes the resonance frequency to increase, see (2.8).

Furthermore, the nonlinear suspension sometimes causes a hysteretic behavior in the displacement with respect to the voice-coil current. An example here is not presented, as equipment for measuring this was not available, but it is shown in greater detail in [Bright, 2002].

At some point at very high displacements a physical limit is reached. Either the suspension will no longer become flexible or the voice-coil will contact the magnet and/or frame. At this point the suspension compliance becomes zero, and no matter how much force applied, the diaphragm can not be moved any further. Because of this, the compliance should be limited to a maximum allowed displacement, when it is linearized.

[1] ??

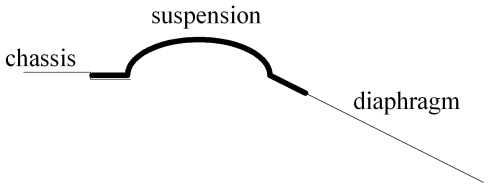

Figure 3.4: Cross section of typical single roll suspension

High levels of sound causes the compliance of the suspension to increase, after a few minutes, and again decreasing slowly when stopped. The compliance at rest position in figure 3.3 is just above 2[mm/N], whereas it is measured to be 1.17[mm/N], see appendix B.1. This is due to the fact that when measuring the linear parameters, only small input signals are applied, but when the nonlinear parameters are measured, as in figure 3.3, then high level pink noise is used in several minutes. When measuring the nonlinearities, the plots are update during the process, and here it can be seen how it slowly increases over time.

Mass and Area

When the diaphragm is moving the suspension is stretched causing a change in the diaphragm area, as shown in [Olsen and Thorborg, 1995] for single-roll suspensions, see figure 3.4. The change is due to how the suspension moves, which seems to roll and bend and will divide it into a part that moves with the diaphragm and a part that does not move. Furthermore, the changes is not necessarily the same when the diaphragm moves forward as when it moves backward.
Changes in area is proportional to changes in the mechanical mass. It can be shown that they both are well modeled with a first order polynomial expansion in x_D:

$$M_D(x_D) = \sum_{n=0}^{1} M_n x_D^n \tag{3.3}$$

Above the resonance frequency of the system the mass and area nonlinearities will to some extend self-compensate. At these frequencies the sound pressure is proportional to the ratio between the diaphragm area and mass.

Diaphragm break up

Usually the diaphragm is considered as a piston, but at high frequencies this not true. In figure 3.5 a measurement of this is seen for the driver used in the test loudspeaker. The impedance is inverted and calculated in dB, and a offset is applied so that the top at 300Hz is equal to the sensitivity on the speaker in 2π space. The sound pressure must follow the impedance if break up of the diaphragm does no happen. But already below 1kHz the sound pressure begins to differ from the impedance, which is due to break up.

As the diaphragm breaks up, the resulting response is extended to a much higher frequency than allowed by the ideal model, see (2.38). This is an advantage for the loudspeaker designer as the working range of the driver is increased, but an disadvantage when the driver must be compensated. When the diaphragm breaks up, the hole diaphragm does not necessarily move. If only a part of it moves, then both the acoustical and mechanical mass is different from the one expected, thus making it impossible to simulated the velocity of it.

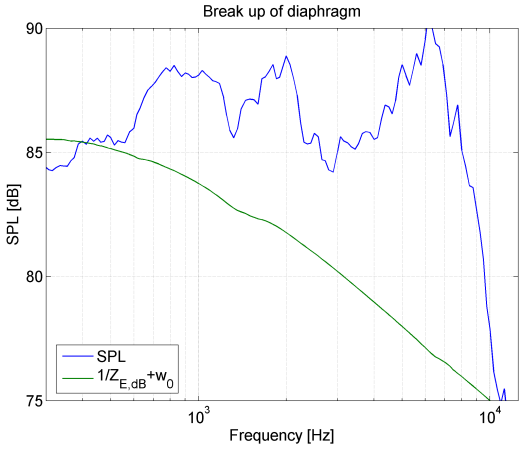

Figure 3.5: Deviation of the sound pressure compared to the inverted impedance

3.1.3 Others

Temperature

As shown in [Klippel, 2003], the increase in the voice-coil temperature ΔT_v is dependent of the music material. This is due to the fact that large low frequency signals cause convection cooling, decreasing the temperature of the coil and the magnetic system. The thermal model in figure 2.12 does not include this effect. A model that include the effect of convection cooling is found in [Klippel, 2003].

The magnet is dependent of the temperature. By increasing temperature causes reversible losses in the magnet. Heating the magnet more might causing irreversible losses, thus re-magnetizing can restore this. By increasing the temperature even more, changes in the structure on microscopic scale, that will make the magnet lose its magnetism forever, is risked; [Janssen, 2004].
Two types of magnets are typically used in loudspeakers:

- Ferrite-magnets: Strontium-ferrite, Sr Fe12 O19 (Br = 0.4 T , Hcb = 190 kA/m)
- Neodymium-magnets: NdFeB, grade N35 (Br = 1.2 T , Hcb = 876 kA/m)

Br is the flux-density inside the magnet when the magnet is inside a fully closed system (no airgap) after the magnet is fully saturated. This is a theoretical value (fully closed system has no practical uses) and is independent of the size of the magnet.
HcB is the demagnetization field strength required for the flux-density inside the magnet (in a fully closed system) to become zero. The value of the HcB depends on the Br, HcJ and the permeability of the material. HcJ is the field strength of the demagnetization field at which the polarization reaches zero. The permeability is the value which states how well the material "conducts" magnetism (this value is dependent on the applied field strength).

The grade of the magnets is not referred to anymore in this report, but when talking about magnets, the grades meant is the ones that are given.

The typically temperature range[2] for ferrite magnets is -40 to 225°C and for Neodymium it is up to 80°C. Within these ranges no irreversible losses can happen.
Unfortunately it is not as simple as this. The diameter to height ratio of the magnet influences these

[2]For the manufacture http://www.goudsmit-magnetics.nl/

range negatively, if the ratio is less than 0.7. Furthermore, the airgap also changes how the magnet reacts on temperature, but in order to conclude anything a finite element program must be used.
In this thesis irreversible loss is assumed not to happen, as it then is considered to be damaged.

The reversible losses related to the temperature can be expressed as:

- Ferrite:
  - Br: -0.2 %/°C, related at 20 °C
  - HcJ: +0.35%°C (higher temp: higher resistance to demagnetizing)
- Neodymium (only from 20 to 100 °C; the decrease by temperature is not completely linear)
  - Br: -0.11 %/°C
  - HcJ: -0.6%/°C (higher temp: lower resistance to demagnetizing)

Ageing

The degradation of the parameters throughout ageing is a topic with very high uncertain, which varies for each manufacture and even for each different transducer model of a given manufacture. This section is based on [Smidth, 2004] from Danish Sound Technology (DST).

The suspension is the worst factor in what causes the loudspeaker to change throughout time. A common rule among the loudspeaker manufacturers is that the outer suspension makes up about 20% of the common stiffness K_D and the spider (inner suspension) makes up about 80%. Sometimes it can be 10% to 90% or 30% to 70%.

Three types of materials are commonly used for the outer suspension:

- Rubber made of Styrol-Butadien basis which is an almost natural product. This is the most used material for the outer suspension, because it does not change with time.
- Gum made of Polynorbomen basis. Not used very often, because some materials evaporates with time and the gum becomes more stiff.
- Foam made of Poly-urethan on Ester basis. This material is not used very often because it starts to crumble after ten to fifteen years.

The spider is made of PAC. Its R_D value changes within the first couples of months of playing, and afterwards it stabilizes. If it is heated up, i.e. by the sun, while the diaphragm is out of its rest position, the rest position for the spider will change.
The material used by DST for the outer suspension is Rubber. This material is very soft and does not influence the stiffness much except when it is stretched out. According to [Smidth, 2004] this material does not change with time.

Variation in a batch

In a production the parameters have some variation among each driver. The variation is biggest when the transducers are new, after a couple of months when the loudspeaker is run in the variation decreases a bit. Furthermore, the resonance frequency drops with about 10% to 15% after it is run in.

According to [Janssen, 2004] there can be a variation of 15% on the magnetic properties, thus it is depending on which manufacture and the grade. Furthermore, the magnetic properties have a normal distribution when produced a batch.

According to [Smidth, 2004], the stiffness R_D of the spider can be modeled with a gaussian distribution.

The tolerances on the parameters at DST, [Smidth, 2004], is:

- R_E: +/- 0.15 ohm or +/- 2% (the maximum of the two is used)
- Bl: +/- 5%
- M_D: +/- 5%
- f_s: +/- 5% after the first couple of months (maybe up to 10% especially in many tweeters)
- SPL: max +/- 1dB (in the frequency range below the brake up of the diaphragm)

3.1.4 Analysis of importance of the nonlinearities

The parametric nonlinearities described in the present section causes distortion, see section 3.2, and therefore they must be linearized. But dependent of the given loudspeaker, and the amount of nonlinearity in each parameter, some are more convenient to linearize than others.

The three parameters, force factor, electrical inductance and the mechanical compliance, are normally assumed to be the most responsible for causing distortion.
The figures 3.1, 3.2 and 3.3 shows a need for linearizing these three parameters, as they exhibits a high nonlinearity with respect to x_D.
Due to the behavior of the suspension, the movement of the diaphragm exhibits a hysteretic movement. In order to remove this problem a memory model is needed, and is thus not included in the compensation algorithm. Furthermore, it has not been possible to measure the effect, as such equipment was not available.
Furthermore, if the physical limit in the suspension is linearized, a limit must be added in order not to brake the loudspeaker.

According to [Olsen and Thorborg, 1995], The changes in mass and area will to some extend be self-compensating above the resonance frequency. Of this reason the mass and area are not dealt with further in this report.

The magnetic attraction force is the most simple one, as the amount of force is not related to a specific loudspeaker. As it only influences the distortion very little, it is not dealt with in this report.

Changes in the temperature changes the electric resistance. This leads to a decreased sensitivity, an increase in the resonance frequency f_s and a higher total quality factor Q_{TS}, see 3.2.1. The temperature change in the voice-coil must be dealt with. Notice, due to the fact that the temperature varies very slow, a feedback control would automatically measure the electric resistance to the given temperature. The temperature is then not to be considered; though in a feedforward control it must be included.
The temperature change in the magnetic circuit is much less than in the voice-coil, and it is not dealt with any further, because it is assumed that the force factor only will vary very little of this reason. Notice, in car hifi this would be different due the large variations in the ambient temperature, which also would change the compliance in the suspension.

Ageing of the loudspeaker is very dependent of material and how it is treated during its lifetime, as written in section 3.1.3. If the right materials are used, after the first couple of months the parameters will only change a bit. If a feedback control is used these changes are automatically handled. In a feedforward control it is not possible to deal with these changes as no model can be derived.

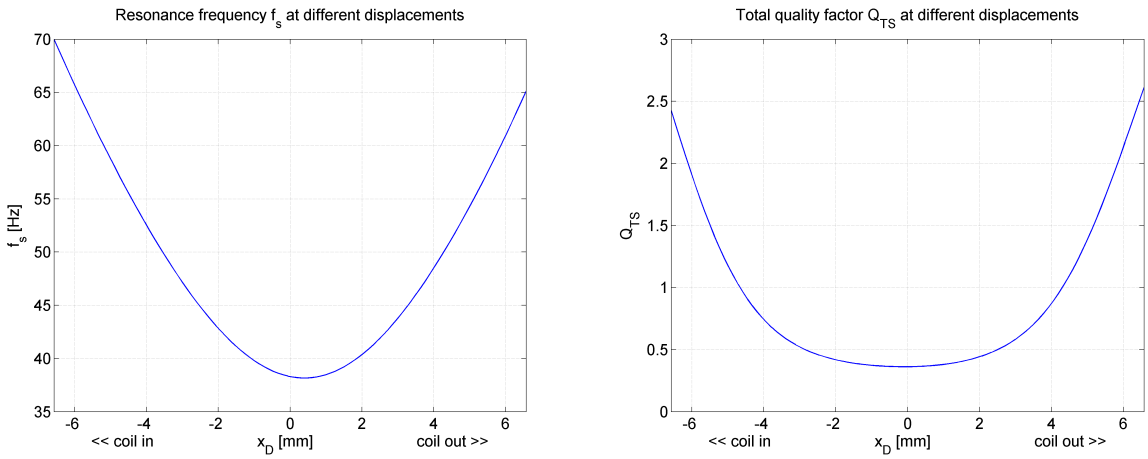

(a) (b)

Figure 3.6: (a) Resonance frequency f_s and (b) quality factor Q_{TS}, at different displacements

3.2 Evaluation of nonlinear loudspeakers

In this section the effects caused by the nonlinearities are evaluated, by measurement of the test loudspeaker and by using the nonlinear plant model derived later in section 5.3; the results of the nonlinear plant model is also evaluated in that section. Only measurements and simulation for the vented box loudspeaker are presented.

3.2.1 Variation in filter characteristic

The resonance frequency (2.8) and quality factor (2.9) for the driver in free air, are affected by the varying compliance and force factor. In figure 3.6 this is seen, where both have been plotted with respect to the displacement. This leads to a transfer function which changes according to the displacement.
In the following, the consequences of this is investigated and plots of the vented box loudspeaker are showed. Furthermore, the effect of changing temperature and varying inductance is investigated.
In figure 3.7 the normalized transfer function is plotted for different levels. As seen, not much happens between a power of 0.1W and 1W on the input. But at 3W and even 5W, the curve starts to peak, indicating an increasing quality factor. Furthermore, the lower -3dB cutoff frequency is increased.

3.2.2 DC offset

Equipment for measuring the DC offset on the loudspeaker has not been available, and thus it must be simulated. In figure 3.8 such a simulation is seen. As seen only very little DC offset is occurring 0.3mm as maximum value. Notice, this simulation is not considered to be true, as it is too small compared to that shown in literature, [Klippel, 2001]. As seen in the paper by Klippel, his simulations were also doubtful when comparing with his measurement. The reason why the DC offset is difficult to simulate, might be that the hysteresis exhibited in the suspension is not included in the plant model.

3.2.3 Total harmonic distortion and Intermodulation distortion

In figure 3.9(a) measurements of the total harmonic distortion is seen. Here the five first harmonics are used. As seen, the THD is high at low frequencies and low at high frequencies. This is what is expected due to the displacement transfer function, which is a low-pass filter. Furthermore, at high levels around

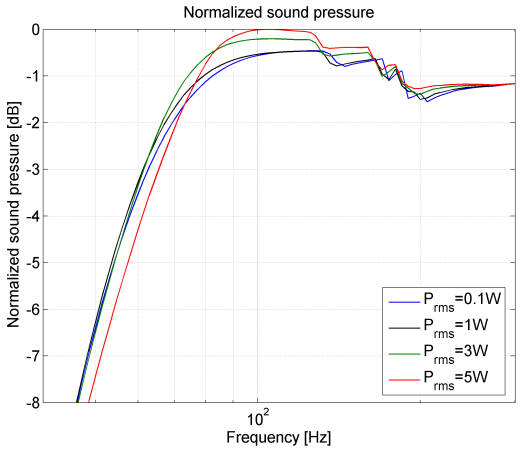

Figure 3.7: Normalized SPL at low frequencies, measured inside box

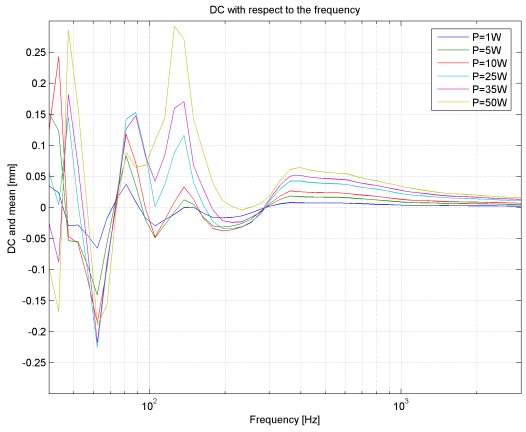

Figure 3.8: DC in diaphragm displacement at different driving levels

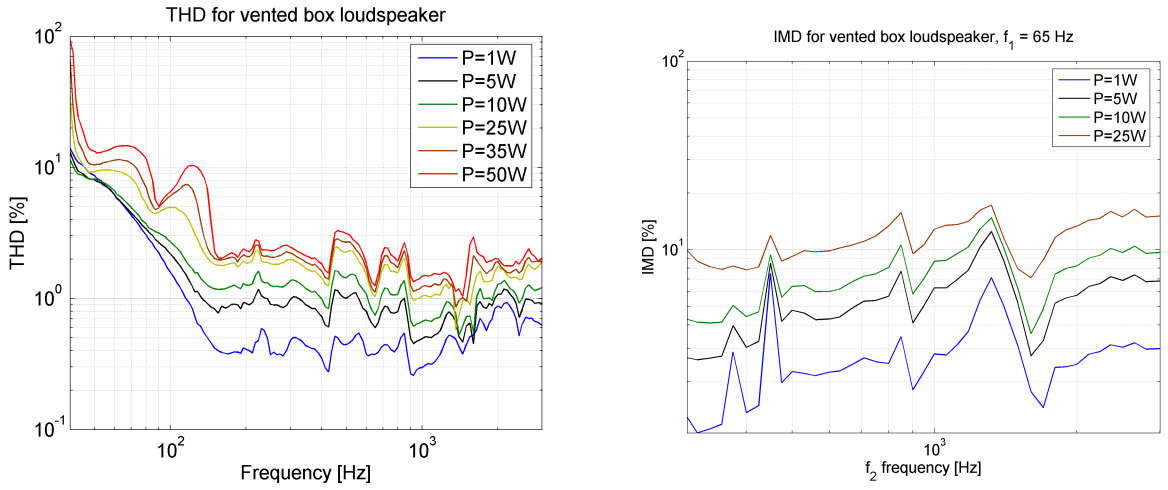

(a) (b)

Figure 3.9: (a) Total harmonic distortion (b) Intermodulation distortion

the Helmholtz frequency, $f_B = 51$Hz, a dip in the curve is seen, which is due to the fact that the diaphragm hardly moves. furthermore, at a multiple of f_B a small dip is seen at very high displacements.
In figure 3.9(b) measurements of the intermodulation distortion is seen. Here the three first harmonics on each side of the high frequency tone is used. As seen, the distortion is increasing slightly towards higher frequencies. This is due to the inductance shown below.
In the following three figure **??**, **??** and **??**, simulations have been done with the plant model, where only one nonlinearity is included in each. As seen, the force factor and suspension compliance contributes a lot to the THD distortion, while the inductance only has a minor influence. This is due to the fact that the resistance is the most dominating component in the electrical impedance at low frequencies. At high frequencies where the inductance is the most dominant, the diaphragm only moves very little and only little distortion is resulted.
In the following three figure 3.13, 3.14 and 3.15 similar simulations have been done, but now with respect to the intermodulation. Now the suspension compliance is the one that contributes very little to the distortion, while the two others contributes much. As seen, the inductance result in the increasing distortion, which is due to the fact that it becomes more and more dominant in the electrical impedance at higher frequencies.

3.2.4 Summary

The following list sums up which distortion effects occurring at high levels:

- At large signal levels, filter characteristic of loudspeaker changes.
- A frequency DC offset occurring on the diaphragm.
- Nonlinear force faction causes high THD distortion at low frequencies and high IMD distortion at all frequencies.
- Nonlinear suspension compliance causes high THD distortion at low frequencies.
- Nonlinear voice-coil inductance causes high IMD distortion increasing towards higher frequencies.

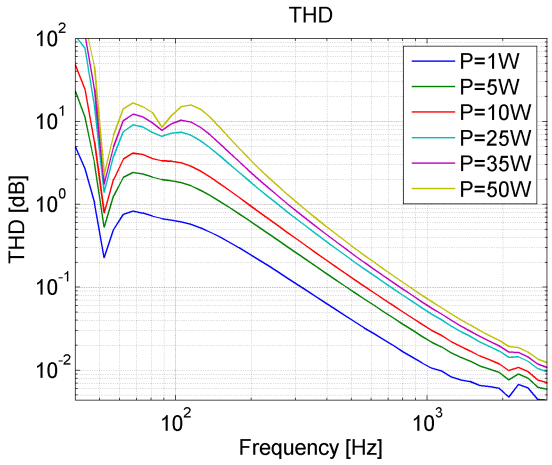

Figure 3.10: Simulated total harmonic distortion, only Bl nonlinearity

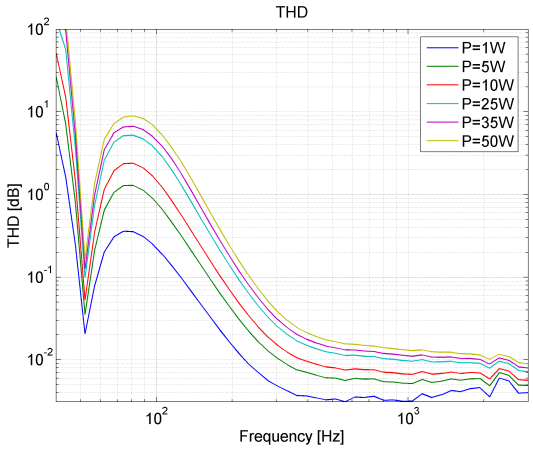

Figure 3.11: Simulated total harmonic distortion, only C_D nonlinearity

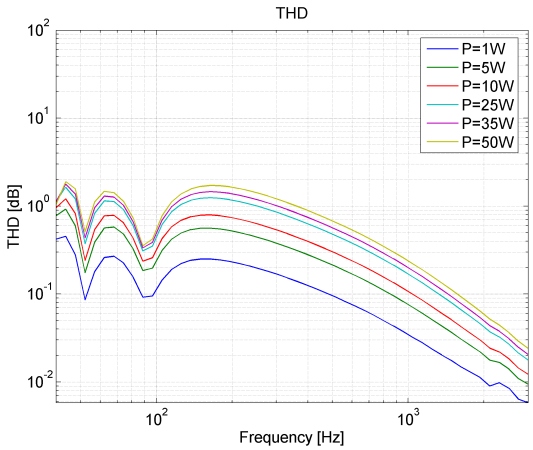

Figure 3.12: Simulated total harmonic distortion, only L_E nonlinearity

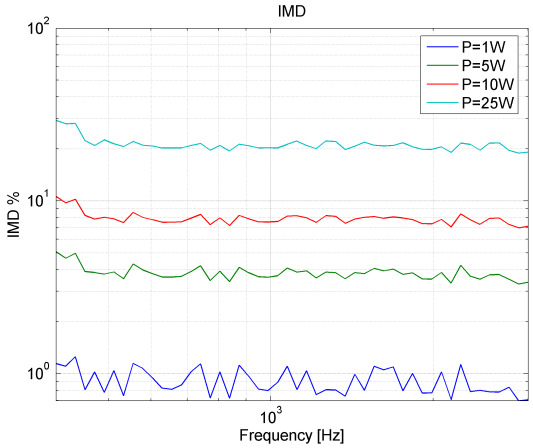

Figure 3.13: Simulated intermodulation distortion, only Bl nonlinearity

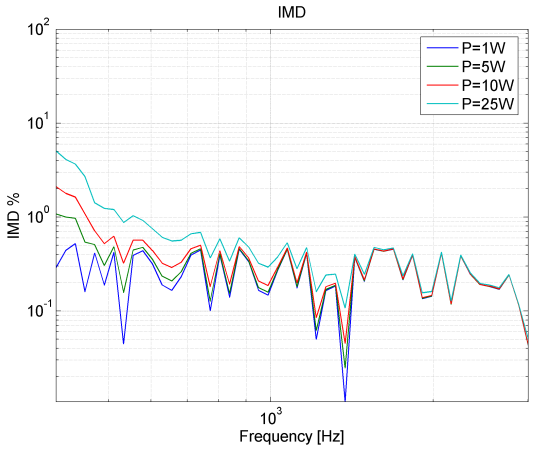

Figure 3.14: Simulated intermodulation distortion, only C_D nonlinearity

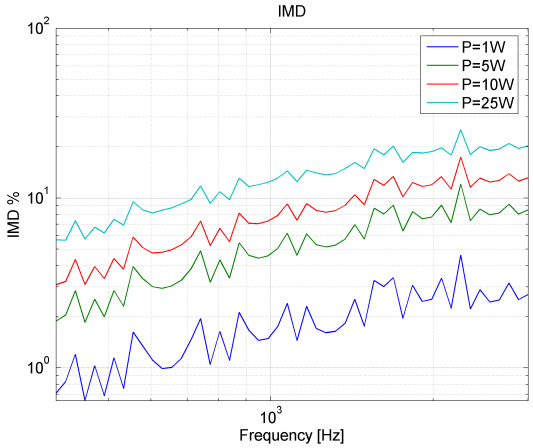

Figure 3.15: Simulated intermodulation distortion, only L_E nonlinearity

Chapter 4

Modeling of nonlinearities

In this chapter, the nonlinear parameter chosen in section 3.1.4 are modeled with respect to the displacement. The nonlinear parameters are:

- Force factor $Bl(x_D)$
- Coil inductance $L_E(x_D)$
- Suspension compliance $C_D(x_D)$

The coefficients found for the mathematical model in the present chapter are listed in appendix B.2.

4.1 Least Squares

The least squares method is used for fitting functions to the nonlinear parameters, and thus will be derived first, [Weisstein, 1].

Given some measured data for a function to be fitted to:

$$\{x_{D,i} = [x_{D,1}, \cdots, x_{D,N_i}]^T, y_i = [y_1, \cdots, y_{N_i}]^T\} \tag{4.1}$$

where N_i is total amount of measurement points, $x_{D,i}$ is the i'th displacement measurement and y_i is the target at input $x_{D,i}$.
The estimated result can be calculated from the basis-function:

$$\hat{y}(x_D) = \sum_{l=0}^{N_l} \omega_l f_l(x_D) = \boldsymbol{f}(x_D)\boldsymbol{\omega} \tag{4.2}$$

where ω is the coefficients of the linear network, f_l is an arbitrary function used to fit, and N_l is the order of the fitting function; $l = 0$ is often used as DC offset. The coefficients are found hereafter.
The sum of squares of the error is the cost function:

$$S(\boldsymbol{\omega}) = \sum_{i=1}^{N_i} (y_i - \boldsymbol{f}(x_{D,i})\boldsymbol{\omega})^2 = (\boldsymbol{y} - \boldsymbol{F\omega})^T(\boldsymbol{y} - \boldsymbol{F\omega}) \tag{4.3}$$

The cost function describes how well the data is fitted and in order to get an optimal fit, it must be minimized with respect to the coefficients:

$$S(\boldsymbol{\omega}) = \arg\min_{\boldsymbol{\omega}}[(\boldsymbol{y} - \boldsymbol{F\omega})^T(\boldsymbol{y} - \boldsymbol{F\omega})] \tag{4.4}$$

The solution is that the gradient of the cost function is 0:

$$\frac{\partial S(\boldsymbol{\omega})}{\partial \boldsymbol{\omega}} = 0 \;\leftrightarrow\; 2\boldsymbol{F}^T\boldsymbol{F}\boldsymbol{\omega} - 2\boldsymbol{F}^T\boldsymbol{y} = 0 \tag{4.5}$$

And at last the Least squares solution

$$\boldsymbol{\omega} = (\boldsymbol{F}^T\boldsymbol{F})^{-1}\boldsymbol{F}^T\boldsymbol{y} \tag{4.6}$$

4.2 Polynomial fit

Polynomial fitting is very popular when modeling the nonlinear parameters in a loudspeaker; [Klippel, 1992b], [Bright, 2002] and [Schurer, 1997] are some among many which use this method.
Using Least squares, as described above, to fit a polynomial involves inserting the polynomial function into f_l from (4.2):

$$f_l(x_D) = x_D^l \tag{4.7}$$

And the coefficients are then found by solving (4.6); see [Weisstein, 2].
In order to find the most optimal order of the polynomial, the order has been varied over several simulations and the sum of squares error is calculated for a comparison as seen in figure 4.1(a). Here the force factor data is fitted. It can be seen that equal orders of the polynomial gives the best result, as the cost is reduced much from an unequal order to an one step higher equal order, but only little when it is vice versa. It is because of the shape of the data, which is like a negative parable (both slopes falls towards minus infinity).
Fitting to the inverse of the data $1/y_i$ is sometimes better, as seen at figure 4.1(b), [Bright, 2002]. It is seen the that an optimal fit is achieved at the order equal to four, and by then, drops off much fast. It results in a better fit and fewer calculations, because of the smaller polynomial order. Furthermore, outside the data range of y_i, the polynomial sometimes drops off to zero much more smoothly, when fitting to the inverse data; it will be shown just below.
When fitting to the inverse, the basis function in (4.2) is rewritten as:

$$\hat{y}(x_D) = \frac{1}{\boldsymbol{f}(x_D)\boldsymbol{\omega}} \tag{4.8}$$

Force factor $Bl(x_D)$

In figure 4.2(a) an eight order polynomial is fitted to the force factor data is seen. Within the data range of $Bl(x_D)$, the fit is good, but outside the polynomial becomes negative, and by then, the polynomial is useless outside of $Bl(x_D)$.
A fourth order polynomial fitted to the inverse data is seen in figure 4.2(b). Besides a lower sum of squares error, the curve behaves much more realistic outside of the data range of $Bl(x_D)$.

Suspension compliance $C_D(x_D)$

As for the force factor the same procedure has been done for the compliance of the suspension. Again the optimal order of polynomial that is found is eight for a normal fit and eight for a fit on the inverse data. The result is seen in figures 4.3(a) and 4.3(b). The same conclusions can be made as for the force factor.

Coil inductance $L_E(x_D)$

Because of the shape of the coil inductance, two things result in a fit different form both the force factor and the suspension compliance. First, the shape is no longer approximately like a parable, which is fitted well with a equally order polynomial. But instead like an s-shape where an unequally polynomial fits

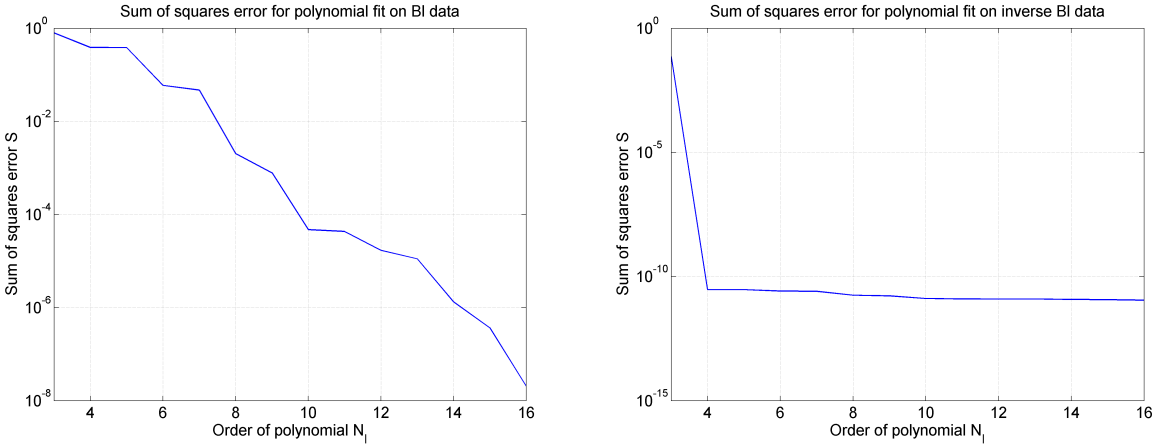

(a) Fit on data

(b) Fit on inverted data

Figure 4.1: Fit on data

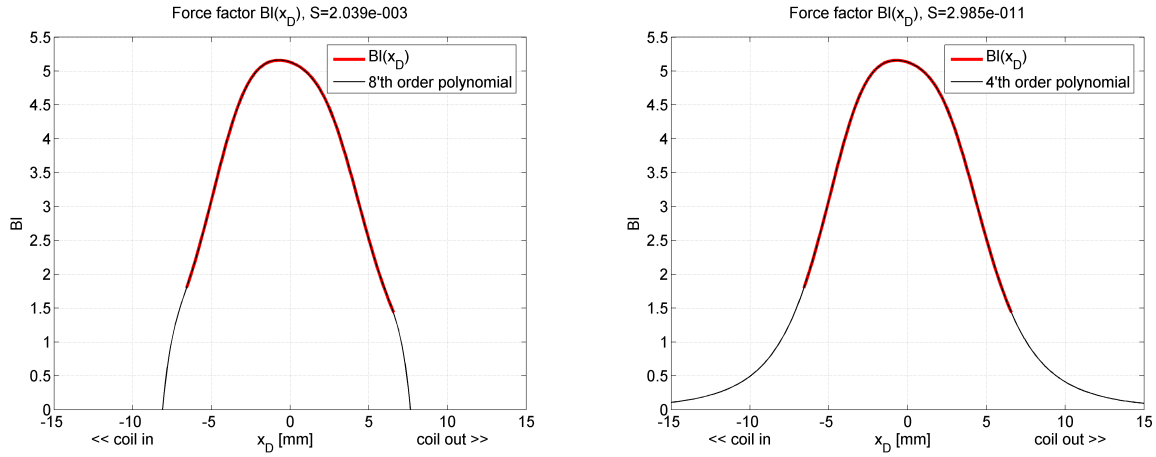

(a) Fit on data

(b) Fit on inverted data

Figure 4.2: Polynomial fit on force factor data data

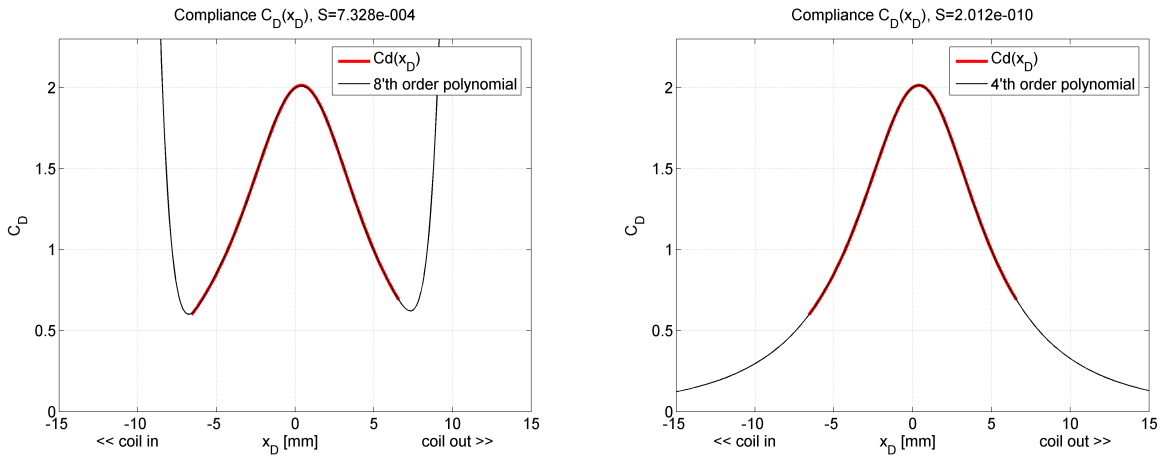

(a) Fit on data

(b) Fit on inverted data

Figure 4.3: Polynomial fit on force factor data data

better. Second, fitting to the inverse data only worsen the behavior outside of $L_E(x_D)$. At figure 4.4(a) and 4.4(b) the results are seen; seven orders polynomials have been used for both fits. It is seen that the normal fit gives the lowest sum of squares error and the that they both behaves poorly outside of $L_E(x_D)$.

4.3 Exponential fit

The use of exponential functions to model the nonlinear parameters have not been done before in this type of application. The advantage of the exponential functions, is that their behavior outside the data range of y_i can be affected to be more optimal.
Again, using Least squares as described above to fit the exponential functions involves inserting them into f_l from (4.2):

$$f_l(x_D) = \exp^{-\frac{1}{2\sigma_l^2}(x_D - x_l)^2} \qquad f_0(x_D) = 1 \tag{4.9}$$

where σ is the standard deviation for each function, x_l is the center of each them and f_0 can be used as offset if wanted. The coefficients are again found by solving (4.6).
In order to do the most optimal fit with the exponential kernels, four things must be clear:

- Number of kernels used
- Distribution of kernel centers
- Standard deviation for exponentials
- Least squares coefficients (heights of exponentials)

The number of kernels used, is estimated in same manner as for the order of the polynomials. The distribution is in this thesis always linear within a range found to be the most optimal.
The standard deviation is also estimated over a given range and evaluated with respect to the sum of squares error. At last the coefficients are found with the Least squares solution (4.6).
In figure 4.5(a) the sum of squares error with respect to the number of kernels is seen. Here is the optimal standard deviation for each number of N_l is used; the force factor data is used.
In figure 4.5(b) the sum of squares error is seen again, but here the number of kernels is fixed at seven and the standard deviation is varied. It is seen that around the optimal value only very little happens,

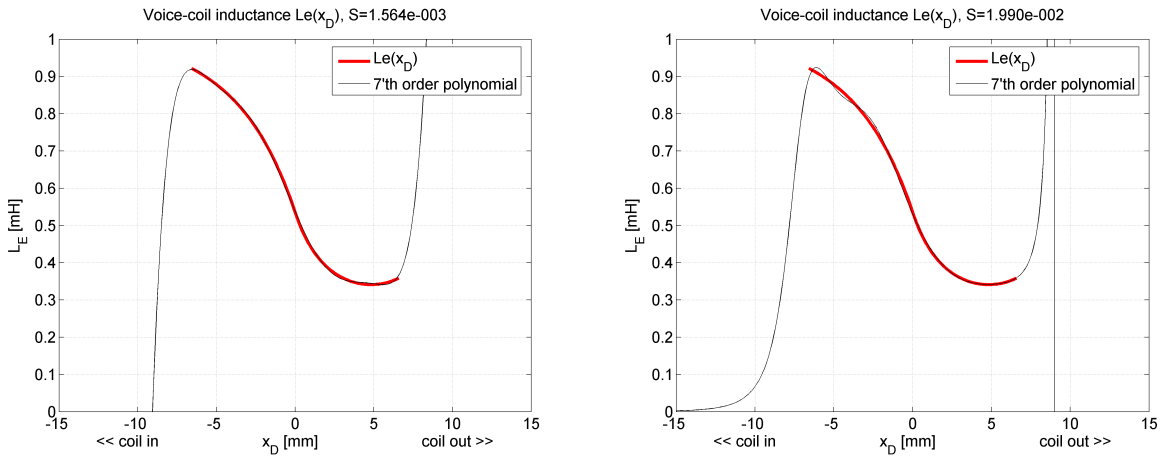

(a) Fit on data

(b) Fit on inverted data

Figure 4.4: Polynomial fit on force factor data data

meaning that the sum of squares error only changes a bit if the standard deviation were varied between two, three or four.
If the standard deviation is to small as in figure 4.6(a), then the exponentials becomes too narrow, which results in a curve with ripple. But if it is too high, then the fit within the data range y_i is good, but outside of the range, problems like the ones with the polynomial fit occurs, as seen in figure 4.6(b).
The solution to these two problems, is to choose a optimal value between the two.

Force factor $Bl(x_D)$

In figure 4.7 the resulting fit with exponential kernels on the force factor data is seen. And as seen, the fit is good both inside and outside the data range of $Bl(x_D)$.

Suspension compliance $C_D(x_D)$

The resulting fit with exponential kernels on the compliance of the suspension data is seen in figure 4.8. And as seen, the fit is good both inside and outside the data range of $Cd(x_D)$.

Coil inductance $L_E(x_D)$

Finally the fit on the coil inductance is shown in figure 4.9. Here an offset has been manually set equal to $L_E(0)$. Again it is seen that a good result can be achieved both inside and outside the data range of $L_E(x_D)$.

4.4 Alternative functions

As seen above, the method for exponential fitting, resulted in fits that behave more appropriate outside of the measured data range. But the fit on the voice-coil inductance, settling at the level equal to the one at $x_D = 0$, is not the most optimal. Instead a 's'-function is better as it remains high and low in each of the ends.

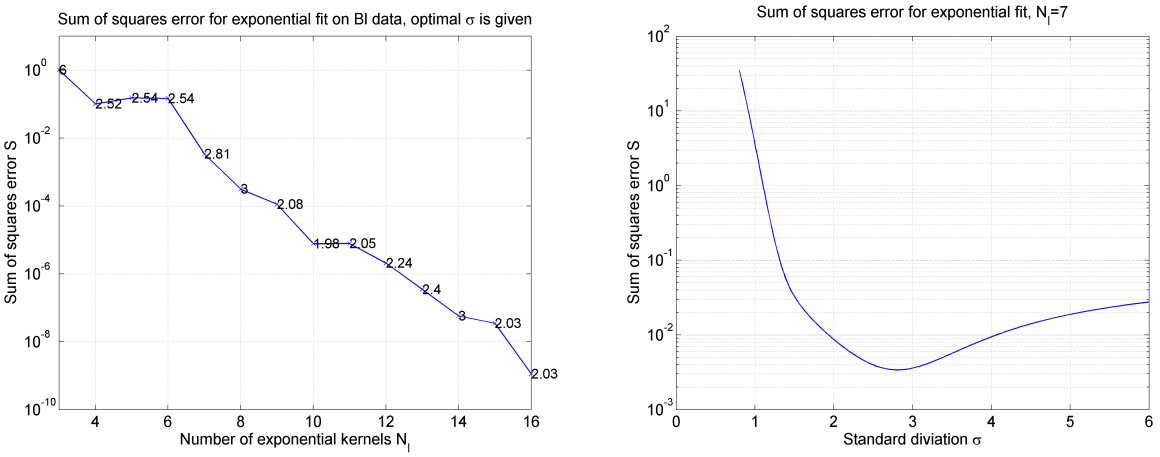

(a) (b)

Figure 4.5: Sum of squares error

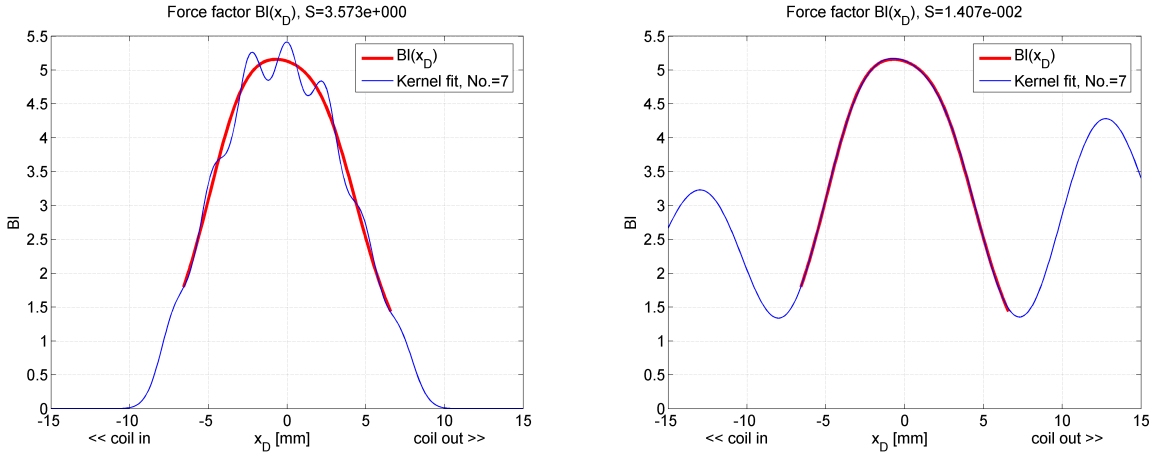

(a) (b)

Figure 4.6: Bad fits, (a) $\sigma_l = 1$, (b) $\sigma_l = 4.5$

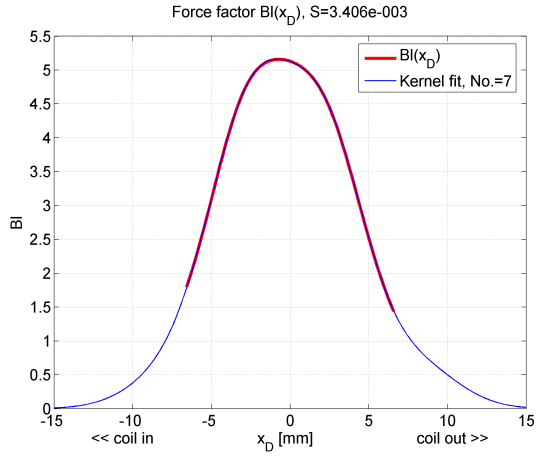

Figure 4.7: $\sigma = 2.81$, range of centers $\{-7\text{mm}; 7\text{mm}\}$, no offset

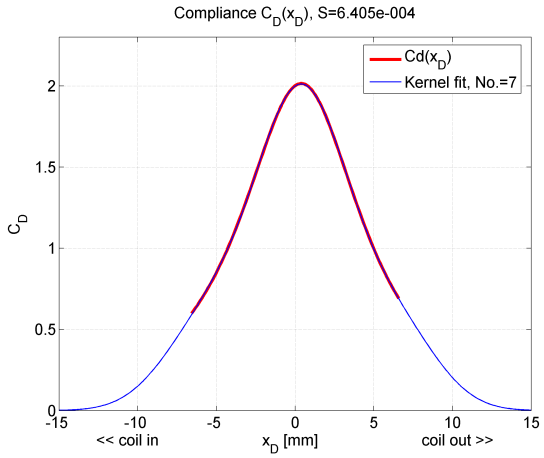

Figure 4.8: $\sigma = 2.55$, range of centers $\{-7\text{mm}; 7\text{mm}\}$, no offset

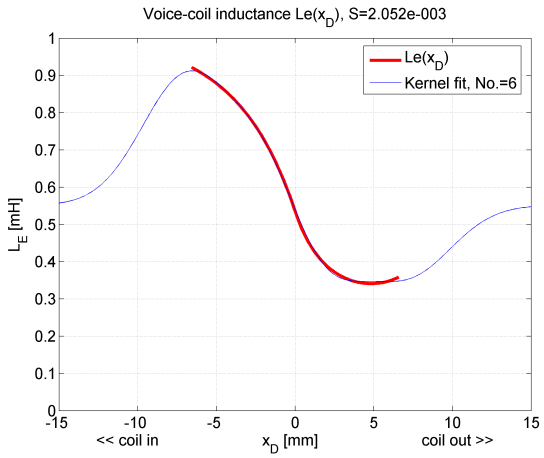

Figure 4.9: $\sigma = 3$, range of centers $\{-6\text{mm}; 6\text{mm}\}$, offset equal to $Bl(0)$

It has been found that the sigmoid function works well [Bishop, 2000][1]:

$$sigmoid(x) = \frac{1}{1+\exp^{-x}} \tag{4.10}$$

It can be shown that this function is the same as a tanh function, but with an offset so it is positive. Of that reason it is more convenient to use the sigmoid function, as the inductance is always positive. Now, adding an offset ω_0, a scalar ω_1 and two variables, one to change the slope of the 's'-function a and one to move is sideways x_0:

$$f(x_D) = \omega_1 \frac{1}{1+\exp^{-(x_D-x_0)a}} + \omega_0 \tag{4.11}$$

This function can not be fitted in one step, as the variable can not be separated and isolated, as above, thus we need a iterative process, [Weisstein, 3].
The error of the present fit is given by:

$$d\beta = y_i - f(x_i; \omega_0, \omega_1, x_0, a) = \boldsymbol{y} - \boldsymbol{f}(\omega_0, \omega_1, x_0, a) \tag{4.12}$$

where $\boldsymbol{y}$ is the measured data. Now obtaining a linearized estimate for the changes $d\lambda_j$ needed to reduce $d\beta_i$ to 0:

$$d\beta_i = \sum_{j=1}^{n} \frac{\partial f}{\partial \lambda_j} d\lambda_j \bigg|_{x_i, \boldsymbol{\lambda}} \tag{4.13}$$

for $i = 1, \ldots, m$, where $\lambda \equiv (\omega_0, \omega_1, x_0, a)$. Written in component form it is given by:

$$d\beta_i = A_{ij} d\lambda_j \tag{4.14}$$

The derivatives used to constructed matrix $\boldsymbol{A}$ are:

$$\begin{aligned}
\frac{\partial f}{\partial \omega_0} &= 1 \\
\frac{\partial f}{\partial \omega_1} &= \frac{1}{1+\exp^{-(x_D-x_0)a}} \\
\frac{\partial f}{\partial x_0} &= -\frac{\omega_1 a \exp^{-(x_D-x_0)a}}{\left(1+\exp^{-(x_D-x_0)a}\right)^2} \\
\frac{\partial f}{\partial a} &= -\frac{\omega_1 \left(-x_D+x_0\right) \exp^{-(x_D-x_0)a}}{\left(1+\exp^{-(x_D-x_0)a}\right)^2}
\end{aligned} \tag{4.15}$$

Writing (4.14) in matrix form gives:

$$\boldsymbol{A} d\boldsymbol{\lambda} = d\boldsymbol{\beta} \tag{4.16}$$

and solving it with respect to $d\boldsymbol{\lambda}$:

$$d\boldsymbol{\lambda} = (\boldsymbol{A}^T \boldsymbol{A})^{-1} \boldsymbol{A}^T \boldsymbol{\beta} \tag{4.17}$$

$d\boldsymbol{\lambda}$ is then added to $\boldsymbol{\lambda}$, and the procedure is repeated until the error is minimized.

In figure 4.10(a) each iteration in fitting the inductance data is seen. Despite the naive guess, $\omega_0 = 1$, $\omega_1 = -1$, $x_0 = 0$ and $a = 0.5$ only four iterations are needed for the coefficients to be minimized. The final result is seen in figure 4.10(b), as seen, the sigmoid function fits well. Though in each end it can be seen that it does not follow the data completely, but it is still considered a better choice compared to the results with the polynomial and exponential.

[1] page 82

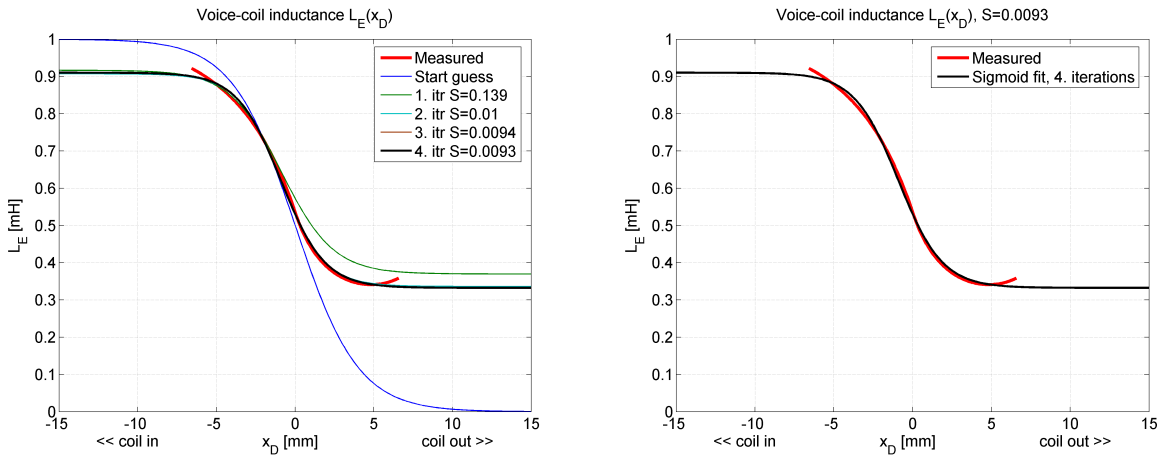

(a) (b)

Figure 4.10: Fit on inductance data with sigmoid function, (a) iterations in fit, (b) final result

If wanted, the fit can be improved by using a sum of sigmoid functions. In that case, the form of the equation is similar to the one of a neural network. Later the continuous time differential equations in chapter 2 are converted into discrete difference equations. In that case, if the three nonlinearities are fitted with sigmoid functions, then it might be possible to write the complete equation for a loudspeaker as a neural network. This has not been done in this thesis, but it could be a very interesting topic in future work.

4.5 Fitting models with soft clipping

In order not to damage the loudspeaker when linearized, some kind of soft clipping must be added. This means that a limit must added to the displacement, but in an appropriate way, such that the de-acceleration near the limit, is low.
Here an idea is presented, but because of to lack of time, further investigations has not been possible.

If a fit to one of the three nonlinearities, force factor, suspension compliance and inductance, could be used in order to not only model the nonlinearity, but also include some soft clipping, as no extra circuit then has to be included to do the soft clipping.
As the force factor alone connects the electrical circuit with mechanical, it is the most optimal one. Looking at the fit in figure 4.7, it can be seen that the force factor decreases when moving away from the rest position, causing a need for increasing voltage for the diaphragm to remain its velocity. If instead the linearizing system was "told" that the force factor instead is increasing close to the wanted limit, then a lower voltage would be applied, breaking and limiting the diaphragm.
Such a function must be found, though it is not done in here.

4.6 Summary

The polynomial fit has been shown to be good within the given data range, but very poor outside. Furthermore, as stated in section 3.1.2, the offset of the compliance change during operation. If using the fit found in figure 4.3(a), and the compliance offset changes to the value found in the linear measurement $C_D = 1.17$, then the polynomial would becomes as in figure 4.11. Here a part of the curve, within the

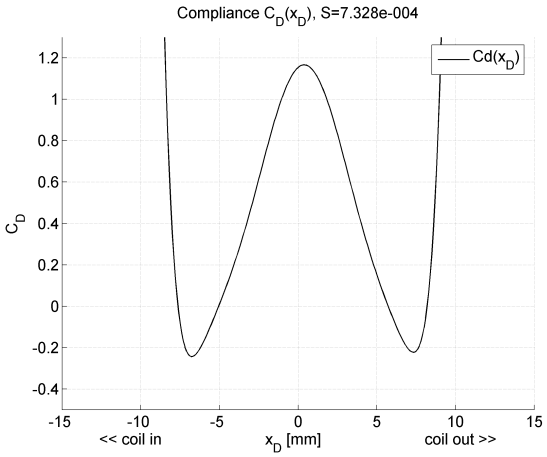

Figure 4.11: Polynomial fit on compliance data, where only offset is changed

measured range, becomes 0. This is fatal, and causes an unstable controller, which would not have happen with the exponential fit; which may add distortion, but it does not become unstable.

Of course this does not conclude that it is not possible avoid such errors. It just shows that it can be a problem if not taken care of, as in [Bright, 2002]; He only updates offset in the polynomial, the rest is fitted before applying the controller.

In this thesis, exponential fitting is used for the force factor and compliance, and the sigmoid function is used for the inductance.

Chapter 5

Discrete nonlinear simulation

Despite that transducer control systems are implemented in a discrete time environment such as a DSP-processor, so far all systems have been derived in continuous time, see [Schurer, 1997] [Klippel, 1992a] and many others, with the exception of [Bright, 2002]. Hans Schurer's solution is to simulate the continuous time system in discrete time by integrating over small time steps. Wolfgang Klippel does not come up with a solution in his papers, but it is assumed that he has a solution, taking in mind of his analyzer system, which implements many of the topics considered in this thesis. Andrew Bright is the only one that have derived the control system directly in discrete time, but his methods are simplified and do not meet the requirements about which nonlinearities that must be compensated, put up in section 3.1.4.
In this thesis all control systems have been derived in discrete time, as it is considered as the most correct method.

In this chapter the continuous time differential equations, from chapter 2, are transformed into corresponding discrete time difference equations. From these difference equations, standard digital filter that are used more than once times in this thesis, are derived.
Later the difference equations are rewritten as a state space model. This model is ideal for computer simulations in the time domain. And finally a toolbox developed during this thesis, is described.

5.1 Discrete representation of differential equations

The discrete time difference equation corresponds to the continues time differential equation. A transformation from one to another most be done.

Looking at the difference equations in the z domain and at the differential equations in the laplace s domain, then the relation is $z = e^{sT_s}$. For a first order filter using this relationship, the result would be:

$$H(s) = \frac{1}{s - p_1} \quad \Rightarrow \quad H(z) = \frac{1}{(1/T_s)ln(z) - p_1} \tag{5.1}$$

Unfortunately the transfer function in the z domain, can not be converted into a difference equation. So some other approach is needed.
Several methods for converting the continuous time differential equations into discrete time exists, such as:

- Impulse invariant technique
- Bilinear transform
- Forward Euler method

where the two first are given in [Denbigh, 1998][1] and the third is found in [Spiegel and Liu, 1999][2]. At low frequencies all three techniques give good results, but near the sample frequency f_s the results differ a great amount and each different from the true analog. Of this reason, the minimum sample frequency must be decided in order to have a wanted frequency range, where the discrete time equations give equivalent results to the continues time equations.

Impulse invariance

The impulse invariance technique performs a discrete time sampling of the impulse response of the continuous time system. This requires a conversion of polynomial ratio in s to a partial fraction expansion, from which the impulse response in continues time may be found by inverse Laplace transform. The discrete time sampling of the impulse response is then z transformed. The conversion from the partial fraction expansion in s domain to z domain can be written as:

$$\frac{r_1}{s-p_1}+\frac{r_2}{s-p_2}\ldots \rightarrow T_s\frac{r_1}{1-e^{p_1T_s}z^{-1}}+T_s\frac{r_2}{1-e^{p_2T_s}z^{-1}}\ldots \tag{5.2}$$

where p_i are the poles and r_i is the numerator coefficient of the partial fraction expansion. The resulting partial fraction in z domain may be rewritten as a standard digital filter.

With this method a filter is first created in continuous time and then transformed into discrete time. But what is wanted is, to transform the differential equations into discrete time and then rewrite them to some filters. The reason for this is that it is easier to deal with when creating a state space model of the system as in section 5.3. For this reason this is method is considered unsuitable for the applications in this thesis.

Bilinear transform

As quoted earlier, using the relationship $z=e^{sT_s}$ results in z transfer function that can not be converted into a difference equation. The bilinear transform modifies $H(s)$ into a new function $H(s')$ which has a different, but similar, frequency response and which gives a result with the relationship $z=e^{s'T_s}$ that can be converted into a difference equation.
By replacing s with $2f_stanh(s'/2f_s)$ a similar frequency response is achieved in most of the frequency range. But moving close to the frequencies $s=s'=i\cdot f_s/2$, where i is an integer, $H(s')$ begins to differ from $H(s)$ and at the frequencies $H(s')$ is singular.
Finally, using the relationship $z=e^{s'T_s}$, results in:

$$s\rightarrow 2f_s\frac{1-z^{-1}}{1+z^{-1}} \tag{5.3}$$

As seen, a difference equation is now achieved. Furthermore, this technique will increase the order of the converted filter, unless the nominator and denominator has equally orders; the one with the lowest order will increase to become of equally order to the other. Of this reason, this method increases the complexity of the differential equations (2.1) and (2.5), and furthermore, this will lead to an increased number of necessary states in the state-space model derived later in section 5.3.

The bilinear technique has the advantage that if used to transform a low-pas filter as i.e. (5.1), the singularities become zeroes in the transfer function and aliasing effects are removed. As the transducer has the properties that its transfer function for the displacement is a low-pass function and the sound pressure is a band-pass function, a transformation from continuous time to discrete time is done without aliasing.

[1] page 403-411
[2] page 225

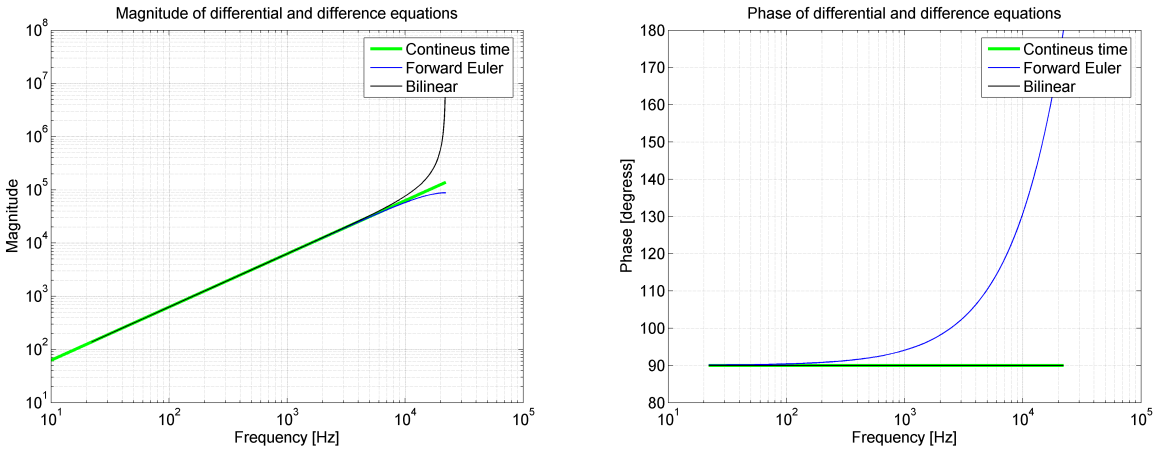

(a) (b)

Figure 5.1: Transfer function of discrete derivatives, $f_s = 48$kHz, (a) magnitude, (b) phase

On the other hand, the sample frequency must be high enough to leave the pass-band of the filter unchanged.

In figure 5.1 the magnitude and phase for a continuous time differential equation and its bilinear transform is seen, as in (5.3); here the sample frequency is 48kHz. The phase is equal to the phase of the continuous time differential equation for all frequencies. For the magnitude the discrete time result is close to the continuous time result up to about 10kHz, above it differs because of the singularity.

Forward Euler method

Of the three methods, the forward Euler method is the simplest and most straightforward method. The principle is to rewrite the differential equation as a expansion series and then approximate it. The expansion series is written as:

$$y(t+T) - y(t) = \frac{dy(t)}{dt}T + \frac{d^2y(t)}{dt^2}\frac{T^2}{2} + \ldots + \frac{d^ny(t)}{dt^n}\frac{T^n}{n!} + o(T^n) \tag{5.4}$$

where y is the function that is about to be differentiated and T is a small time step. By removing all higher order differentials and putting T equal to the sample time T_s, the expansion series is approximated to something that is identical to a discrete difference equation:

$$\frac{dy(t)}{dt} \approx \frac{1}{T_s}(y(t+T_s) - y(t)) \equiv \frac{1}{T_s}(y(n+1) - y(n)) \tag{5.5}$$

Or described by Laplace transformation and the z transformation:

$$s \to \frac{1}{T_s}(z-1) \tag{5.6}$$

where n is the discrete time number. The magnitude and phase response of the continues time differential equation compared with its discrete time version, where the forward Euler method has been used, is seen in figure 5.1. As seen, the magnitude response agrees well with the true response, only at half the sample frequency it differs a bit. Furthermore, it is seen that it performs better that the bilinear transform.
The phase response is plotted in figure 5.1(b), and as seen, the phase error increases when moving towards

the half of the sample frequency. Of this reason, the lowest sample frequency that is allowed must be decided in order to make the discrete time model fit well to the continues time model. If a second order differential where converted, the phase error would be twice as big, and therefore the minimum allowed sample frequency must be decided from the response of each of the two compensator systems dealt with in this thesis.
But as the loudspeaker model describing the true loudspeaker is unprecise near its higher frequencies, the sample frequency is not a problem. First, as the diaphragm is breaking up at relatively low frequencies compared to its actual working range, the model is probably unprecise above 1kHz as its does not model this effect, see section 3.1.2. Second, the eddy currents that changes the impedance at towards higher frequencies, is also not included in the model, causing it to be even more un-precise. Of these two reasons, compensation of distortion above 1kHz is not be achieved.
Third, the application, in this thesis, is hifi systems, where the sample frequency normally is 44.1kHz. With this frequency, the phase is small at 1kHz some multiple of this (harmonics), and the sample frequency is considered to be high enough.
Other applications or even other drivers, this might be different, and more optimal sample frequency must be found. This must e done with simulation of the complete system, with compensation, as the phase error is different for different systems.
The forward Euler method is used throughout this thesis, because it is the most simple, both in terms of deriving the equations and in terms that it does not increase the order of the system as the bilinear transform does.

5.1.1 Discrete difference

Now the technique, for converting the continuous time system into discrete time, has been derived, and conversion must be done. Furthermore, the nonlinearities picked in section 3.1.4 are added.

The voltage equation (2.1) becomes:

$$\begin{aligned} u(n) \;=\; & R_E i_c(n) + L_E(x_D(n))\frac{1}{T_s}\left(i_c(n+1) - i_c(n)\right) + i_c(n)\frac{dL_E(x_D(n))}{dx_D(n)}\frac{1}{T_s}\left(x_D(n+1) - x_D(n)\right) \\ & + Bl(x_D(n))\frac{1}{T_s}(x_D(n+1) - x_D(n)) \end{aligned} \tag{5.7}$$

As seen, each differential term is simply replaced with the forward Euler equation (5.5). Furthermore, an extra term is added. The reason for this is when the inductance becomes nonlinear and change with respect to the displacement which change with respect to time, it can not be moved outside of the differential as in (2.1), it must be differentiated with respect to time.

Closed box

The mechanical second order differential equation in (2.5), with the combined mechanical and acoustical coefficient (2.17), is then written in discrete time as:

$$\begin{aligned} i_c(n)Bl(x_D(n)) \;=\; & M_t\frac{1}{T_s^2}(x_D(n+2) - 2x_D(n+1) + x_D(n)) + R_t\frac{1}{T_s}(x_D(n+1) - x_D(n)) \\ & + \frac{1}{C_t(x_D(n))}x_D(n) \end{aligned} \tag{5.8}$$

Notice the second order difference term in first term on the right hand side, which is the difference equation to (5.5).

Vented box

The mechanical second order differential equation in (2.5) is added with the mechanical equivalent of the acoustical mass in front and back of the diaphragm (2.18). Furthermore, the impedance of the mechanical equivalent of the vented box (2.29) is added; this is the transfer function of the pressure inside the box (2.21). The resulting difference equation is given by:

$$\begin{aligned} i_c(n)Bl(x_D(n)) &= M_t\frac{1}{T_s^2}(x_D(n+2)-2x_D(n+1)+x_D(n))+R_D\frac{1}{T_s}(x_D(n+1)-x_D(n)) \\ &\quad +\frac{1}{C_D(x_D(n))}x_D(n)+p_c(n)S_D \end{aligned} \tag{5.9}$$

In (2.19) U_P is replaced by the equivalent term for p_c in (2.20). By putting these two equal to each other and then rewrite the equation, p_c can be found with respect to U_P:

$$p_c(n) = M_{AP}\frac{1}{T_s}(U_P(n+1)-U_P(n)) \tag{5.10}$$

And finally, rewriting (2.20) U_P is given by:

$$U_P(n) = S_D\frac{1}{T_s}(x_D(n+1)-x_D(n)) - C_{AB}\frac{1}{T_s}(p_c(n+1)-p_c(n)) - \frac{p_c(n)}{R_{AL}} \tag{5.11}$$

5.2 Digital filter description of transducer

During this thesis, some general filters will be used more than once and in different sections; they are presented here and are:

- Linear movement of diaphragm: displacement, velocity and acceleration.
- Linear and nonlinear current flow through voice-coil.
- Acoustical circuit of vented box system.

As the displacement is going to be used, a filter must be derived with the voltage $w(n)$ as input, where $w(n)$ is the input to the control system see section 6.1. Because the movement of the diaphragm is linearized, this filter must be linear in relation with $w(n)$.
Furthermore, the current flow through the voice-coil must be found and because the displacement is found with a linear filter, the current must be found with a nonlinear filter. But actually, also the linear current flow is needed, so the final filter is linear and then the nonlinearities are added afterwards.
At last two filters for the vented box system must be derived, one for the sound pressure inside the box and one for the volume velocity in the vent. These are linear and with the displacement x_D as input.

But before deriving these filters, three simple filters must be derived. As the forward Euler method is non-causal, the displacement must be delayed with two samples in order for the resulting filters to become causal. This can also be seen in (5.8) and (5.9), which is used later for calculating the current, the current is given by samples in the future. Notice, if the backward Euler method was used, this would not be necessary. The filters for the displacement, velocity and acceleration, each delayed two samples, are given by:

$$\begin{aligned} H_{x_D}(z) &= \frac{x_D(z)}{x_{D+2}(z)} = z^{-2} \\ H_{u_D}(z) &= \frac{u_D(z)}{x_{D+2}(z)} = \frac{1}{T_s}(z^{-1}-z^{-2}) \\ H_{a_D}(z) &= \frac{a_D(z)}{x_{D+2}(z)} = \frac{1}{T_s^2}(1-2z^{-1}+z^{-2}) \end{aligned} \tag{5.12}$$

where x_{D+2} is the displacement before delayed, x_D is the delayed displacement, u_D is the diaphragm velocity and a_D is the acceleration of the diaphragm.

Closed box

Because the filter for extracting the linear displacement, in standard z transformation form, is very long, it is moved to appendix A.1. Instead a more simple form of the filter is presented. It is derived from (5.7) and (5.8):

$$H_{x_D+2}(z) = \frac{x_{D+2}(z)}{w(z)} = \frac{Bl(0)}{\left(L_E(0)\frac{1}{T_s}(z-1) + R_E\right)\left(M_t\frac{1}{T_s^2}(z^2-2z+1) + R_t\frac{1}{T_s}(z-1) + \frac{1}{C_t(0)}\right)} \tag{5.13}$$

Instead of writing the filter for the linear current in normal difference form, it is calculated from the displacement, velocity and acceleration in (5.12), which is inserted in (5.8):

$$i_{c,lin}(n) = \frac{M_t}{Bl(0)} \cdot a_D(n) + \frac{R_t}{Bl(0)} \cdot u_D(n) + \frac{1}{C_t(0)Bl(0)} \cdot x_D(n) \tag{5.14}$$

And adding the nonlinearities, again according to (5.8):

$$i_c(n) = \frac{Bl(0)}{Bl(x_D(n))}\left(i_{c,lin}(n) + \frac{1}{(C_t(x_D(n)) - C_t(0))Bl(0)} \cdot x_D(n)\right) \tag{5.15}$$

Vented box

Again, the filter for extracting the linear displacement for a vented box system, is moved to appendix A.1. The filter is derived from (5.7) and (5.9) and in a simple form written as:

$$H_{x_D+2}(z) = \frac{x_{D+2}(z)}{u(z)} = \frac{Bl(0)}{\left(L_E(0)\frac{1}{T_s}(z-1) + R_E\right)\left(M_t\frac{1}{T_s^2}(z^2-2z+1) + R_D\frac{1}{T_s}(z-1) + \frac{1}{C_D(0)} + S_D p_c(z)\right)} \tag{5.16}$$

where $p_c(z)$ is the sound pressure inside the box. The linear current flow in the voice-coil is derived from (5.9) and given by:

$$i_{c,lin}(n) = \frac{M_t}{Bl(0)} \cdot a_D(n) + \frac{R_t}{Bl(0)} \cdot u_D(n) + \frac{1}{C_t(0)Bl(0)} \cdot x_D(n) + \frac{S_D}{Bl(0)} \cdot p_c(n) \tag{5.17}$$

As no nonlinearities is present are the acoustical circuit for the vented box, (5.15) is used again for calculating the nonlinear current flow, but with the new $i_{c,lin}(n)$ as entry.
Finally, the sound pressure inside the box and volume velocity in the vent, derived from (5.10) and (5.11), are written as:

$$H_{p_c}(z) = \frac{p_c(z)}{x_D(z)} = \frac{M_{AP}S_D\frac{1}{T_s} - 2M_{AP}S_D\frac{1}{T_s}z^{-1} + M_{AP}S_D\frac{1}{T_s}z^{-2}}{C_{AB}M_{AP}\frac{1}{T_s} + \left(-2C_{AB}M_{AP}\frac{1}{T_s} + \frac{M_{AP}}{R_{AL}}\right)z^{-1} + \left(T_s + C_{AB}M_{AP}\frac{1}{T_s} - \frac{M_{AP}}{R_{AL}}\right)z^{-2}} \tag{5.18}$$

$$H_{U_p}(z) = \frac{U_p(z)}{x_D(z)} = \frac{S_D z^{-1} - S_D z^{-2}}{C_{AB}M_{AP}\frac{1}{T_s} + \left(-2C_{AB}M_{AP}\frac{1}{T_s} + \frac{M_{AP}}{R_{AL}}\right)z^{-1} + \left(T_s + C_{AB}M_{AP}\frac{1}{T_s} - \frac{M_{AP}}{R_{AL}}\right)z^{-2}} \tag{5.19}$$

In a given application only one of either H_{p_c} or H_{U_p} needs to be implemented as in (5.18) and (5.19), the other one is simply found by (5.10) or (5.11); i.e. H_{p_a} is implemented and (5.10) is rearranged and used for calculating U_p.

5.3 State space model of transducer

The state space model has the advantages that it is simple to implement a nonlinear system in time, for computer simulations. The discrete state-space model is written as:

$$\begin{aligned} \mathbf{x}(n+1) &= \mathbf{F}(n)\mathbf{x}(n) + \mathbf{g}(n)u(n) \\ y(n) &= \mathbf{h}\mathbf{x}(n) \end{aligned} \tag{5.20}$$

where n is a integer and the discrete time number, $\mathbf{F}$ is the time varying matrix, $\mathbf{g}$ is the time varying input vector and $\mathbf{h}$ is the time invariant output vector.

5.3.1 Closed box

The discrete time states are defined as:

$$\mathbf{x}(n) = \begin{bmatrix} x_1(n) \\ x_2(n) \\ x_3(n) \end{bmatrix} = \begin{bmatrix} i_c(n) \\ x_D(n) \\ \frac{1}{T_s}(x_D(n+1) - x_D(n)) \end{bmatrix} \tag{5.21}$$

According to the general state space model (5.20) and the definition of the states (5.21), the equation for the following time sample of each state can be written. x_1 is found from (5.7), x_3 from (5.8) and given x_3, x_2 can be found by using (5.5).
Finally the matrix $\mathbf{F}$ and vectors $\mathbf{g}$ and $\mathbf{h}$ in the state-space model for the closed-box loudspeaker can be written as:

$$\begin{aligned} \mathbf{F}(n) &= \begin{bmatrix} -\frac{R_E}{L_E(x_2(n))}T_s + 1 & 0 & -\frac{z_1(n)L_{EX}(x_2(n))}{L_E(x_2(n))} - \frac{Bl(x_2(n))}{L_E(x_2(n))}T_s \\ 0 & 1 & T_s \\ \frac{Bl(x_2(n))}{M_t}T_s + \frac{x_1(n)L_{EX}(x_2(n))}{2M_t} & -\frac{1}{C_t(x_2(n))M_t}T_s & -\frac{R_t}{M_t}T_s + \frac{1}{T_s} \end{bmatrix} \\ \mathbf{g}(n) &= \begin{bmatrix} \frac{T_s}{L_E(x_2)} \\ 0 \\ 0 \end{bmatrix} \\ \mathbf{h} &= \begin{bmatrix} 0 & 1 & 0 \end{bmatrix} \end{aligned} \tag{5.22}$$

5.3.2 Vented box

The states in the state space model, for the vented box loudspeaker, are defined as:

$$\mathbf{x}(n) = \begin{bmatrix} x_1(n) \\ x_2(n) \\ x_3(n) \\ x_4(n) \\ x_5(n) \end{bmatrix} = \begin{bmatrix} i_c(n) \\ x_D(n) \\ \frac{1}{T_s}(x_D(n+1) - x_D(n)) \\ U_P(n) \\ p_c(n) \end{bmatrix} \tag{5.23}$$

x_1 and x_2 are calculated in same manor as for the closed box. x_3 is found from (5.9), x_4 from (5.10) and x_5 from (5.11).

Finally the state-space model for the vented-box loudspeaker is given by:

$$
\begin{aligned}
\mathbf{F}(n) &= \\
&\begin{bmatrix}
-\frac{R_E}{L_E(x_2(n))}T_s + 1 & 0 & -\frac{x_1(n)L_{EX}(x_2(n))}{L_E(x_2(n))} - \frac{Bl(x_2(n))}{L_E(x_2(n))}T_s & 0 & 0 \\
0 & 1 & T_s & 0 & 0 \\
\frac{Bl(x_2(n))}{M_t}T_s & -\frac{1}{C_D(x_2(n))M_t}T_s & -\frac{R_D}{M_t}T_s + 1 & 0 & -\frac{S_D}{M_t}T_s \\
0 & 0 & 0 & 1 & \frac{1}{M_{ap}}T_s \\
0 & 0 & \frac{S_D}{C_{AB}}T_s & -\frac{T_s}{C_{AB}} & -\frac{T_s}{R_{AL}C_{AB}} + 1
\end{bmatrix} \\
\mathbf{g}(n) &= \begin{bmatrix} \frac{T_s}{L_E(x_2)} \\ 0 \\ 0 \\ 0 \\ 0 \end{bmatrix} \\
\mathbf{h}(n) &= \begin{bmatrix} 0 & 1 & 0 & 0 & 0 \end{bmatrix}
\end{aligned}
\tag{5.24}
$$

where L_{EX} denotes the first order derivative of L_E.

$\mathbf{h}$ defines the output of the states space model and above x_D is the output. If the diaphragm volume velocity U_D or the total volume velocity U_0 is wanted instead, the vector must be defined as:

$$
\begin{aligned}
\mathbf{h}(n) &= \begin{bmatrix} 0 & 0 & S_D & 0 & 0 \end{bmatrix} \\
\mathbf{h}(n) &= \begin{bmatrix} 0 & 0 & S_D & -1 & 0 \end{bmatrix}
\end{aligned}
\tag{5.25}
$$

5.4 Matlab simulation toolbox

During this thesis a text based toolbox for Matlab has been made. With this it is easy and fast to evaluated a loudspeaker and/or compensation algorithm, before implementing in hardware.
In figure 5.2 a flow diagram of the toolbox is seen. As seen, it is constructed of five layers, which each handles a specific job.
In the following each layer is described. Finally simulations of the THD and IMD are done and compared with the measured.

5.4.1 Layer 1: Settings

The text based user interface setups the simulation, and works by specifying the setting for the following four layers.

5.4.2 Layer 2: Signal generation

In this layer all signals are generated specific to the settings in layer 1. The available signals are:

- Single-tone sinusoid: This signal is used in many simulations. First, it is used in THD simulations where several sinusoids are made and run through the system in a for loop. Second, it is also used for simulating the frequency depend DC offset, in the same manner as the THD simulation. Third, it can be used in FFT plots. Fourth, it can be used for simulating a nonlinear transfer function that changes with respect to the signal level. Fifth, it can be saved to a wave file and played back on a loudspeaker for measuring the compensator influence on the loudspeaker.
- Two-tone sinusoidal: This signal is only used in two types of simulation. First, it is used for simulating IMD. And second, it can be saved in a wave file and played back on a loudspeaker in order to compensate IMD.

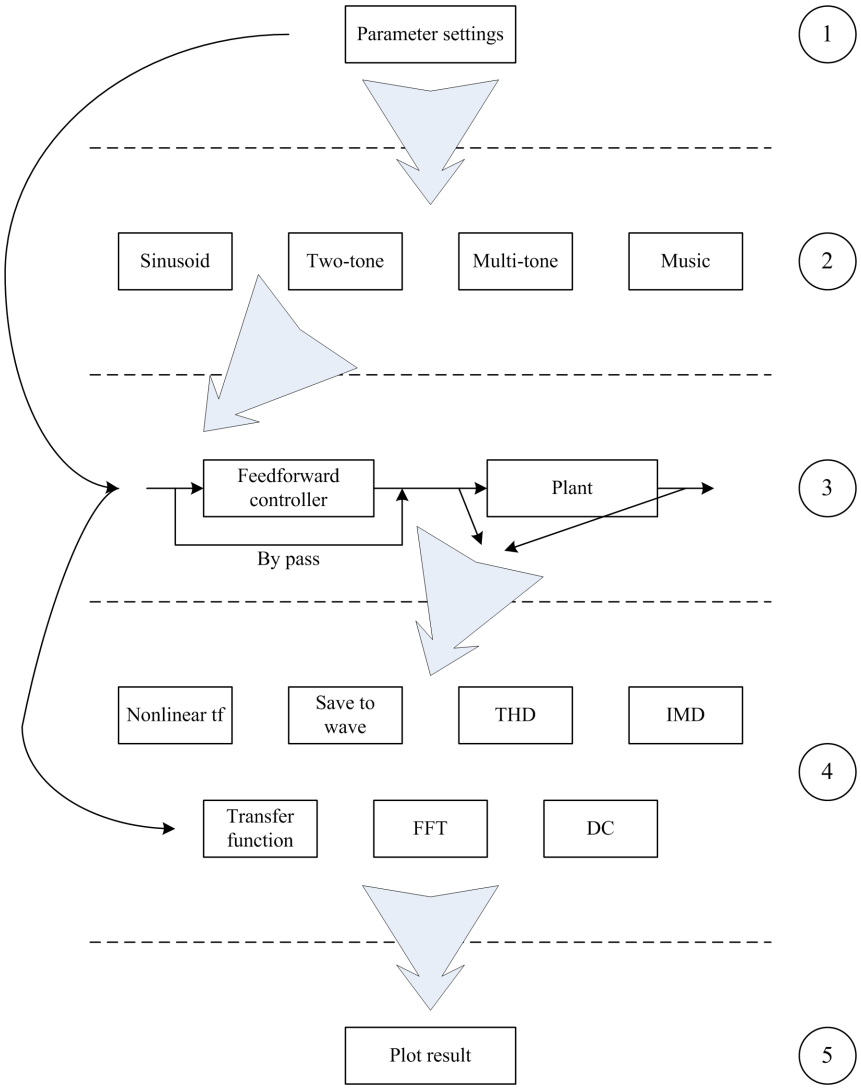

Figure 5.2: Block diagram of loudspeaker compensation toolbox in Matlab

- Multi-tone signal: This signal is for simulating nonlinear transfer functions and generating FFT plots.
- Music (loads a wave-file): Is used for compensating the distortion added when played on a loudspeaker.

5.4.3 Layer 3: Simulation

Layer 3 simply simulates the loudspeaker, represented as the plant model derived in section 5.3 with the nonlinearities given in 4, and the compensators, that are found in chapter 6.2 and 6.3. It is possible both to by pass the controller but also the plant if wanted.

Further more, both the plant model and the compensator has been implemented in c language, in order to optimize the simulation time. Furthermore, this has the advantage that if processed on a long music signal for listening impressions, it can be done within reasonable time.

5.4.4 Layer 4: Signal processing

In this layer the output of either the plant model or controller is processed.

When calculating the amplitude of tone from a frequency response, as with THD, IMD and nonlinear transfer function simulations, the sum of the bins at and a few around that specific frequency are taken. This is due to the fact that when applying a window to the time signal, the energy of a frequency is spread out over a narrow frequency range, rather than being concentrated to the frequency. Though, if the amplitude of the tone is close to the noise floor, then it may affect the result as some energy of the noise floor are added and influences the result; the user must be aware of this as normally a few extra bins are used rather than not enough. The number of bins used is setup in layer 1.

Furthermore, in this layer, the simulated signal can be saved in wave file.

5.4.5 Layer 5: plotting

Finally the last layer plot the results achieved in the four first layers. These results are plotted specific to the given simulation:

- Nonlinear tf and transfer function: Plotted in dB both for the sound pressure, but also for the displacement response.
- THD and IMD: plotted in percent with respect to the frequency.
- DC offset: plotted in millimeters with respect to the frequency.
- FFT. Normally frequency plot in dB.

5.5 THD and IMD evaluation of nonlinear plant model

In figure 5.3 THD simulations compared with corresponding measurements, is seen. At high frequencies the results achieved in the simulations are too low; This is expected as only the most significant nonlinearities are included in the model, resulting in a false image at low distortions. Furthermore, the Helmholtz resonance is much more significant in the simulation. When simulating, the overall pressure response is used in the calculation. But when measuring the THD, the microphone is placed closed to the diaphragm (less than 20cm) and not as close to the vent, then the sound pressure from the diaphragm and vent do not necessary contributes equally at the point of the microphone.

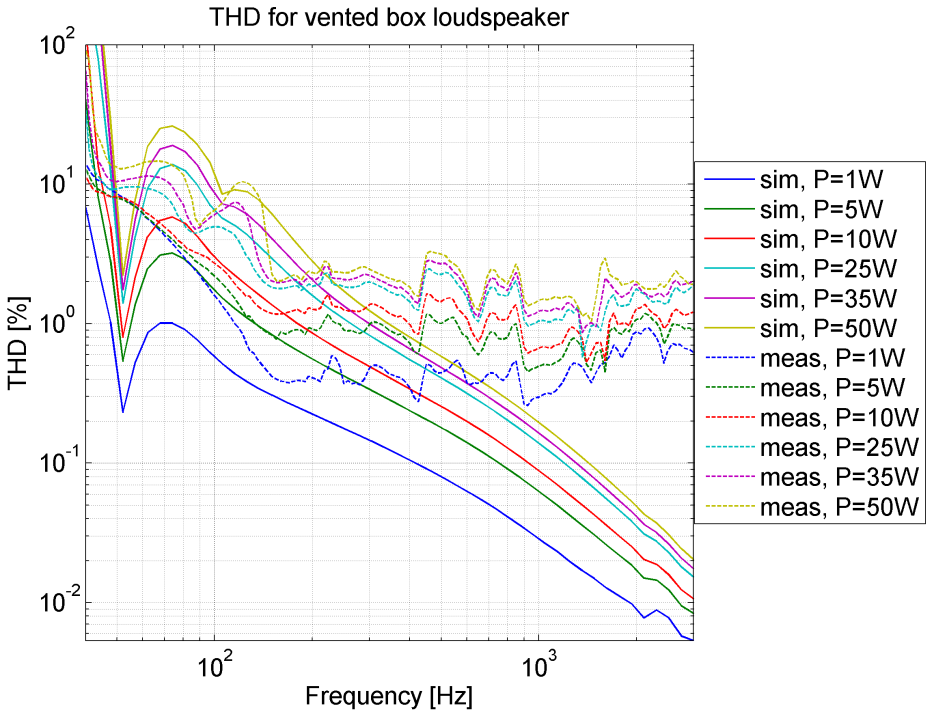

Figure 5.3: THD simulation plotted along with belonging measurements

From $70Hz$ to $200Hz$ the simulations and measurements are comparable, but differs a bit. Though the measurement where 1W input signal is applied, differs much from the simulations.
In figure 5.3 simulations and measurements of intermodulation distortion are compared. As seen, the amount of distortion in the simulation differs from the measured, but the increasing from are very comparable.

New measurements, in order to validate the ones presented, would have appreciable, but because of time lack, this has not been done.

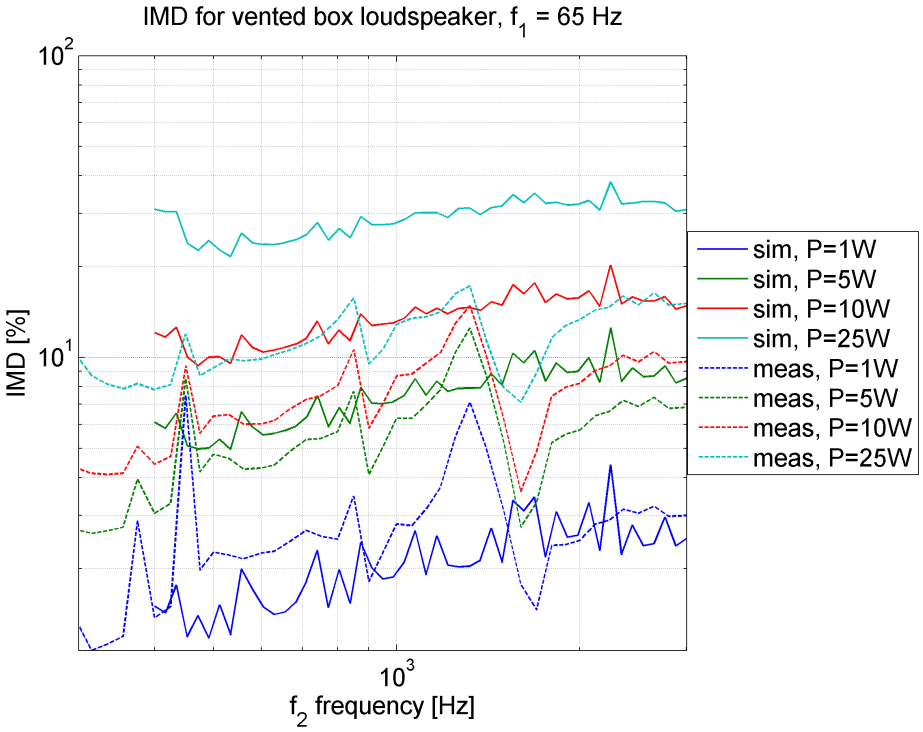

Figure 5.4: IMD simulation plotted along with belonging measurements

Chapter 6

Controllers

Before a compensator is made, some general control theory is presented. In this chapter the three most commonly used controllers are presented, as well as practical issues about applying the controllers to a transducer.

Next, two compensator algorithms are presented. So far, these are the two most popular method; the first is the state-space compensator and finally, the second is Klippel's mirror filter.

6.1 Controller theory

The three controller systems that are dealt with in this thesis are:

- Feed-forward controller (or open-loop)
- Feedback controller (or closed-loop)
- Adaptive feed-forward controller

Feed-forward controller

The feed-forward controller is seen in figure 6.1a. This is the simplest and cheapest control design. It compensates for the unwanted nonlinearities in the plant by changing the input $w(t)$ to $u(t)$ by adding the inverse of the nonlinearities, and the wanted output $y(t)$ is then achieved. Its disadvantage is, however, if the dynamics of the plant model changes with age, temperature and other factors, then it might fail to do the job.

Feedback controller

Another control method is the feedback model, or servo controller, as seen in figure 6.1b. Closed-loop feedback systems feed the plant output back to the controller. The plant output that is feed back, is some kind of information on how the loudspeaker is reproducing the audio input signal.
The advantage of this method is that it is very robust to changes in the plant as the output of it is measured $y_m(t)$ all the time. So any changing nonlinearity as the compliance, would be recognized immediately.
The disadvantage of the feedback controller, is that the output is impractical to obtain, see [Bright, 2002][1], which is explained as why no type of closed-loop controller for a loudspeaker system has seen much commercial success, despite the big interest in loudspeaker linearization.
Even more problematic is it that delay introduced in the feedback link, might cause the feedback system to fail the Nyquist stability criteria.

[1] Page 25

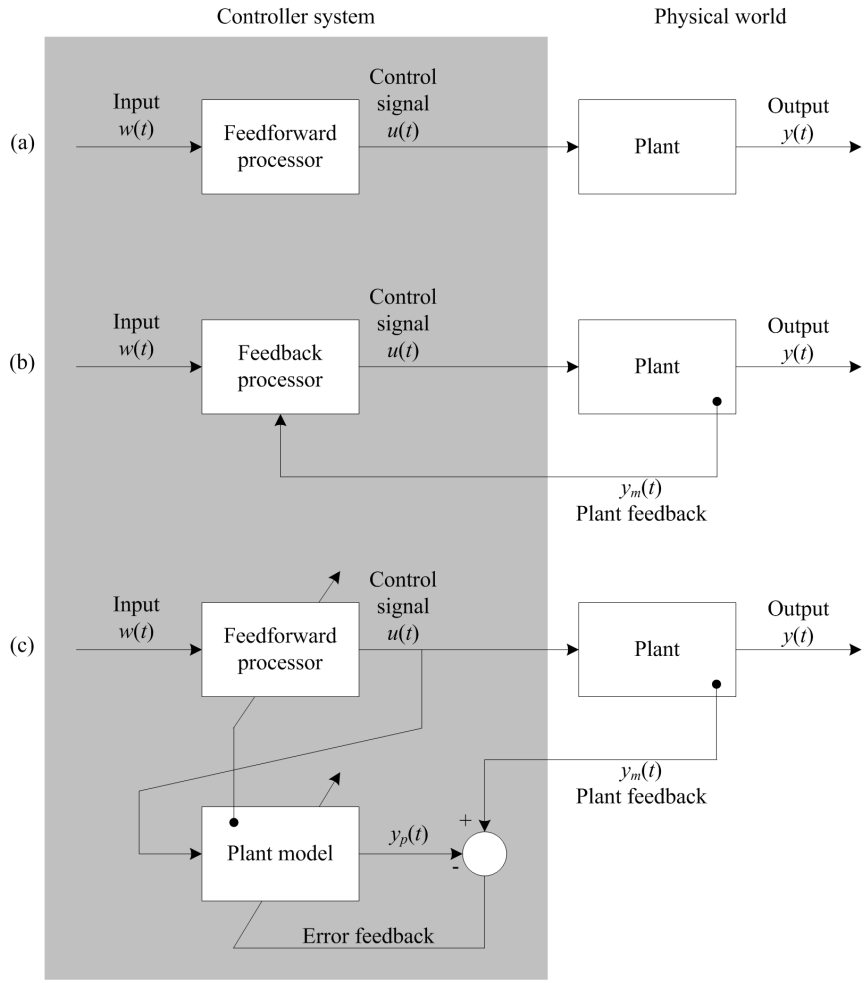

Figure 6.1: Three types of controller systems, (a) feed-forward, (b) feedback, (c) adaptive feed-forward

Adaptive feed-forward controller

The third method is the adaptive feedforward model, which is a combination of the two first, as seen in figure 6.1c. Here a feedforward controller is applied where its states are updated once in a while. The update is done by a feedback to a system identification block, which finds the state of the loudspeaker and applies it to the feedforward model. The advantages is that the Nyquist stability criteria does not have to be achieved, but still the changes caused by age, temperature and many other things is adapted by the controller.

6.1.1 Plant measurement

The feedback used in two of the controllers, can be done in the following ways:

- The sound pressure is measured with a microphone and with the signal the diaphragm displacement and velocity is possible to find.
- The motion of the diaphragm is recorded directly.
- The voltage and current are measured and hereof the states in the loudspeaker are found.

Sound pressure

On first hand it might be most convenient to measure the sound pressure and use it as feedback. But actually it is the most problematic method, as the sound field changes with the microphone position. One could say that the most obvious position for the microphone would be at the listeners, but as the far-field response is changed because of the room response (wall reflections that are frequency dependent), a false picture of the loudspeaker would be achieved.
Close to the loudspeaker, where the wavelength is big compared to the distance between the microphone and the loudspeaker, it will be the dominant and the effect of the room can be neglected.
Another disadvantage is that it has to be calibrated once in a while.

The sound pressure can be used in two ways. Either the expected sound pressure can be calculated and compared with the true, or the true acceleration can be calculated from the measured sound pressure and then compared with the calculated acceleration. The sound pressure is defined in section 2.5.3.

Motional feedback

The first publication describing what is more commonly thought of as motional feedback appeared in 1927. Since several attempt has been made with different kinds of plant measurements:

- An accelerometer mounted on the diaphragm.
- Secondary magnet circuit and voice-coil.
- Conducting voice-coil former as a secondary winding.
- Laser that measures the displacement.

The accelerometer is a good choice when the mass of the diaphragm with assembly is big compared with the mass of the accelerometer. If not it will change the properties of the loudspeaker, which is not wanted. If a closed box loudspeaker is considered, then the measured acceleration will be proportional to the sound pressure. Unfortunately, the high price makes it less interesting.

If a secondary magnet circuit and voice-coil is used, the voltage created by the back EMF can be measured and the velocity of the diaphragm can be derived. But because the magnet is the most expensive part of

the loudspeaker, the price would increase dramatically. A less expensive strategy is to add a secondary winding to the primary coil, or if a conducting voice-coil former is used, then use it as a secondary winding [Poulsen, 2004][2]. Although a conducting voice-coil former increases the eddy currents, see section 2.6.2.

Voltage and current

The voltage is always known as the amplifier considered is a constant voltage amplifier. The current is measured by adding a small resistor in series with the loudspeaker, and then measuring the voltage drop. The current flow in the resistor, which is equal to the flow in the loudspeaker, can then be calculated. The voltage and current measurement can be used to identify the state of the loudspeaker.
This method is the cheapest of them all because of the low cost Delta-Sigma A/D-converters, and is therefore often used.

[2] Page 138

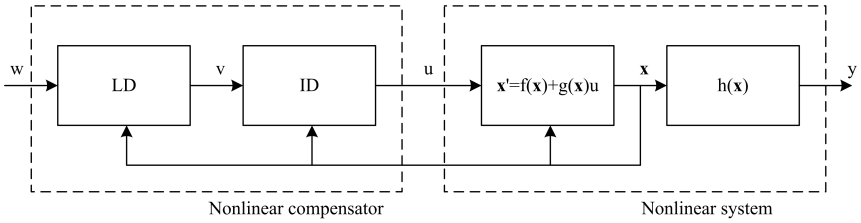

Figure 6.2: State-space compensator

6.2 State-space compensator

The state space compensation is in fact a feedback linearization system, wherein the state space notation is used. Feedback linearization is a general, abstract, complete formal theory for the control of nonlinear dynamic systems. The method uses elements of feedforward control, in that it utilizes a complete model of the system's dynamics, and feedback control, as it uses a measurement of the system state. So although the word 'feedback' forms a part of its name, it is not a pure feedback control system.
The compensator is first derived in general form, with a state feedback from the plant. Later the system is changed to estimate the states with a state observer, and finally it is shown that the states can be estimated in a pure feedforward form.

6.2.1 Inverse dynamics

The first who applied feedback linearization to loudspeakers was [Johan Suykens and Ginderdeuren, 1992], wherein an inverse dynamics processor uses feedback signals from a model of the loudspeaker to create a feedforward distortion compensator. Later both [Schurer, 1997] and [Bright, 2002] have done the same; all as continuous time formulations.

If considering the state space model from section 5.3, then the basic goal is to create a linear relationship between input signal $u(n)$ and the output $y(n)$.
The essential feature of feedback linearization, is that by taking a sufficient number of time intervals $n+1$ of the output $y(n)$, given certain conditions, one will eventually arrive at an expression that depends exactly on the input. Such an expression can be inverted by simple algebraic expressions. The resulting expression can then be used as a controller, which compensates the nonlinearities in the system.
Theory about applying feedback linearization in discrete time, is given in [Bright, 2002], but only applied in a more simple form where certain nonlinearities are excluded.
In figure 6.2 a diagram of the principle is seen. The nonlinear system is the loudspeaker, modeled by the state space model in section 5.3. The nonlinear compensator consist both of the inverse dynamic system (ID) and the a linear dynamic system (LD). The inverse dynamics not only compensates the nonlinearities but also the linear system, and of that reason the linear dynamic block must be included.

If considering the system output at time interval $n+1$:

$$\begin{aligned} y(n+1) &= \mathbf{h}(x(n+1)) \\ &= \mathbf{h}(\mathbf{F}(x(n)) + \mathbf{g}(x(n))u(n)) \end{aligned} \tag{6.1}$$

Then if the derivative of the right hand side with respect to the input $u(n)$ is not zero:

$$\frac{\partial y(n+1)}{\partial u(n)} \neq 0 \tag{6.2}$$

an input-output link is established, and the output can be solved in terms of the input. If this derivative is zero, then it is necessary to take the next output sample in same manor as (6.1). This procedure is

repeated until one finds the derivative of the r^{th} composition with respect to the input to not be zero, represented as:

$$y(n+r) = \mathbf{h}^r \circ (\mathbf{F}, \mathbf{g}u(n)) \tag{6.3}$$

When the input-output link is established and the output $y(n+r)$ depends directly on the input $u(t)$, the expression is inverted to form a compensator in terms of the inverse dynamics. This controller will process the signal $v(n)$ according to the inverse of (6.3), and feed this to the input to the plant. The compensator will create a linear relationship between the input $v(n)$ and the output $y(n)$ as so:

$$y(n+r) = v(n) \quad \begin{matrix} z\{\} \\ \Rightarrow \end{matrix} \quad \frac{y(z)}{v(z)} = \frac{1}{z^r} \tag{6.4}$$

where r is the relative degree of the system, defined above. As seen, a delay through the controller and the plant of r samples is happening.

Linear dynamics

As the linear dynamics are compensated in the inverse dynamics, it must be reintroduced by filtering the input to the inverse-dynamics controller $v(n)$ by a linear filter with the frequency response of the linear dynamics of the system. As the output is set to the displacement $y(n) = x_D(n)$, see (5.22) or (5.24), the linear filter in (5.13) or (5.16) is used with $w(n)$ as input and $v(n)$ as output, see figure 6.2.

Closed box

For the nonlinear system defined in (5.22), the above theory about taking the next output sample $n+1$, see 6.3, results in:

$$\begin{aligned}
y(n) &= x_2(n) \\
y(n+1) &= x_2(n) + T_s x_3(n) \\
y(n+2) &= \frac{Bl(x_2(n))}{M_t} T_s^2 x_1(n) + \left(1 - \frac{1}{C_t(x_2(n))M_t} T_s^2\right) x_2(n) + \left(2T_s - \frac{R_t}{M_t} T_s^2\right) x_3(n) \\
y(n+3) &= \left[\frac{Bl(x_2(n))}{M_t} T_s^2 - \frac{Bl(x_2(n+1))}{M_t} T_s^2 \left(\frac{R_E}{L_E(n)} T_s - 1\right) - \frac{Bl(x_2(n))}{M_t} T_s^2 \left(\frac{R_t}{M_t} T_s - 1\right)\right] x_1(n) \\
&\quad + \left(1 - \frac{1}{C_t(x_2(n))M_t} T_s^2 - \frac{1}{C_t(x_2(n))M_t} T_s^2\right) x_2(n) + \left(2T_s - \frac{R_t}{M_t} T_s^2 + 1\right) x_3(n) \\
&\quad - \frac{Bl(x_2(n+1))}{M_t L_E(x_2(n))} T_s^3 x_3(n) \left[L_{EX}(x_2(n)) x_1(n) + Bl(x_2(n))\right] - \frac{1}{C_t(x_2(n+1))M_t} T_s^2 (x_2(n) + T_s x_3(n)) \\
&\quad + \frac{R_t}{M_t} T_s^2 \left(\frac{1}{C_t(x_2(n))M_t} T_s x_2(n) + \left(\frac{R_t}{M_t} T_s - 2\right) x_3(n)\right) + \frac{Bl(x_2(n+1))}{M_t L_E(x_2(n))} T_s^3 u(n)
\end{aligned} \tag{6.5}$$

As seen, with a relative degree of the system $r = 3$ depends directly on the input $u(n)$. The expression is easily inverted into a controller and $y(n)$ replaced with $v(n)$ (though it has been done, the result is not shown here because of its size), and the relationship between $v(n)$ and $y(n)$ can be established:

$$y(n+3) = v(n) \quad \begin{matrix} z\{\} \\ \Rightarrow \end{matrix} \quad \frac{y(z)}{v(z)} = \frac{1}{z^3} \tag{6.6}$$

Vented box

Again for the nonlinear system in (5.24), the above theory results in:

$$
\begin{aligned}
y(n) &= x_2(n) \\
y(n+1) &= x_2(n) + T_s x_3(n) \\
y(n+2) &= \frac{Bl(x_2(n))}{M_t} T_s^2 x_1(n) + \left(1 - \frac{1}{C_t(x_2(n))M_t} T_s^2\right) x_2(n) + \left(2T_s - \frac{R_t}{M_t} T_s^2\right) x_3(n) - \frac{S_D}{M_t} T_s^2 x_5(n) \quad (6.7) \\
y(n+3) &= \left[\frac{Bl(x_2(n))}{M_t} T_s^2 - \frac{Bl(x_2(n+1))}{M_t} T_s^2 \left(\frac{R_E}{L_E(n)} T_s - 1\right) - \frac{Bl(x_2(n))}{M_t} T_s^2 \left(\frac{R_t}{M_t} T_s - 1\right)\right] x_1(n) \\
&\quad + \left(1 - \frac{1}{C_t(x_2(n))M_t} T_s^2 - \frac{1}{C_t(x_2(n))M_t} T_s^2\right) x_2(n) + \left(2T_s - \frac{R_t}{M_t} T_s^2 + 1\right) x_3(n) \\
&\quad - \frac{Bl(x_2(n+1))}{M_t L_E(x_2(n))} T_s^3 x_3(n) \left[L_{EX}(x_2(n)) x_1(n) + Bl(x_2(n))\right] - \frac{1}{C_t(x_2(n+1))M_t} T_s^2 (x_2(n) + T_s x_3(n)) \\
&\quad + \frac{R_t}{M_t} T_s^2 \left(\frac{1}{C_t(x_2(n))M_t} T_s x_2(n) + \left(\frac{R_t}{M_t} T_s - 2\right) x_3(n)\right) + \frac{Bl(x_2(n+1))}{M_t L_E(x_2(n))} T_s^3 u(n) \\
&\quad - \frac{S_D}{M_t} T_s \left(\frac{S_D}{C_{AB}} T_s x_3(n) - \frac{1}{C_{AB}} T_s x_4(n)\right) \\
&\quad + \left(\frac{R_t}{M_t^2} S_D * Ts^2 - \frac{S_D}{M_t} T_s - \frac{S_D}{M_t} T_s \left(-\frac{1}{(R_{AL} C_{AB}} T_s +\right) - \frac{S_D}{M_t} T_s^2\right) x_5(n)
\end{aligned}
$$

where at the relative degree of the system is $r = 3$. Again a similar relationship can be found:

$$
y(n+3) = v(n) \quad \begin{matrix} z\{\} \\ \Rightarrow \end{matrix} \quad \frac{y(z)}{v(z)} = \frac{1}{z^3} \quad (6.8)
$$

6.2.2 State observer

The state space compensator developed above suffers from the same problem as traditional feedback processors described in section 6.1, namely that the controller requires states measurement of the state vector $\mathbf{x}(n)$.
A solution to this can be to make a partial state measurement, i.e. to measure one state, and simulated the others by using a state observer. One example is Beerling et al. [Marcel A. H. Beerling and Hermann, 1998], which presented a system with an accelerometer mounted on the diaphragm, and from that he calculated the velocity, displacement and current.

Schurer et al. presented in [Hans Schurer, 1997] a feedback linearization controller that employed a state observer which made no measurement on the plant. In the system, the input to the state observer was the output from the controller $u(n)$. This is theoretically possible with an accurate plant model, and the resulting controller is a pure feed forward type.
A diagram of the system is seen in figure 6.3, and the state observer is the state space plant model in (5.20). The states in the model are read and fed back to the compensator.

One disadvantage with this approach is that is might become unstable, as a feedback loop is created between $u(n)$ and $\hat{\mathbf{x}}(n)$, see [Bright, 2002].

6.2.3 Pre-estimation of states assuming ideal alignment

As a result of (6.4), stating that the r^{th} next sample output is given by the input to the nonlinear controller $v(n)$, the states can be simulated from the input to the compensator, in a more simple manner than using the state observer.

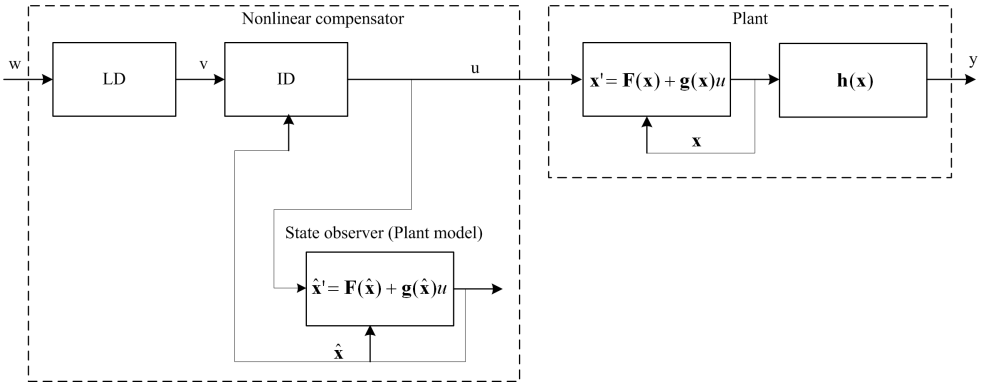

Figure 6.3: State-space compensator with state observer

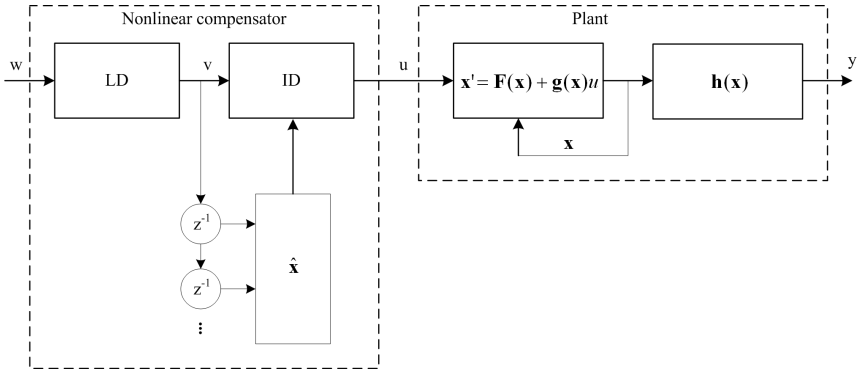

Figure 6.4: State-space compensator with pre-simulated states

In figure 6.3 this principle is seen. Here the delays are added to fulfill (6.4), whereafter the states are estimated. As the displacement is calculated in the linear dynamics (LD) block, see section 6.2.1, and given in the input to the inverse dynamics $v(n)$, it only needs to be delayed with three time samples. If applying (5.12), but with an extra delay (multiplying with z^{-1}), state x_2 and x_3 are found. The estimation of the last states are different for the closed box and vented box loudspeaker.

Closed box

As the system is nonlinear, and as the displacement states x_2 is calculated by its linear filter, the current must be nonlinear in order to describe the nonlinear system.
First the linear current filter is used (5.14) and then the nonlinearities are added (5.15).

Now all three states are estimated, and the compensator for the closed box is complete.

Vented box

For the application of the vented box speaker, the estimated current must be with a nonlinear filter. The linear filter used first is (5.17) and then the nonlinearities added are the as for the closed box case (5.15).

Furthermore the two states for both the inside box pressure and the volume velocity in the vent is estimated. It can be done respectively with (5.18) and (5.19), although computations would be saved if the

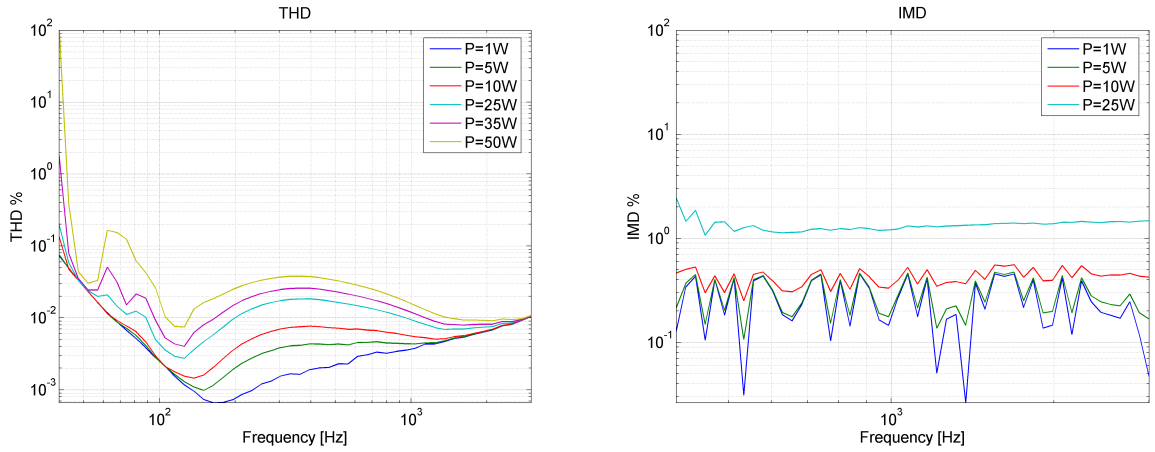

(a) (b)

Figure 6.5: THD and IMD simulations at different driving levels, (a) THD, (b) IMD

pressure inside the box first is calculated (5.18), and then rewriting (5.10) to calculate the volume velocity.

The feedforward compensator the vented box loudspeaker is now complete.

6.2.4 Simulation

In order to evaluate how well the state space compensator in theory, compensates for the total harmonic distortion and intermodulation distortion, it is applied on the nonlinear plant model derived in section 5.3 for the vented box loudspeaker.

In figure 6.5(a) the THD measurement is seen at different driving levels. Notice, below the helmholtz resonance frequency $f_B = 51$Hz the distortion is very high. This is due to the fact that the sound from the diaphragm is close to being in inverse phase with the sound from the vent, see figure 2.10, thus producing very low sound pressure at large displacement. At and above the Helmholtz resonance, the distortion is very low, even at the highest input level the distortion is below 0.1%. The distortion for the low level signal, is lower than the noise floor.
In figure 6.5(b) the IMD measurement is seen at different driving levels. Nearly the same conclusions can be drawn as for the THD measurement, though the distortion for the highest level, increases slightly, and is thus still low.
As seen, in theory the state space compensator compensates for the distortion very well.

6.3 Mirror filter

In this section the Mirror filter is presented. The Mirror filter is a feed-forward controller system for compensation of nonlinearities in transducers. It was developed and patented by Klippel [Klippel, 1992c] and applied to a loudspeaker [Klippel, 1992a]. Later in [Klippel, 1998] Klippel finally recognized that the mirror filter is simply a feedforward case of the integrator decoupled form of feedback linearization. Herein the system states are determined by processing the input to the compensator, instead of by a observer model processing the output of the compensator.

Notice, the mirror filter normally includes a term for compensating the magnetic attraction force, section 3.1.1. In this thesis this is left out, because it was concluded in section 3.1.4 that this nonlinearity only contributes very little to the overall distortion.

6.3.1 Algorithm

The mirror filter algorithm is very simple and is derived by subtracting the desired linear dynamics from the nonlinear dynamics.
First the nonlinear dynamics equation is written by combining and z transforming (5.7) and (5.9):

$$\begin{aligned} Bl(x_D(z))u(z) \;=\; & R_E\left(M_t\frac{1}{T_s^2}(z^2-2z+1)+R_D\frac{1}{T_s}(z-1)+Z_a\right)x_D(z)+R_E\frac{1}{C_D(x_D(z))}x_D(z) \quad (6.9)\\ & +Bl(x_D(z))L_E(x_D(z))\frac{1}{T_s}(z-1)i_c(z)+Bl(x_D(z))L_{EX}(x_D(z))\frac{1}{T_s}(z-1)i_c(z)x_D(z)\\ & +Bl(x_D(z))^2\frac{1}{T_s}(z-1)x(z) \quad (6.10)\end{aligned}$$

Notice the notation of the mechanical parameters. Only the mechanical equivalent of the acoustic mass is added to the mechanical mass. The Z_a is the acoustic radiation impedance, where both the closed box and vented box acoustic impedance can be inserted. The vented box impedance is given in (2.21) and the closed box impedance in (2.13), where the mass is not included for the last one. The acoustic impedances are continuous time equations, but as shown below they are canceled out.
The desired dynamics of the overall system is found by rewriting the linear filter (5.16):

$$\begin{aligned} Bl(0)w(z) \;=\; & R_E\left(M_t\frac{1}{T_s^2}(z^2-2z+1)+R_D\frac{1}{T_s}(z-1)+Z_a\right)x_D(z)+R_E\frac{1}{C_D(0)}x_D(z) \quad (6.11)\\ & +Bl(0)L_E(0)\frac{1}{T_s}(z-1)i_{c,lin}(z)+Bl(0)L_{EX}(0)\frac{1}{T_s}(z-1)i_{c,lin}(z)x_D(z)+Bl(0)^2\frac{1}{T_s}(z-1)x(z)\end{aligned}$$

Again it can be seen that both the closed box and the vented box can be used. And finally the control law is derived by subtracting (6.11) from (6.9):

$$\begin{aligned} u(z) \;=\; & \left[w(z)+\left(\frac{1}{C_D(x_D(z))}-\frac{1}{C_D(0)}\right)\frac{R_E}{Bl(0)}x_D(z)+\left(\frac{Bl(x_D(z))^2}{Bl(0)}-Bl(0)\right)\frac{1}{T_s}(z-1)x_D(z) \quad (6.12)\right.\\ & \left.-L_E(0)\frac{1}{T_s}(z-1)i_{c,lin}(z)\right]\cdot\frac{Bl_0}{Bl(x_D(z))}+L_E(x_D(z))\frac{1}{T_s}(z-1)i_c(z)+i_c(z)\frac{dL_E(x_D(z))}{dx_D(z)}\frac{1}{T_s}(z-1)x_D(z)\end{aligned}$$

As seen, no acoustical parameters are left, and the only mechanical parameter is the compliance of the suspension.
The states that are inputs to the mirror compensator, are calculated from $w(n)$ as a feedforward form.

- The displacement, velocity and acceleration of the diaphragm are calculated from (5.12).
- The linear current is calculated from (5.14) for the closed box and from (5.17) for the vented box.

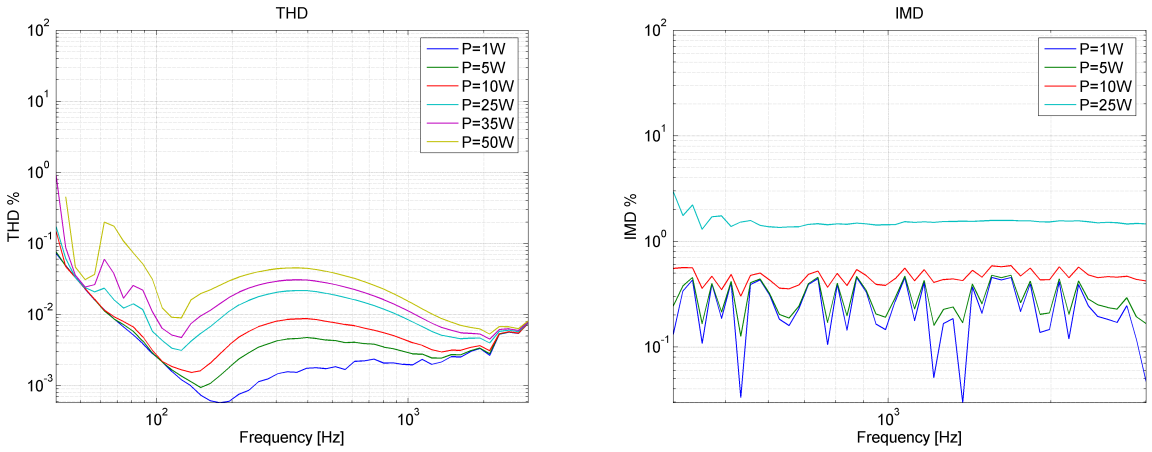

(a) (b)

Figure 6.6: THD and IMD simulations at different driving levels, (a) THD, (b) IMD

- (5.15) is used in order to calculated the nonlinear current.

As seen, only the calculation of the current differs from the closed box to the vented box loudspeaker. Though if the vented box is used, (5.18) must be used before calculating the current.

6.3.2 Simulation

In figure 6.6(a) and 6.6(b), THD and IMD simulations for the mirror filter is seen at different driving levels. When comparing to figure 6.5 it can be seen that the compensators nearly performs equally, thus the same conclusions can be drawn with the mirror filter

Chapter 7

Future work

During this thesis many topics have been investigated, but because of a limited time schedule, many remain untouched. In this chapter it is discussed how to continue on this thesis. The topics are written in the order that they must be done.

Many of the acoustic measurements must be done one more times, in order to validate the ones which are already given. This was originally planned, but failed due to bad luck with the loudspeaker. Simulations have shown that both the compensation algorithms worked with in this thesis, compensate the plant model, which they are derived from, perfectly well. But in order to get a true image of the performance, they must be applied on the test loudspeaker; all work for this has been done within the Matlab toolbox, it only needs to be applied.

Afterwards some listening tests with several persons with different relations to hifi must be established. This is very important as the improvement in the subjective listening pleasure must be estimated.

An idea of where to implement soft clipping was given, but how it is done must be further investigated.

As already indicated, in a batch, feedforward compensators are impractical as every transducer is different and as they change during operation. Of this reason investigation on system identification must be done for a later implementation of a adaptive feedforward compensator.

Finally the evaluation of the performance must be done again, both by measurements and by listening tests.

Another direction could be done by investigating the opportunity to rewrite the difference equations for the transducer into a neural network. This is a hole new way of looking at compensation algorithms as normally physical model are used.

Chapter 8

Conclusion

For now the investigation, on compensation of nonlinearities in loudspeakers is over, and the following conclusions can be drawn.
As shown in figure 3.5, break up in the diaphragm, for the driver used in the test loudspeaker, occurs at relatively low frequencies when taking in mind that its working range is somewhat higher. Furthermore, eddy currents causing the electric impedance to behave differently than a coil at high frequencies. These two issues are making the plant model inaccurate at high frequencies. Looking at the distortion caused by the inductance in section 3.2.3, it can be seen that its main contribution, is intermodulation distortion at high frequencies. A plant model that is unprecise in that area, might cause problems when compensating for the nonlinearity in the inductance.
During the thesis, no compensation algorithm studied, include break up in the diaphragm or eddy currents, but all models compensates the nonlinear inductance.

Next it was shown in chapter 4 that polynomials for modeling the nonlinearities as commonly used, can causes some problems, an even worse, the system can become unstable. Exponential functions were proposed instead, which have been shown to always be stable and behave more appropriately outside of the measured data. But also the sigmoid function is used when modeling the inductance, due to its special 's' form. Finally, the given section, an idea to implement a soft clipping system with respect to the displacement, was given.

A toolbox in Matlab was made to simulated both closed box and vented box loudspeaker. In the toolbox compensation algorithms could be applied, simulated and evaluated, see section 5.4.

In general all proposes so far, with the exception of the one from Andrew Bright, are derived in continuous time for later to be implemented in discrete time. During this thesis the two most popular compensators have been derived from scratch with the intension on discrete time from the start. The compensators are the state space compensator, see section 6.2 and Klippel's mirror filter, see section 6.3. It is believed that it is much more appropriate to work in the domain which the application is to be used. To do this, methods for describing the nonlinear transducers in discrete time were used, see chapter 5.

Finally, the two compensators were evaluated, and in theory, both of them are close to being ideal, but in real world applications they will fail as they in this thesis, only are considered as feedforward controllers. They must be adaptive, including a system identification block for updating the feedforward controller.

Bibliography

[Beers and Belar, 1981] Beers, G. L. and Belar, H. (1981). Frequency-modulation distortion in loudspeakers. *J. Audio Eng. Soc.*, Vol. 29(No. 5):pp. 320–326.

[Behler and Bernhard, 1998] Behler, G. K. and Bernhard, A. (1998). Measuring method to derive the lumped elements of the loudspeaker thermal equivalent circuit. *Audio Eng. Soc.*, 104th Convention.

[Bishop, 2000] Bishop, C. M. (2000). *Neural Networks for Pattern Recognition*. Oxford University Press Inc.

[Bright, 2002] Bright, A. (2002). *Active Control of Loudspeakers: An Investigation of Practical Applications*. PhD thesis, The Technical University of Denmark, Department of Acoustic Technology - Ørsted·DTU.

[Button, 1992] Button, D. J. (1992). Heat dissipation and power compression in loudspeakers. *J. Audio Eng. Soc.*, Vol. 40(No. 1/2):pp. 32–41.

[Chapman, 1998] Chapman, P. J. (1998). Thermal simulation of loudspeakers. *Audio Eng. Soc.*, 104th Convention.

[Chapman, 2000] Chapman, P. J. (2000). Complete thermal protection of an active loudspeaker. *Audio Eng. Soc.*, 104th Convention.

[Cunningham, 1949] Cunningham, W. J. (1949). Non-linear distortion in dynamic loudspeakers due to magnetic effects. *J. Acoustical Society of America*, 21:pp. 202–207.

[Denbigh, 1998] Denbigh, P. (1998). *System Analysis & Signal Processing*. Addison-Wesley, 1. edition.

[Hans Schurer, 1997] Hans Schurer, A. G. J. Nijmeijer, M. A. B. C. H. S. O. E. H. (1997). Identification and compensation of the electrodynamic transducer nonlinearities. *Procedings of ICASSP-97*, (3):pp. 2381–2384. ISBN: 0-8186-7919-0.

[Henricksen, 1987] Henricksen, C. A. (1987). Heat-transfer mechanisms in loudspeakers: Analysis, measurement, and design. *J. Audio Eng. Soc.*, Vol. 35:pp. 778–791.

[Janssen, 2004] Janssen, N. (2004). Personal correspondence. (14 and 15 october, 2004). Goudsmit Magnetic Supplies B.V., http://www.goudsmit-magnetics.nl/.

[Johan Suykens and Ginderdeuren, 1992] Johan Suykens, J. V. and Ginderdeuren, J. V. (April 22, 1992). Control of distortion in an electrodynamic loudspeaker, part 1. *Leuven*.

[Klippel, 1992a] Klippel, W. (1992a). The mirror filter - a new basis for reducing nonlinear distortion and equalizing response in woofer systems. *J. Audio Eng. Soc.*, Vol. 40(No. 9):pp. 675–691.

[Klippel, 1992b] Klippel, W. (1992b). Nonlinear large-signal behavior of electrodynamic loudspeakers at low frequencies. *J. Audio Eng. Soc.*, Vol. 40(No. 6):pp. 483–496.

[Klippel, 1992c] Klippel, W. (1992c). Schaltungsanordnung zur korrektur des linearen und nichtlinearen Übertragungsverhaltens elektroakustischer wandler. *European Patant*, No. EP-A-0 508 392.

[Klippel, 1998] Klippel, W. (1998). Direct feedback linearization of nonlinear loudspeaker systems. *J. Audio Eng. Soc.*, Vol. 46(No. 6):pp. 499–507.

[Klippel, 2000] Klippel, W. (2000). Diagnosis and remedy of nonlinearities in electrodynamical transducers. *Audio Eng. Soc.*, 109th Convention.

[Klippel, 2001] Klippel, W. (2001). Prediction of speaker performance at high amplitudes. *Audio Eng. Soc.*, 111th Convention.

[Klippel, 2003] Klippel, W. (2003). Nonlinear modeling of the heat transfer in loudspeakers. *Audio Eng. Soc.*, 114th Convention.

[Leach, 1999] Leach, W. M. (1999). *Introduction to Electroacoustics and Audio Amplifier Design.* Kendall/Hunt Publiching Company, 2. edition.

[Marcel A. H. Beerling and Hermann, 1998] Marcel A. H. Beerling, C. H. S. and Hermann, O. E. (1998). Reduction of nonlinear distortion in loudspeakers with digital motional feedback. *Audio Eng. Soc.*, 96th Convention. Preprint 3820.

[Moir, 1974] Moir, J. (1974). Doppler distortion in loudspeakers. *Wireless World*, pages pp. 65–69.

[Olsen and Thorborg, 1995] Olsen, E. S. and Thorborg, K. (1995). Diaphragm area and mass nonlinearities of cone loudspeakers. *Audio Eng. Soc.*, 99th Convention.

[Poulsen, 2004] Poulsen, S. (2004). *Towards Active Transducers.* PhD thesis, The Technical University of Denmark, Department of Automation - Ørsted·DTU.

[Schurer, 1997] Schurer, H. (1997). *Linearization of Electroacoustic transducers.* PhD thesis, University of Twente Enschede.

[Small, 1971] Small, R. H. (1971). Direct-radiator loudspeaker system analysis. *IEEE Transactions on Audio and Electroacoustics*, Vol. AU-19:pp. 269–281.

[Small, 1972] Small, R. H. (1972). Closed-box loudspeaker systems, part i: Analysis. *J. Audio Eng. Soc.*, Vol. 20:pp. 798–808.

[Small, 1973a] Small, R. H. (1973a). Closed-box loudspeaker systems, part ii: Synthesis. *J. Audio Eng. Soc.*, Vol. 21:pp. 11–18.

[Small, 1973b] Small, R. H. (1973b). Vented-box loudspeaker systems, part 1: Small-signal analysis. *J. Audio Eng. Soc.*, Vol. 21:pp. 363–372.

[Small, 1973c] Small, R. H. (1973c). Vented-box loudspeaker systems, part 2: Large-signal analysis. *J. Audio Eng. Soc.*, Vol. 21:pp. 483–444.

[Small, 1973d] Small, R. H. (1973d). Vented-box loudspeaker systems, part 3: Synthesis. *J. Audio Eng. Soc.*, Vol. 21:pp. 549–554.

[Small, 1973e] Small, R. H. (1973e). Vented-box loudspeaker systems, part 4: Appendices. *J. Audio Eng. Soc.*, Vol. 21:pp. 635–639.

[Smidth, 2004] Smidth, U. (2004). Personal correspondence. (8 october, 2004). Danish Sound Technology, www.d-s-t.com.

[Spiegel and Liu, 1999] Spiegel, M. R. and Liu, J. (1999). *Mathematical Handbook of Formulas and Tables.* Schaum's Outline Series, 2. edition.

[Thiele, 1961] Thiele, A. N. (1961). Loudspeakers in vented boxes. *Proceedings of the IRE Australia; "reprinted in J. Audio Eng. Soc., 19: pp. 382-392 (May 1971)"*, Vol. 22:pp. 487–508.

[Vanderkooy, 1989] Vanderkooy, J. (1989). A model of loudspeaker driver impedance incorporating eddy currents in the pole structure. *J. Audio Eng. Soc.*, Vol. 37(No. 3):pp. 119–128.

[Weisstein, 1] Weisstein, E. W. (1). Least squares fitting. from mathworld–a wolfram web resource. http://mathworld.wolfram.com/LeastSquaresFitting.html.

[Weisstein, 2] Weisstein, E. W. (2). Least squares fitting–polynomial. from mathworld–a wolfram web resource. http://mathworld.wolfram.com/LeastSquaresFittingPolynomial.html.

[Weisstein, 3] Weisstein, E. W. (3). Nonlinear least squares fitting. http://mathworld.wolfram.com/NonlinearLeastSquaresFitting.html.

Appendix A

Data coefficients

A.1 Digital filters

A.1.1 Closed box

$$H_{x_D+2}(z) = \frac{x_{D+2}(z)}{u(z)} = S_0 \frac{b_x(2)z^{-2}}{a_x(0) + a_x(1)z^{-1} + a_x(2)z^{-2}} \tag{A.1}$$

where:

$$\begin{aligned} S_{0,x_D} &= \frac{C_t Bl}{R_E} \\ \mathbf{b}_{x_D,CB}(2) &= \frac{1}{C_t M_t} T_s^2 \\ \mathbf{a}_{x_D,CB}(0) &= 1 \\ \mathbf{a}_{x_D,CB}(1) &= -2 + \frac{R_t}{M_t} T_s + \frac{Bl^2}{R_E M_t} T_s \\ \mathbf{a}_{x_D,CB}(2) &= 1 - \frac{R_t}{M_t} T_s + \frac{1}{C_t M_t} T_s^2 - \frac{Bl^2}{R_E M_t} T_s \end{aligned}$$

A.1.2 Vented box

$$H_{x_D+2}(z) = \frac{x_{D+2}(z)}{u(z)} = S_0 \frac{b_{x_D,VB}(2)z^{-2} + b_{x_D,VB}(3)z^{-3} + b_{x_D,VB}(4)z^{-4}}{a_{x_D,VB}(0) + a_{x_D,VB}(1)z^{-1} + a_{x_D,VB}(2)z^{-2} + a_{x_D,VB}(3)z^{-3} + a_{x_D,VB}(4)z^{-4}} \tag{A.2}$$

where:

$$
\begin{aligned}
S_{0,x_D} &= \frac{C_t Bl}{R_E} \\
\mathbf{b}_{x_D,VB}(2) &= M_{AP} C_{AB} \frac{1}{T_s^2} \\
\mathbf{b}_{x_D,VB}(3) &= -2 M_{AP} C_{AB} \frac{1}{T_s^2} + \frac{M_{AP}}{R_{AL} T_s} \\
\mathbf{b}_{x_D,VB}(4) &= C_{AB} \frac{1}{T_s^2} - \frac{M_{AP}}{R_{AL} T_s} + 1 \\
\mathbf{a}_{x_D,VB}(0) &= C_D M_t \frac{1}{T_s^2} M_{AP} C_{AB} \frac{1}{T_s^2} \\
\mathbf{a}_{x_D,VB}(1) &= C_D M_t \frac{1}{T_s^2} \left(-2 M_{AP} C_{AB} \frac{1}{T_s^2} + \frac{M_{AP}}{R_{AL} T_s} \right) \\
&\quad + \left(-2 C_D M_t \frac{1}{T_s^2} + C_D R_D \frac{1}{T_s} + \frac{C_D Bl^2}{Re * Ts} \right) M_{AP} C_{AB} \frac{1}{T_s^2} \\
\mathbf{a}_{x_D,VB}(2) &= C_D M_t \frac{1}{T_s^2} \left(C_{AB} \frac{1}{T_s^2} - \frac{M_{AP}}{R_{AL} T_s} + 1 \right) + \left(-2 C_D M_t \frac{1}{T_s^2} + C_D R_D \frac{1}{T_s} + \frac{C_D Bl^2}{Re * Ts} \right) \\
&\quad \left(-2 M_{AP} C_{AB} \frac{1}{T_s^2} + \frac{M_{AP}}{R_{AL} T_s} \right) + \left(C_D M_t \frac{1}{T_s^2} - C_D R_D \frac{1}{T_s} - \frac{C_D Bl^2}{Re * Ts} + 1 \right) M_{AP} C_{AB} \frac{1}{T_s^2} \\
&\quad + C_D S_D M_{AP} S_D \frac{1}{T_s^2} \\
\mathbf{a}_{x_D,VB}(3) &= \left(-2 C_D M_t \frac{1}{T_s^2} + C_D R_D \frac{1}{T_s} + \frac{C_D Bl^2}{Re * Ts} \right) \left(C_{AB} \frac{1}{T_s^2} - \frac{M_{AP}}{R_{AL} T_s} + 1 \right) \\
&\quad + \left(C_D M_t \frac{1}{T_s^2} - C_D R_D \frac{1}{T_s} - \frac{C_D Bl^2}{Re * Ts} + 1 \right) \left(-2 M_{AP} C_{AB} \frac{1}{T_s^2} + \frac{M_{AP}}{R_{AL} T_s} \right) - 2 C_D S_D^2 M_{AP} \frac{1}{T_s^2} \\
\mathbf{a}_{x_D,VB}(4) &= \left(C_D M_t \frac{1}{T_s^2} - C_D R_D \frac{1}{T_s} - \frac{C_D Bl^2}{Re * Ts} + 1 \right) \\
&\quad \left(C_{AB} \frac{1}{T_s^2} - \frac{M_{AP}}{R_{AL} T_s} + 1 \right) + C_D S_D^2 M_{AP} \frac{1}{T_s^2}
\end{aligned}
$$

A.2 Bessel and Struve functions

Bessel function of first kind:

$$J_1(x) = \frac{x}{2} - \frac{x^3}{2^2 \cdot 4} + \frac{x^5}{2^2 \cdot 4^2 \cdot 6} - \cdots \tag{A.3}$$

Struve function of order one:

$$H_1(x) = \frac{2}{\pi} \left[\frac{x^2}{3} - \frac{x^4}{3^2 \cdot 5} + \frac{x^6}{3^2 \cdot 5^2 \cdot 7} - \cdots \right] \tag{A.4}$$

Appendix B

Parameters of the test loudspeaker

B.1 Linear parameters

	SI	s1	s2	tweeter
Electrical Parameters				
R_E	Ω	5.54	5.57	3.57
L_E	mH	0.337	0.346	0.1
R_2	Ω		3.02	-
L_2	mH		0.482	-
f_s	Hz	50.1	45.8	1348
Mechanical Parameters				
M_t	g	8.629	8.439	0.3
M_D	g	8.22	8.03	-
R_D	kg/s	0.979	0.973	0.93
C_D	mm/N	1.17	1.43	0.05
K_D	N/mm	0.85	0.70	-
Bl	N/A	5.13	5.21	2
Sd	cm^2	80.00	80.00	6.2
Loss factors				
Q_M	N/A	2.77	2.49	2.94
Q_E	N/A	0.57	0.5	3.95
Q_{TS}	N/A	0.47	0.41	1.68
V_{AS}	l	10.6	12.99	-
η_0	%	0.224	0.241	-
L_m	dB	85.70	86.02	90.1

B.2 Nonlinear coefficients

B.2.1 Polynomial fit

	Bl	C_D	L_E
(0)	5.132	1.999	$5.367e-1$
(1)	$-8.231e-2$	$6.533e-2$	$-9.897e-2$
(2)	$-5.429e-2$	$-8.370e-2$	$6.387e-3$
(3)	$-1.638e-3$	$-4.166e-3$	$3.638e-3$
(4)	$-4.101e-3$	$2.627e-3$	$-2.757e-4$
(5)	$1.544e-4$	$1.121e-4$	$-9.789e-5$
(6)	$1.31e-4$	$-4.965e-5$	$7.088e-6$
(7)	$-2.034e-6$	$-1.094e-6$	$1.022e-6$
(8)	$-1.171e-6$	$3.924e-7$	$-6.626e-8$

B.2.2 Exponential fit

Bl

$$\begin{aligned} N_l &= 5 \\ \sigma &= sqrt5 \\ \\ x_l &= [-5; -2.5; 0; 2.5; 5] \\ \omega_{opt} &= [1.5131; 2.6684; 2.1999; 2.4490; 1.0571] \end{aligned}$$

C_D

$$\begin{aligned} N_l &= 5 \\ \sigma &= sqrt7 \\ \\ x_l &= [-7; -3.5; 0; 3.5; 7] \\ \omega_{opt} &= [0.3746; 0.3421; 1.5851; 0.5998; 0.2997] \end{aligned}$$

L_E

$$\begin{aligned} N_l &= 6 \\ \sigma &= sqrt7 \\ \\ x_l &= [-6; -3.6; -1.2; 1.2; 3.6; 6] \\ \omega_{opt} &= [0.4517; -0.2731; 0.5095; -0.5164; 0.2274; -0.2689] \\ \omega_0 &= 0.5513 \end{aligned}$$

B.2.3 Sigmoid fit

L_E

$$\begin{aligned} \omega_1 &= -0.5776 \\ \omega_0 &= 0.9102 \\ a &= 0.7145 \\ x_0 &= -0.9131 \end{aligned}$$